Towards reliable correlation of microporous layer physical characteristics and PEMFC electrochemical performance

BY

Gregory Crymble

Submitted in partial fulfilment of the requirements for the degree of
Master of Science in Engineering

Centre for Catalysis Research
Department of Chemical Engineering
University of Cape Town

2014

PLAGIARISM DECLARATION

I know the meaning of plagiarism and declare that all the work in this document, save for that which is properly acknowledged, is my own.

Name: **Gregory A. Crymble**

Signed by Candidate

Signature: _____

Signature Removed

Date: 18 November 2014

SYNOPSIS

Polymer electrolyte membrane (PEM) fuel cells are promising clean energy alternatives to non-sustainable fossil fuels. During fuel cell operation, external humidification of reactant gases is typically required in order to increase PEM conductivity for improved performance. However, the use of external humidification is costly and increases system complexity.

Recently it has been found that by including a cathode microporous layer (MPL) in the membrane electrode assembly (MEA), performance under dry conditions (no external humidification) can be significantly improved. However, the precise function of the MPL is not well understood and therefore there is little theoretical basis to optimisation of physical properties. One possible reason for this lack of understanding is the absence of a well established fabrication, characterization and electrochemical testing methodology for MPL research. In particular, current research places little emphasis on the effect of MEA variance on the uncertainty in MPL electrochemical performance results.

In this study a methodology is developed for fabricating, characterizing and testing MPLs to accurately correlate physical properties with *in-situ* electrochemical performance. MPLs of two significantly different thicknesses (approximately 20 and 50 µm in the thickest regions) were fabricated in-house using a doctor blade method and varying the ink composition. The pore structure and thickness of MPLs were characterized by mercury intrusion porosimetry (MIP), scanning electron microscopy (SEM) and X-ray micro computed tomography (µCT).

Using µCT, a procedure is developed to holistically quantify the thickness distribution of the MPL after electrochemical testing and while still within the MEA. The obtained thickness distributions suggest that conventional SEM measurements do not provide sufficient information for accurate and complete characterization of MPL thickness. The variation in pore structure of Sigracet® SGL 25BA, SGL 25BC and Freudenberg H2315 I6 was quantified by repeat MIP analysis. It is found that SGL 25BC has the largest variability in measured pore size distribution relative to the other two commercial GDLs which is possibly due to the MPL.

MEA electrochemical performance was measured by polarization curves with high frequency resistance measurements and electrochemical impedance spectroscopy performed in a 25 cm^2 active area balticFuelCells single cell connected to a FuelCon test station. Procedures were implemented to ensure reliable and reproducible testing conditions with a particular focus on relative humidity control and contamination mitigation. MEA performance variance at high and low (inlet gas) relative humidity

operation with both air and oxygen was quantified by repeat electrochemical testing of Ion Power DuPont® NAFION® NR-211 catalyst coated membranes with Sigracet® SGL 25BC at the anode and three different gas diffusion layer combinations at the cathode; SGL 25BC, SGL 25BA and Freudenberg H2315 I6. It is found that there is significant performance variance under a variety of controlled testing conditions which is attributed to non-uniformity across MEAs. MEAs with SGL 25BC at the cathode showed a larger variation than those with the two commercial GDLs without MPLs. This suggests that the effect of the SGL 25BC MPL on measured pore structure is a contributing factor to MEA variance. The largest MEA performance variation for all three cathode GDLs is observed at low relative humidity operation with air as the oxidant, however by comparing the performance results of SGL 25BA and SGL 25BC the MPL is still shown to have a statistically significant beneficial effect on performance at these conditions. The beneficial effect of the MPL when operating under high relative humidity and air (which is well established in literature) is not observed in this study and in fact the results here suggest that the MPL has a detrimental effect on performance for this specific MEA combination.

The MPL characterization and MEA performance results from this study show that careful consideration of experimental testing conditions, MEA components, physical characterization methods and a statistical treatment of MEA performance variations are all necessary for reliable MPL electrochemical *in-situ* studies. Using the methodology developed in this study may allow for an improved understanding of the function of the MPL thus providing a better theoretical basis for optimisation.

ACKNOWLEDGEMENTS

Thank you to the HySA/Catalysis team and in particular my supervisors Dr Olaf Conrad and Mr Nabeel Hussain for giving me the freedom to pursue my own research ideas while still providing valuable guidance along the way.

In no particular order I would like to thank all those that helped with the collection of data for this research. Ms Stephanie Snoek and Dr Sivakumar Pasupathi and his team for mercury intrusion porosimetry measurements, Ms Miranda Waldron for assistance with scanning electron microscopy and Dr Anton du Plessis and Stephan le Roux for their extensive help with X-ray computed tomography.

Additionally I am grateful for the funding provided by Sasol and the assistance from my mentor Vimal Bhimsan over the duration of this study.

To my parents, your support throughout my life has been instrumental to me achieving my academic goals thus far. Finally to my sisters and friends, for all the love and support during all my University studies, **thank you**.

TABLE OF CONTENTS

LIST OF FIGURES

LIST OF TABLES

LIST OF SYMBOLS

Symbol	Description	Units
d_p	Pore diameter	µm
$\tilde{d}_p$	Median pore diameter	µm
ε	Porosity	%
i	Current density	A/cm^2
Im (Z)	Imaginary component of (area specific) impedance	$m\Omega.cm^2$
P	Pressure (absolute)	bar
p-value	Probability value (of null hypothesis)	-
Q	Flow rate at normal conditions (273K , 1 atm)	nL/min
Re(Z)	Real component of (area specific) impedance	$m\Omega.cm^2$
RH	Relative humidity	%
s_x	Stoichiometry for species 'x'	-
$S_{X_1X_2}$	Pooled standard deviation	-
T	Temperature	^oC
t_{stat}	t-test statistic	-
V	Cell voltage (potential difference relative to RHE)	V
$\bar{X}$	Sample mean	-
Z	Impedance	$m\Omega.cm^2$

GLOSSARY

CD	Current density
CL	Catalyst layer
CCM	Catalyst coated (polymer electrolyte) membrane
CTR	Charge transfer resistance
DM	Diffusion medium
EIS	Electrochemical impedance spectroscopy
GC	Gas channel
GDL	Gas diffusion layer
GDE	Gas diffusion electrode
GDM	Gas diffusion media
HFR	High frequency resistance
HySA	Hydrogen South Africa
MEA	Membrane electrode assembly
MIP	Mercury intrusion porosimetry
MPL	Microporous layer
µCT	Micro-computed tomography
NWD	Net water drag (coefficient)
OCV	Open circuit voltage
ORR	Oxygen reduction reaction
PC	Polarization curve
PCx	**‘**x’th successive repeat of a polarization curve
PDM	Porous diffusion media
(PEM)FC	(Polymer electrolyte membrane) fuel cell
PSD	Pore size distribution
Pt	Platinum
PTFE	Polytetrafluoroethylene
RH	Relative humidity
RHE	Reference hydrogen electrode
Run	Repeat testing at same conditions but with a different MEA
SEM	Scanning electron microscopy
wt%	Solids (PTFE and carbon) weight percentage of total MPL ink mass
XCT	X-ray computed tomography
2D	Two dimensional
3D	Three dimensional

1 Introduction

Polymer electrolyte membrane fuel cells (PEMFCs) produce electricity from the electrochemical oxidation and reduction of hydrogen and oxygen respectively. Advantageously, PEMFCs can operate continuously at relatively low temperatures (< 100 °C) producing a high power density with only liquid water as the chemical by-product. Additionally, hydrogen is extractable from a variety of (potentially sustainable) sources abundant on the planet and therefore PEMFC technology is a promising candidate as a large scale, clean alternative to non-sustainable fossil fuel based energy.

The electrochemical reactions in PEMFCs require catalysis to improve the kinetics during low temperature operation (Starz et al., 1999). Platinum group metals (PGMs) are commonly used electrocatalysts in PEMFCs due to their high activity and durability under fuel cell conditions (Larminie and Dicks, 2003). Over 70 % of the world's discovered PGM resources are found in South Africa (Zientek et al., 2014: 74) and therefore the development of fuel cell technology in this region is particularly important for resource beneficiation and economic gain. As a result, the South African Government has launched the Hydrogen South Africa programme (HySA) with the primary goal to generate wealth for the country by developing value added PGM catalysts for the emerging fuel cell market.

HySA has established three Competence Centres focusing on hydrogen catalysis and catalytic devices (HySA/Catalysis), hydrogen infrastructure (HySA/Infrastructure) and hydrogen systems integration and validation (HySA/Systems). The Hydrogen Catalysis Competence Centre (HySA/Catalysis) is jointly hosted by the University of Cape Town's Chemical Engineering Department and South Africa's national Minerals Research Council, Mintek. This division focuses on fuel processing, portable power technologies, direct methanol fuel cells and H_2 PEM devices. The main research activities with regard to H_2 PEM devices include catalyst technology, membrane electrode assembly (MEA) development and fuel cell stack engineering.

The microporous layer (MPL) is an important but not well understood component of the MEA. This study develops a methodology for the reliable fabrication and characterization of the MPL and accurate correlation of MPL physical properties with *in-situ* MEA electrochemical performance. Using this methodology the functions and optimal properties of the MPL can be better studied and understood.

2 Background

The proton exchange/polymer electrolyte membrane fuel cell (PEMFC) is the most promising candidate for portable application of fuel cell technology due to its high power density and dynamic response characteristics (Larminie and Dicks, 2003: 67). Figure 2.1 illustrates the half cell reactions and electron flow during PEMFC operation. Humidified hydrogen and oxygen (as either air or pure gas) are fed to either side of a separating electrolyte boundary and are oxidised and reduced respectively. The electrons generated at the anode travel through an external circuit before completing the electrochemical reaction at the cathode producing heat and water.

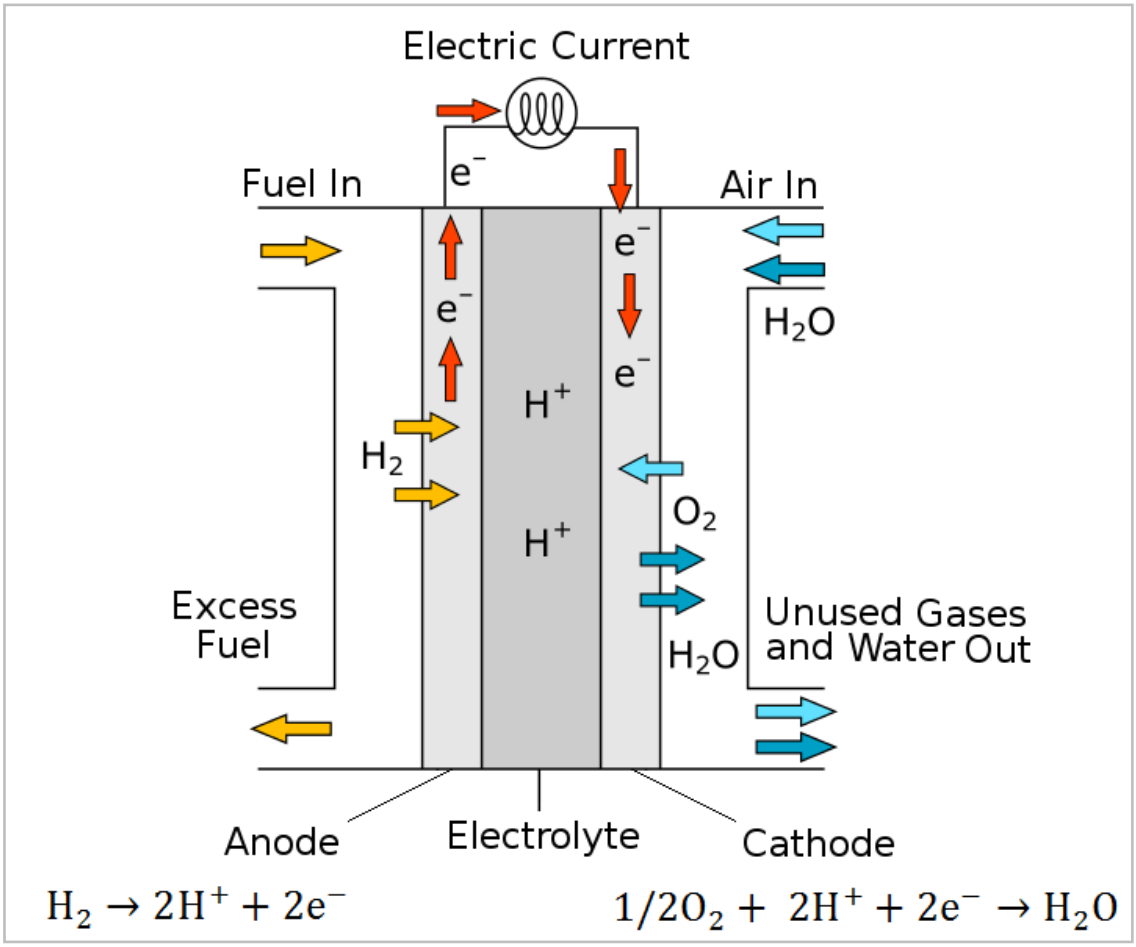

Figure 2.1: PEMFC schematic showing electrochemical reactions (Wikimedia public domain)

In general, the aim of PEMFC research is to maximise performance relative to the cost of producing the fuel cells (Li et al., 2008) and in this regard each component of the fuel cell must be carefully studied and optimised. The membrane electrode assembly is a combination of porous diffusion media, catalyst layers and a polymer electrolyte membrane and is a major focus of fuel cell research.

2.1 The membrane electrode assembly

All fuel cells contain two catalyst electrodes with an electronically insulating electrolyte between them. Porous diffusion layers are placed between the catalyst layer and the reactant gas flow field to improve reactant gas dispersion and product water management. This five layer MEA is about 500 µm thick allowing for the manufacture of compact (high energy density) fuel cells well suited to portable applications (Larminie and Dicks, 2003: 67). Figure 2.2 illustrates a typical five layered MEA with dual layer porous diffusion media composed of a gas diffusion layer and microporous layer. Each layer of the MEA (and interaction between the layers) is important for optimal PEMFC performance.

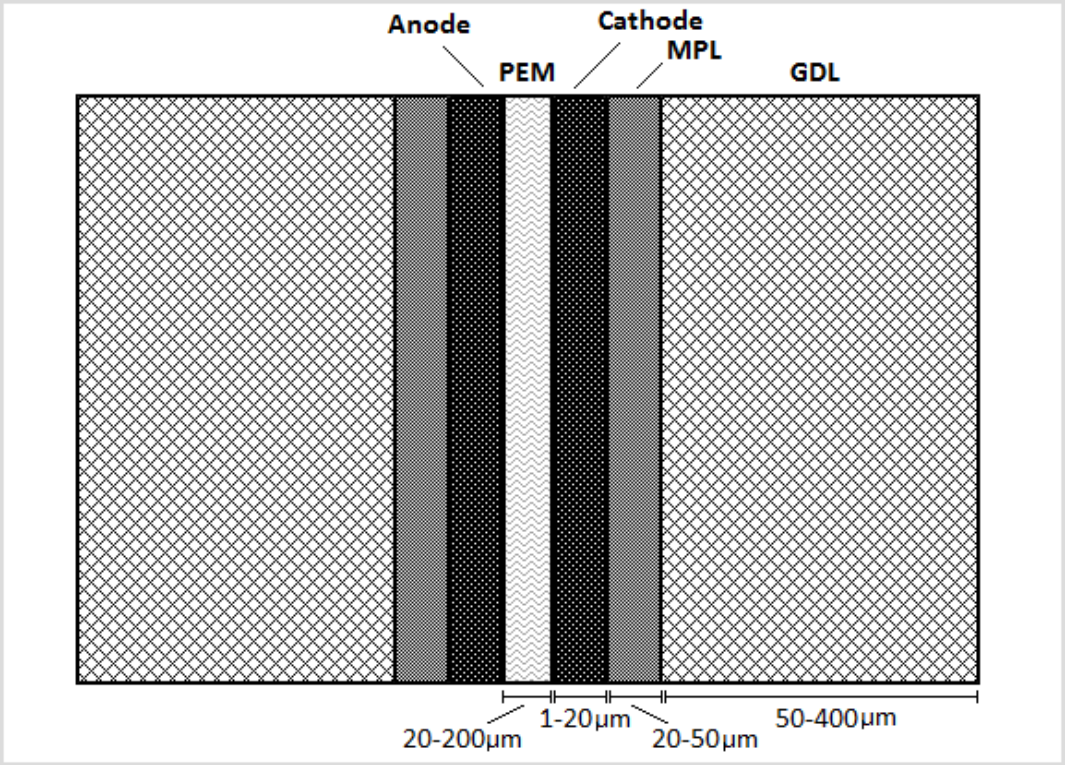

Figure 2.2: Membrane electrode assembly

A polymer electrolyte membrane (PEM) must be proton conductive while separating the anode and cathode electronically and physically to prevent electronic shorting and mixing of reactant gases. Additionally the PEM must be chemically and mechanically stable in the fuel cell environment and therefore is typically composed of perfluoro-sulfonic acid (PFSA) polymers such as Nafion®. These polymers are also known as ionomers because of the presence of ionically bonded H^+ and SO_3^- groups within the structure. The sulphonated regions of the polymer are able to absorb large amounts of water reducing the strength to which the H^+ ions are attracted to SO_3^- group and allowing H^+ ions to move through the long molecule structure (Larminie and Dicks, 2003). As such, membrane hydration is essential to

facilitate proton conduction across the PEM during fuel cell operation. PEM ionic conductivity also increases with temperature (Rieke and Vanderborgh, 1987) however at temperatures above 80 ^{o}C PFSA membranes experience dehydration, loss of ionic conductivity, loss of mechanical strength and increased gas permeability (Viswanathan and Aulice Scibioh, 2006).

The fuel cell electrode is essentially a thin catalyst layer which contains small (≈ 4 nm) platinum particles dispersed over larger (≈ 40 nm) carbon particles usually in powder form e.g. Vulcan® XC72R by Cabot (Babir, 2005). PFSA ionomer is added to the platinum coated carbon to form a three phase region which is accessible to reactant gas, protons and electrons necessary for the electrochemical reaction. The anode (hydrogen oxidation) reaction is facile relative to oxygen reduction reaction (Viswanathan and Aulice Scibioh, 2006) and therefore the cathode is the main focus for MEA performance improvement.

One major concern with regard to platinum electrocatalyst is degradation and the resulting MEA performance loss with time. Catalyst activity may be reduced due to contamination, platinum particle sintering, platinum dissolution into the electrolyte and carbon support corrosion (Yu and Ye, 2007). Carbon corrosion can occur as a result of fuel starvation at the anode causing oxidation of either carbon or water by cross-over oxidant from the cathode. However carbon corrosion in a PEMFC is negligible at electrode potentials lower than 1.1 V (vs. RHE) and furthermore water in the electrode protects carbon from corrosion due to favoured water oxidation (Wu et al., 2008a). The rate of platinum sintering is temperature dependant and the rate of dissolution depends on electrical potential. Platinum gas-phase sintering in Pt/C is insignificant at low temperatures but is greatly accelerated in the liquid phase (Shao et al., 2007). Darling and Meyers (2003) developed a mathematical model for the oxidation and dissolution of Pt/C in PEMFCs which agrees with experimental data which shows a rapid increase in Pt dissolution above 0.8 V in acidic environments. These conditions are experienced at very low current densities in the PEMFC and therefore prolonged periods at open circuit voltage (OCV) should be avoided.

The gas diffusion layer (GDL) is important for electrical and thermal conduction, physical support, diffusion and dispersion of reactant gases and water management (Cindrella et al., 2009). It is typically a hydrophobic, macroporous carbon based substrate such as woven carbon cloth or non-woven carbon fibre paper (Park et al., 2012). The non-woven GDL is composed of carbon fibres randomly orientated to form a porous structure as shown in Figure 2.3. Physical properties such as porosity and thickness (Zhan et al., 2007), pore geometry (Park and Popov, 2009) and PTFE content (Eom et al., 2013) all have been shown to have a significant effect on GDL efficacy and the resulting PEMFC performance.

Due to the random nature of the GDL structure, there is intrinsic variation in local physical properties which may result in performance variation as shown in a study by Reshetenko et al. (2012).

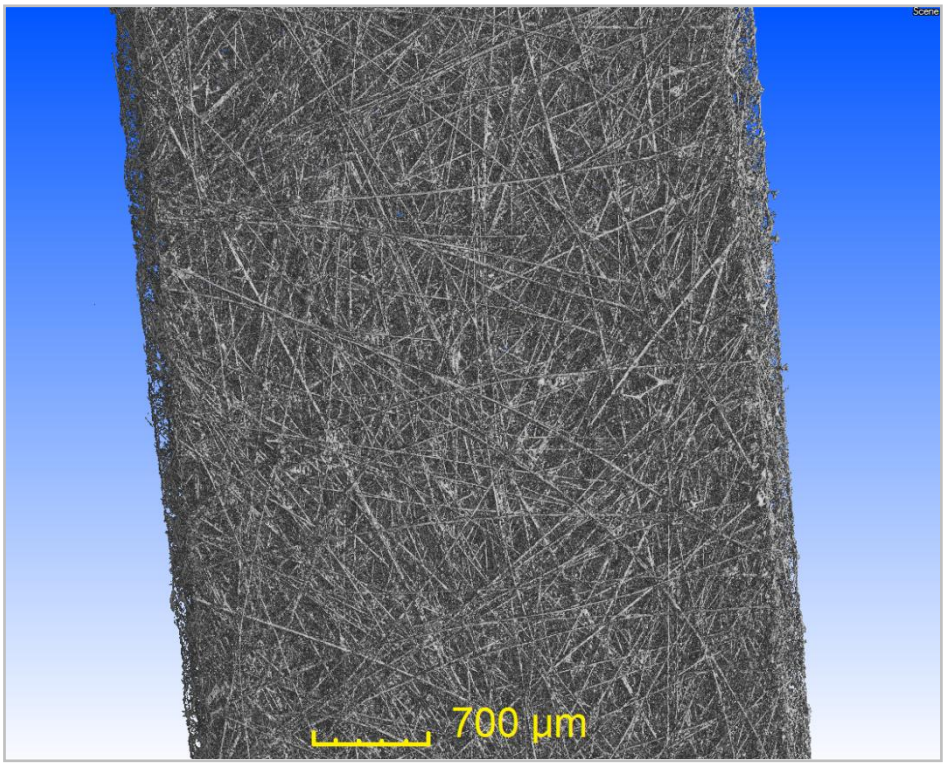

Figure 2.3: X-ray computed tomography image showing GDL fibre structure of SGL 25BC sample (see Section 5.2.1 for scan parameters)

Studies focusing on GDL optimization require characterization of physical properties and correlation of these properties to electrochemical performance. Arvay et al. (2012) provide a review of characterization techniques for GDLs. Intrusion porosimetry and porometry are methods commonly used to quantify pore size distribution and porosity. These methods involve measuring the pressure required to either force liquid into or out of the porous material allowing for the quantification of pore structure from simplifying assumptions. However, due to these assumptions, complex structural information of the GDL such as variable pore geometry is not captured (Arvay et al., 2012). A further disadvantage of these methods is their destructive nature due to the high pressures required to force the liquid into (or out of) small pores. As such, a GDL sample cannot be characterized directly before being used for electrochemical testing and therefore a representative sample is required. Due the previously discussed intrinsic variability in the GDL, a representative sample may not accurately quantify the tested GDL especially if the sample size is small and therefore more sensitive to random structural variation.

The GDL is sometimes coated with a thin carbon layer known as the MPL, which acts as a boundary between the GDL and catalyst layer and has been found to significantly improve PEMFC performance at high current densities under a variety of operating conditions (Lin and Nguyen, 2006; Atiyeh et al., 2007; Tseng and Lo, 2010). Microporous materials are classified by the IUPAC system (IUPAC, 2014: 916) as having pore diameters less than 2 nm however this definition does not strictly apply to microporous layers (MPLs) in MEAs which can have pore sizes of the order of 100 nm (Atiyeh et al., 2007; Pant et al., 2012; Park et al., 2012; Chan et al., 2012). It should also be noted that the size range definition of micro, meso and macro-pores varies throughout PEMFC literature. Though the precise function of the MPL is not well understood, it is generally believed that the MPL alters the liquid water distribution in the MEA in such a way as to improve reactant gas mass transfer (Deevanhxay et al., 2013; Gostick et al., 2009; Nam et al., 2009; Pasaogullari and Wang, 2004). It is also proposed that the MPL improves electrical and thermal conduction between the catalyst layer and GDL by providing a smoother contact surface (Park et al., 2012; Karimi et al., 2010; Gostick et al., 2009; Paganin et al., 1996). An in-depth review of MPL literature is presented in Section 3.2.

2.1.1 Membrane electrode assembly preparation

Complete five layer MEAs can be purchased commercially (e.g. Alfa Aesar Hydrogen Screener Membrane Electrode Assembly (MEA-5 layer) 45362). This is useful for benchmarking purposes and validation of newly commissioned fuel cell testing equipment. However, for the purposes of researching a specific layer of the MEA such as the cathode GDL, the other layers need to be carefully controlled. The usual practice is to purchase the other components separately from a commercial supplier and then to assemble the MEA manually with all components kept uniform except the layer under investigation. The subject of MEA preparation deals with the selection of MEA components and assembly and treatment of these components prior to fuel cell testing.

MEAs are prepared in two ways; either an electrolyte membrane is sandwiched between two catalyst coated substrates (also known as gas diffusion electrodes) or a catalyst coated membrane (CCM) is sandwiched between GDLs. In the field of GDL/MPL research the latter method is typically used prior to electrochemical testing. An additional hot pressing step may be performed to laminate the MEA and improve contact between the layers (Frey and Linardi, 2004). Hot pressing is usually conducted at pressures of 50 - 150 bar and temperatures between 120 and 160 ^{o}C for a period of 1 to 5 minutes (Kocha, 2003). However hot-pressing can also result in excessive membrane dry-out and electrode delamination due to swelling of the protonic form of the membrane (Kocha, 2003).

It is debatable whether there is a distinct advantage for hot pressing MEAs and according to Zhang (2008: 898) hot pressing is not necessary. Escribano et al. (2006) suggest that the high compressive forces applied to the GDL during hot-pressing could dramatically affect the durability of the MEA and increase mass transfer polarization at high current and low pressure. Furthermore Tang et al. (2007b) found that CCMs without hot pressing significantly outperformed hot-pressed MEAs due to a higher electrochemical surface area, lower cell ohmic resistance and lower charge transfer resistance. Prasanna et al. (2008) also found that MEAs made from CCMs without hot pressing perform better than hot-pressed MEAs and showed less degradation during long term galvanostatic operation.

2.1.2 Microporous layer fabrication and characterization

The MPL is typically fabricated from an ink containing carbon powder mixed with PTFE-dispersed water and an organic surfactant (e.g. Triton X-100) which is deposited onto one side of a GDL and heat treated to evaporate all remaining liquid and disperse the PTFE (Park et al., 2012). Two common methods of depositing the MPL ink onto the GDL are doctor blade spreading and spraying. The important physical properties of the final microporous layer are material type, thickness, pore microstructure and water wetting character.

The doctor blade technique involves using a highly accurate mechanical drive to move a blade at constant speed and fixed height in order to spread ink over a flat surface/substrate. In this way, both catalyst ink and microporous diffusion layer ink can be deposited with high speed and precision (Latorrata et al., 2012; Park et al., 2010; Bender et al., 2003). The ink rheology and blade properties such as height, speed and angle relative to the substrate affect the ink flow dynamics during deposition and the resulting properties of the deposited layer (Davard and Dupuis, 2000).

Stampino et al. (2009) studied the effect of varying ink composition on coating deposition of the MPL and the resulting thickness and morphology of the final layer. They found that MPL thickness is a function of ink rheology and that viscosities in the range of 0.05 - 0.06 Pa.s at a shear rate of 100 s^{-1} were suitable for coating deposition, producing MPLs of measured thickness between 30 and 50 µm. They also found that the type of GDL substrate (woven carbon cloth or carbon fibre paper) affects the final MPL thickness but PTFE content in the ink does not.

There are a number of ways in which the pore structure in the MPL can be modified and controlled. Kitahara et al. (2010) were able to vary the mean flow pore diameter in the MPL from 1 to 10 µm by changing the water concentration in the MPL slurry ink from 76 to 89 %

respectively. After drying their applied catalyst ink, Tseng and Lo (2010) used an additional baking step (at 350 °C) which modified MPL pore structure. Increasing the baking time (between 1 h and 9 h) resulted in larger pores in the MPL but baking for longer than 9 h caused no additional change. A similar increase in pore size as a result of heat treatment at 350 °C was observed by Kong et al. (2002). As shown by Chen et al. (1999) PTFE melts at temperatures above 340 °C and therefore the change in pore structure at elevated temperatures may be due to the melting and re-dispersion of PTFE (Kong et al., 2002).

Pore forming agents can be used to control MPL microstructure (see Section 3.2.2). These agents (usually salts) are added to the MPL ink which is deposited onto the GDL. After drying the MPL slurry, the salts are removed (e.g. by treatment with acid and washing with distilled water) creating void spaces in the MPL. In this way porosity can be varied and controlled.

The incorporation of PTFE into the MPL binds the carbon particles into a cohesive layer and imparts hydrophobic properties which influence water management. The PTFE content in the MPL is controlled by varying the amount of PTFE solution added to the MPL ink prior to deposition onto the GDL. Dispersion of PTFE through heat treatment above 340 ^{o}C will also affect the water management properties of the MPL.

The MPL pore size distribution and thickness are typically measured using mercury intrusion porosimetry (MIP) and scanning electron microscopy (SEM) respectively. These techniques have limitations as well as being sample destructive. X-ray micro-computed tomography (µCT) is a potentially non-destructive GDL/MPL characterization technique which can overcome the limitations of MIP and SEM. Recently µCT is being used more frequently to better analyse the complex micro-structure and morphology of the GDL and MPL.

2.1.2.1 Mercury intrusion porosimetry

Intrusion porosimetry is a technique whereby pressure is used to selectively force a liquid into the differently sized pores of a sample. Using the simplifying assumption that the pore structure can be approximated by cylinders with a range of radii, the cumulative intruded volume of liquid over a pressure range can be related to the pore size distribution by a form of Washburn's equation (Arvay et al., 2012):

$$P_c = 2\sigma \frac{cos\theta}{r_{min}}$$

Where σ is the surface tension and θ is the wetting angle of the liquid with the sample material. When the applied pressure is equal to the capillary pressure (P_c), all pores with radii $r > r_{min}$ become filled with liquid.

For MPL characterization, mercury is used due to its high surface tension making it non-wetting and allowing for the measurement of both hydrophobic and hydrophilic pores down to radii of 10 nm (Arvay et al., 2012).

The disadvantages of mercury intrusion porosimetry are that it does not provide complex structural information (e.g. distinguishing between open and closed pores and different pore geometries) and it is sample destructive. Additionally, the technique requires high pressure application to characterize the small pores of the MPL and could therefore alter the MPL structure possibly resulting in inaccurate measurements (Krantz et al., 2013; Arvay et al., 2012).

2.1.2.2 Scanning electron microscopy

Scanning electron microscopy (SEM) is used to visualize MPL thickness after deposition onto the GDL and to study surface and cross-section morphology. For thickness measurements, the MPL coated GDL is freeze-fractured after submersion in liquid nitrogen and then mounted vertically for analysis. Figure 2.4 shows a typical SEM cross sectional image with MPL and GDL regions highlighted.

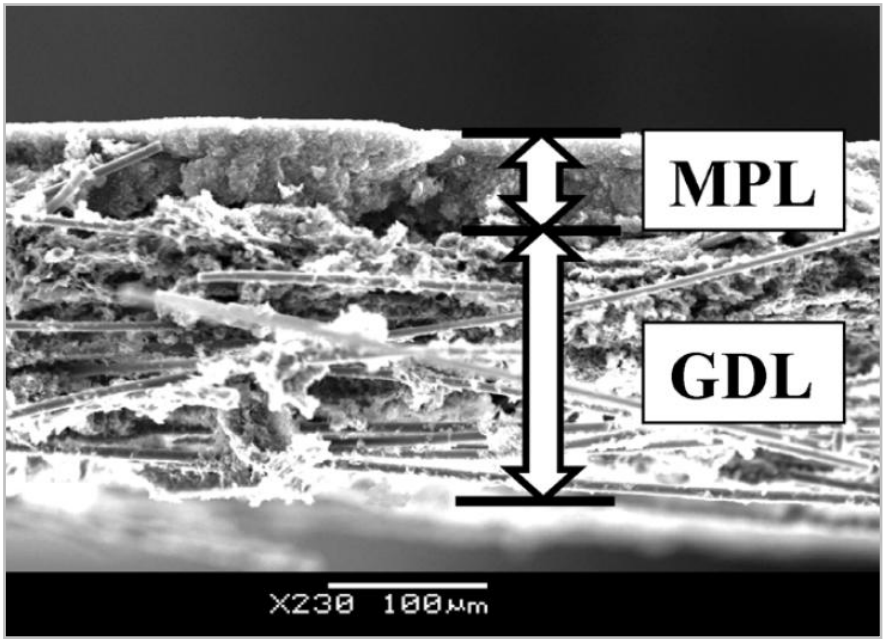

Figure 2.4: SEM cross section of 'SolviCore Type A' showing MPL and GDL regions (Chan et al., 2012)

A disadvantage of MPL characterization using SEM is that the sample preparation is destructive and can disturb the porous structure. Additionally, thickness measurements are localized along the cross-section and as such do not provide holistic information of MPL thickness variation in all dimensions. The region in which the thickness measurement is made may also be subjective and affected by the efficacy of the freeze-fracture preparation.

2.1.2.3 X-ray computed tomography

A relatively new method to characterize the morphology of the GDL and MPL is X-ray computed tomography. This technique measures 3D volume data at high resolution and is non-destructive.

X-ray radiation is attenuated by matter by a degree dependent on material thickness and density. Computed tomography (CT) is a technique by which many two dimensional radiographic images of an attenuated X-ray beam around an axis of rotation (360^{o}) are reconstructed to obtain three dimensional volume information (Maire and Withers, 2014; Herman, 2009). Recent advances in CT technology have allowed for the measurement of microscale (μCT) and even sub-micron volume information providing a new method for obtaining structural data on the GDL and MPL in PEMFCs (Maire and Withers, 2014). Particularly μCT can be used to measure GDL and MPL thicknesses non-destructively over a much larger sample area than conventional SEM methods. Additionally 3D volumes can be virtually manipulated in such a way that individual layers (of differing density) can be extracted and separately analyzed. An example of this is shown in Figure 2.5 where a platinum catalyst layer (of high density relative to the carbon fibres of the GDL) is segmented using grey-value thresholding from the sample 3D volume data set. In this way μCT can be applied to an assembled MEA after electrochemical testing and the layer(s) of interest (e.g. GDL) separately analyzed non-destructively.

Due to the similar compositions of the GDL and MPL, the two layers attenuate X-rays similarly and therefore cannot be completely separated using simple grey level thresholding. However, more advanced segmentation methods do exist which could assist in this task (Pfrang et al., 2013).

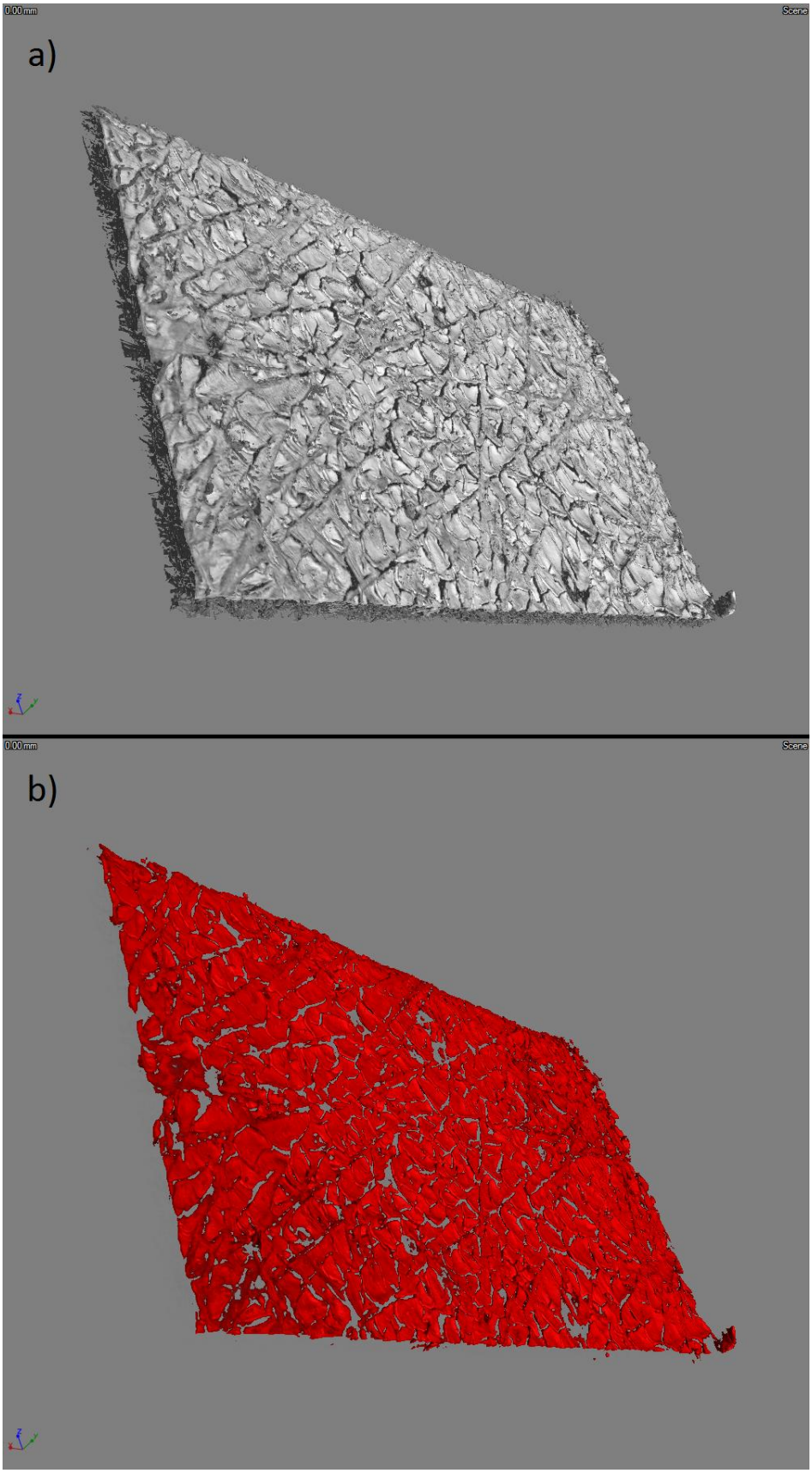

Figure 2.5: µCT 3D volume of a) gas diffusion electrode (Alfa Aesar® 045357) and b) virtually extracted catalyst layer (See Section 5.2.1 for scan parameters)

2.2 Performance evaluation

Due to the complex electrochemical, thermodynamic, kinetic and transport phenomena occurring during PEMFC operation, testing of MEAs under real and controlled fuel cell operating conditions is essential for validation and optimization of performance. Fuel cell test stations contain electronic diagnostic tools allowing for the analysis of (Cooper et al., 2005):

- Membrane permeability
- Electronic short
- Catalytic activity and utilization
- Membrane and catalyst layer ohmic resistance
- Performance curves
- Kinetic parameters such as exchange current density and Tafel slope
- Mass transfer phenomena

Real fuel cell systems use a series of cells (called a stack) to generate large power output. Assuming the heat management and gas delivery to the stack is well designed, single cell performance should give a reliable indication of the expected real fuel cell performance. For this reason single cell testing is an essential step in the assessment and optimization of PEMFC systems (Miller and Bazylak, 2011).

2.2.1 Single cell testing

A fuel cell test station is designed to measure and control reactant gas properties such as temperature, pressure, flow rates and relative humidity and fuel cell properties such as voltage, current and temperature. To achieve this, the station is equipped with mass flow controllers, a load bank, pressure and temperature controllers, humidifiers and a data acquisition and control unit (Cooper et al., 2005: 31). Typically external humidification is used whereby dry gases are bubbled through water to achieve saturation at a fixed temperature. By setting the relative temperatures of the 'bubblers' and the fuel cell, the inlet gas relative humidity can be controlled.

The test cell may vary depending on the flow field design, material design, and the type of sealing and assembly/compression strategies. The MEA is compressed between flow fields using either a gasket or O-ring to prevent internal and external gas leakage. The primary goal of the flow field is to ensure uniform distribution of reactant gas over the active area of the MEA and to effectively remove product water (Babir, 2005). Flow field geometry and configuration both influence gas delivery and thermal and electrical conductivity and

therefore fuel cell performance. Two common flow field configurations are parallel and serpentine. Parallel channels are straight, without any bends or turns and therefore benefit from low pressure drop between inlet and outlet however these channels are not suited for low temperature PEMFCs due to flooding susceptibility. A serpentine flow field does not suffer from channel blockage, but due to the path length and number of turns excessive work is required for gas delivery (Larminie and Dicks, 2003).

The electrodes which contact flow fields are porous to allow gas diffusion and therefore the edges must be sealed to prevent leakage. This is usually achieved by making the electrolyte membrane larger than the electrodes and fitting a sealing gasket or O-ring around each electrode. Figure 2.6 shows a CCM (Ion Power NR-211) secured by support pegs over the flow field of a balticFuelCells single cell fixture. The electrolyte membrane extends beyond the electrodes and over the rubber O-ring encapsulating the flow field.

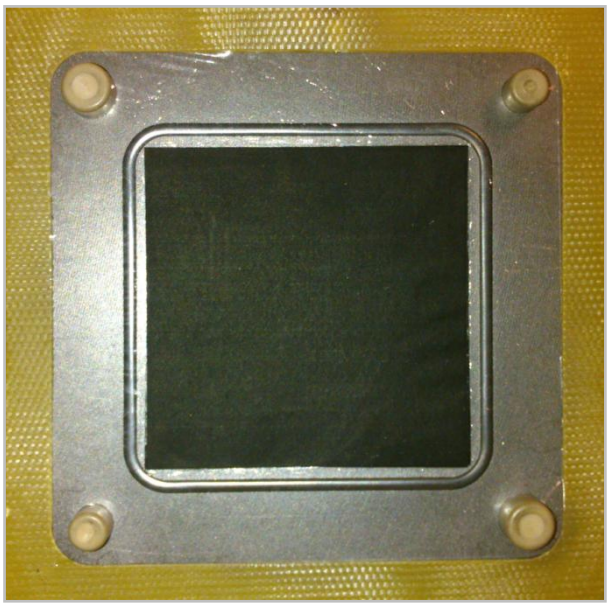

Figure 2.6: Placement of the CCM within a Baltic single cell with O-ring sealing

Apart from preventing gas leakage, cell compression is required to lower contact resistance at the interfacial regions between layers in the MEA. Mason et al. (2013) showed that increasing the compression of the MEA during operation reduces the high frequency (ohmic) resistance but also increases mass transfer overpotential at high current densities due to a reduction in GDL porosity. Depending on the cell fixture hardware, compression is either achieved by applying torque to bolts passing through the fixture or by using a compression unit such as the balticFuelCells FC25/100 quickCONNECT fixture. This fixture allows for rapid and dynamic changes in compression and is convenient for MEA research.

After cell assembly and before electrochemical testing, some pre-test diagnostics are required for safety and to confirm MEA integrity inside the cell. Additionally the MEA requires conditioning to ensure stable and reproducible performance for comparative results.

2.2.2 Contamination mitigation

Fuel cell performance can be severely and unpredictably reduced as a result of impurities in the reactant and water feeds. Therefore high purity reactant and oxidant gases and distilled water should be supplied for reliable testing. The USFCC (2006: p6) recommend testing with hydrogen gas purity greater than 99.999 % and de-ionized water with a resistivity greater than 250 kOhm.cm.

2.2.3 Pre-testing and MEA conditioning

Conventional pre-test diagnostics expose problems relating to gas leakage or crossover and electrical shorting. The US Fuel Cell Council's Single Cell Testing Task Force established a protocol for the assembly, pre-test diagnosis, conditioning, testing and shut down of single cell PEMFCs (USFCC, 2006).

Mixing of hydrogen with oxygen due to leakage (either internally or externally from the fuel cell) is a safety concern. If the flammability limit for hydrogen is exceeded, ignition and an explosion may result. Additionally a substantial upstream leak (relative to the feed flow rate of reactants) will reduce the expected flow of gas to the fuel cell and compromise the integrity of fuel cell data for stoichiometrically sensitive studies. One method for testing external leaks is to pressurize the entire system to about 1.7 bara and measure the pressure drop with time. A leak of less than 0.07 bar over 10 minutes is acceptable according to the US Fuel Cell Council (USFCC, 2006: 14). Leak testing is especially important when performing studies at elevated pressures.

Permeation of hydrogen and oxygen across the electrolyte membrane degrades the performance of the fuel cell by reducing the open circuit voltage (through generation of mixed potentials) lowering fuel efficiency. A large gas crossover is indicative of a hole in the PEM which poses a safety concern as discussed previously. Internal short circuits are essentially equivalent to fuel crossover and both phenomena can be detected by OCV measurements or linear sweep voltammetry experiments as described by Cooper et al. (2005: 66).

Following pre-testing diagnostics, cell break-in/conditioning is required to hydrate the electrolyte membrane and bring the fuel cell to a maximum stable level of performance

prior to electrochemical testing. Many different break-in protocols exist with variations in load cycles and cell conditions. Zhiani and Majidi (2013) studied the effect of three common conditioning procedures on final MEA performance. They found that constant voltage (0.6 V) and cyclic conditioning (between 0.7 and 0.5 V) were more effective than constant current (0.25 Acm^{-2}) conditioning for an MEA composed of in-house fabricated gas diffusion electrodes and a Nafion 212 membrane. Cooper and Smith (2006) found that 10 conditioning cycles between 0.7 V and 0.3 V gave stable MEA performance.

2.2.4 Polarization curve analysis

Increasing the load on a PEMFC increases irreversible losses in the system. The difference between the theoretical reversible potential and the actual voltage is called overpotential. There is a characteristic manner in which overpotential varies with current density (shown in Figure 2.7) known as a polarization curve.

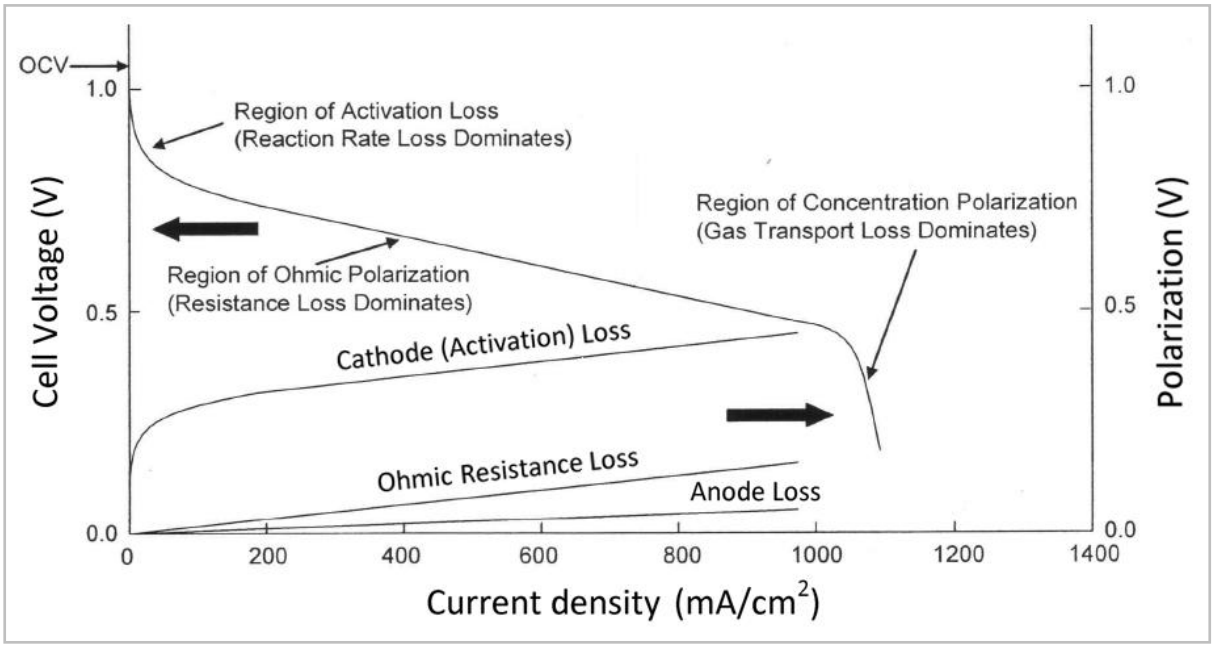

Figure 2.7: Representative polarization curve for a PEMFC operating at 25 °C, 1 atm (Adapted from Cooper et al., 2005)

The polarization curve can be separated into three distinct regions depending on the major underlying process causing the overpotential. Activation polarization is the voltage loss required to overcome the energy barrier of the electrode reactions. The hydrogen oxidation reaction at the anode is facile relative to the oxygen reduction reaction (ORR) at the cathode and therefore does not contribute significantly to activation polarization (Larminie and Dicks, 2003). At moderate current densities overpotential is dominated by resistance to

ionic current through the electrolyte and electronic current through the electrodes. A major factor affecting membrane (ionic) conductivity is the level of hydration.

The net rate of the electrochemical reaction is proportional to the current density and therefore as current density increases, the rate at which reactants are supplied to the electrode must also increase. The rate of oxidant diffusion is limited, and is a function of partial pressure and temperature. Therefore for systems where the oxygen partial pressure is low (e.g. air at ambient conditions), the rate of reaction is limited by the rate of mass transfer at high current density resulting in substantial (concentration) polarization. All of the irreversible loss mechanisms are dependent on the fuel cell characteristics (geometry, materials, MEA properties) and the operating conditions such as temperature, pressure, cell compression, relative humidity and reactant flow rate.

Measuring the polarization behaviour of a fuel cell system is an important tool for identifying the causes of inefficiencies and optimizing performance. The USFCC (2006) describes the general considerations required to develop a reliable protocol for polarization curve measurement. Reactant flows should be increased before increasing the load and when decreasing the load, drop the load first and then the gas flow. Additionally stabilization times after load changes should be sufficiently long to allow for equilibration of the test station and the fuel cell. Typically this requires between 5 and 10 minutes with changes in temperature taking the longest to re-stabilize. It is therefore important to monitor the temperature throughout the polarization curve analysis (particularly at high current density) as temperature has a large impact of PEMFC performance both directly and indirectly through the effect on relative humidity.

Another important electrochemical diagnostic tool is electrochemical impedance spectroscopy (EIS). Different processes in the fuel cell system such as diffusion and charge transfer have different associated time constants. As a result of this, the effects of these processes are revealed at different frequencies when the cell is perturbed. EIS uses this phenomenon to separate individual effects of processes by analysing the fuel cell response to wide frequency range (usually 1 Hz to 10 kHz).

2.2.5 Electrochemical impedance spectroscopy

EIS involves applying a small AC voltage or current signal to the fuel cell and measuring the amplitude and phase of the resulting response signal as a function of frequency. It is commonly used to study the oxygen reduction reaction, mass transfer limitations, ohmic resistance and electrode properties such as charge transfer resistance (Wu et al., 2008b). The separation of individual processes contributing to fuel cell overpotential under variable

load makes EIS a useful tool for optimizing fuel cell and MEA design and for identifying optimal operating conditions. EIS spectra are commonly plotted as the imaginary part against the real part of impedance over a frequency range. This is called a Nyquist plot and is shown in Figure 2.8.

The high frequency arc is associated with interfacial kinetics and the low frequency arc with mass transfer limitations. Due to the fast hydrogen reduction reaction, the impedance spectrum is mainly affected (and approximately equal to) the cathode impedance. By applying models to impedance spectra different losses such as interfacial kinetics, catalyst layer conductivity and membrane conductivity can be independently resolved e.g. Wu et al. (2008b).

In order to study cathode kinetic behaviour, impedance should be measured at low overpotential using pure hydrogen and oxygen whereby mass transfer limitations will be insignificant and only one impedance arc (kinetic loop) will show in the impedance spectrum (Yuan et al., 2007).

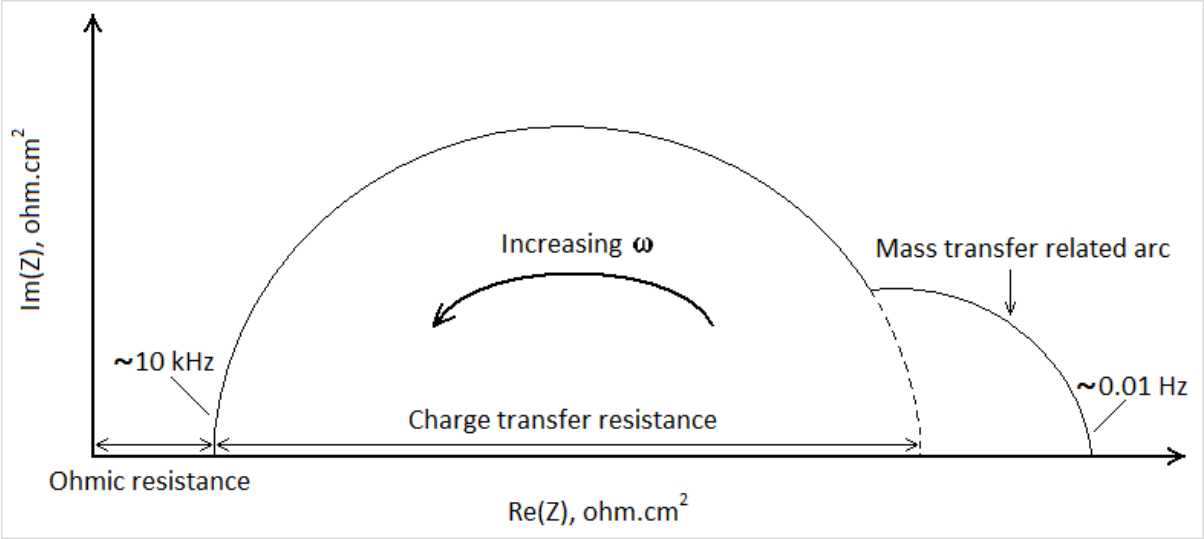

Figure 2.8: Typical high current density impedance spectrum for a PEMFC operating with H_2/air

At high frequencies, charge and mass transfer resistances are eliminated from the frequency response, leaving only the ohmic resistance of the fuel cell. As such, the intercept of the kinetic loop of the impedance spectrum with the x-axis (Im(Z) = 0) is used to determine fuel cell ohmic resistance which includes the ionic resistance of the electrolyte and the electronic resistance of circuit (including the GDL, flow field and contact resistances) but does not include electrode ohmic resistance (Cooper et al., 2005). A full impedance spectrum is not necessary to obtain the ohmic resistance, which can be determined from an impedance measurement at a single (high frequency). This is known as a high frequency resistance

(HFR) measurement and is a useful tool for diagnosing fuel cell performance during operation and in particular monitoring the change in electrolyte conductivity (e.g. during conditioning).

After electrochemical testing, the test station should be shut down safely whilst mitigating MEA damage such as excessive dry-out of the electrolyte or catalyst support degradation.

2.2.6 Test station shut down

The purpose of the shut down procedure is to cool the cell to ambient temperature without causing excessive condensation or membrane dry-out and to purge the system of any residual reactant gas. The protocol as described by the USFCC (2006) is to disengage the electrical load and cool the cell to ambient conditions ensuring that the cell temperature is about 5 ^{o}C higher than the gas line temperature which should be higher than the saturation temperature of water at the system pressure. As an additional step, the cell can be purged with dry nitrogen for about 10 minutes once the cell has reached ambient temperature to remove any residual hydrogen and liquid water.

For this study FuelCon test stations are used for single cell testing. The test station software (FuelWork) is conceived in such a way that all settings and processes can be regulated automatically by test programs. These programs are written in FuelWorkScript which is an extension of the Microsoft® Visual Basic Script (VBScript®).

2.2.7 Automated testing procedures

In addition to the standard VBScript statements, FuelWork test programs can read and write 'Tags' associates with set-point and actual process variable values. For example the following line of code can be used to set the cell temperature to 80 ^{o}C:

$$\text{Tag}(\text{“T901000\_W1”}) = 80$$

The user interface (shown in Figure 5.18) provides Tag identifiers for major system parameters.

3 Literature review

The focus of this research is to develop a methodology to reliably correlate MPL physical characteristics with PEMFC electrochemical performance to better understand the beneficial role of the MPL. In this section the literature is reviewed to illustrate the current state of MPL research to contextualise the importance of this study.

3.1 Water management

Water has both positive and negative roles in the fuel cell and therefore water management is particularly important during PEMFC operation. Water originates from both humidified reactant gases and internal generation via the oxygen reduction reaction. Ionic conductivity of the polymer electrolyte membrane is strongly dependant on the level of water saturation (Zawodzinski et al., 1993; Li et al., 2008;) and as such a highly saturated/humidified membrane is desirable to facilitate proton movement for the electrochemical reaction. However if liquid water accumulates in the gas diffusion layer (GDL), mass transfer of reactants to the catalyst layer is inhibited resulting in a loss of performance at high current density operation (Benziger et al., 2005; Li et al., 2008). This is known as GDL flooding and is particularly evident on the cathode side of the MEA due to localized water generation (Cindrella et al., 2009). Reactant starvation due to water accumulation can also result in degradation of the anode side catalyst carbon support by oxidation (Yang et al., 2012; Kang et al., 2010; Yousfi-Steiner et al., 2009).

The movement of water within the MEA is governed by a variety of factors as illustrated in Figure 3.1 obtained from Larminie and Dicks (2003: 77). Net water movement across the PEM is governed by the relative rates of electro-osmotic drag from the anode to the cathode and back-diffusion of water from the cathode to the anode side of the MEA (Lee and Bae, 2009). These processes have been found to be affected by membrane thickness, cell temperature, current density and gas relative humidity and stoichiometry (Colinart et al., 2009; Janssen and Overvelde, 2001;). Janssen and Overvelde (2001) found that the effective water drag is not a function of current density at fixed feed gas stoichiometry. This is not a general result and only applies up to moderate current densities (≈ 1 A/cm^2) as tested in their study. For higher current densities the fast rate of proton transfer/flux increases the electro-osmotic drag resulting in dry-out of the membrane at the anode side and an increase in ohmic resistance (Cooper et al., 2005: 41). For this reason it is found that hydrogen humidification has a larger impact on PEMFC performance than oxidant humidification (Hyun and Kim, 2004).

Hydrophobic treatment of the GDL and the use of a microporous layer (MPL) between the gas diffusion layer and catalyst layer (Gostick et al., 2009) have both been used to improve water management in the MEA. Research has shown that loading the GDL with a hydrophobic agent such as polytetrafluoroethylene (PTFE) results in improved performance particularly at high relative humidity operation (Park et al., 2008). This is attributed to improved water removal thereby reducing the saturation level of the GDL which results in improved mass transfer of reactant gas (Park et al., 2012). The incorporation of an MPL (typically a thin layer of carbon black powder and hydrophobic agent PTFE) has also been shown to assist with water management and improve cell performance at high current densities (Qi and Kaufman, 2002; Weber and Newman, 2005). However the particular functions of the MPL and the key design parameters affecting its performance are under debate and not well understood (Gostick et al., 2009).

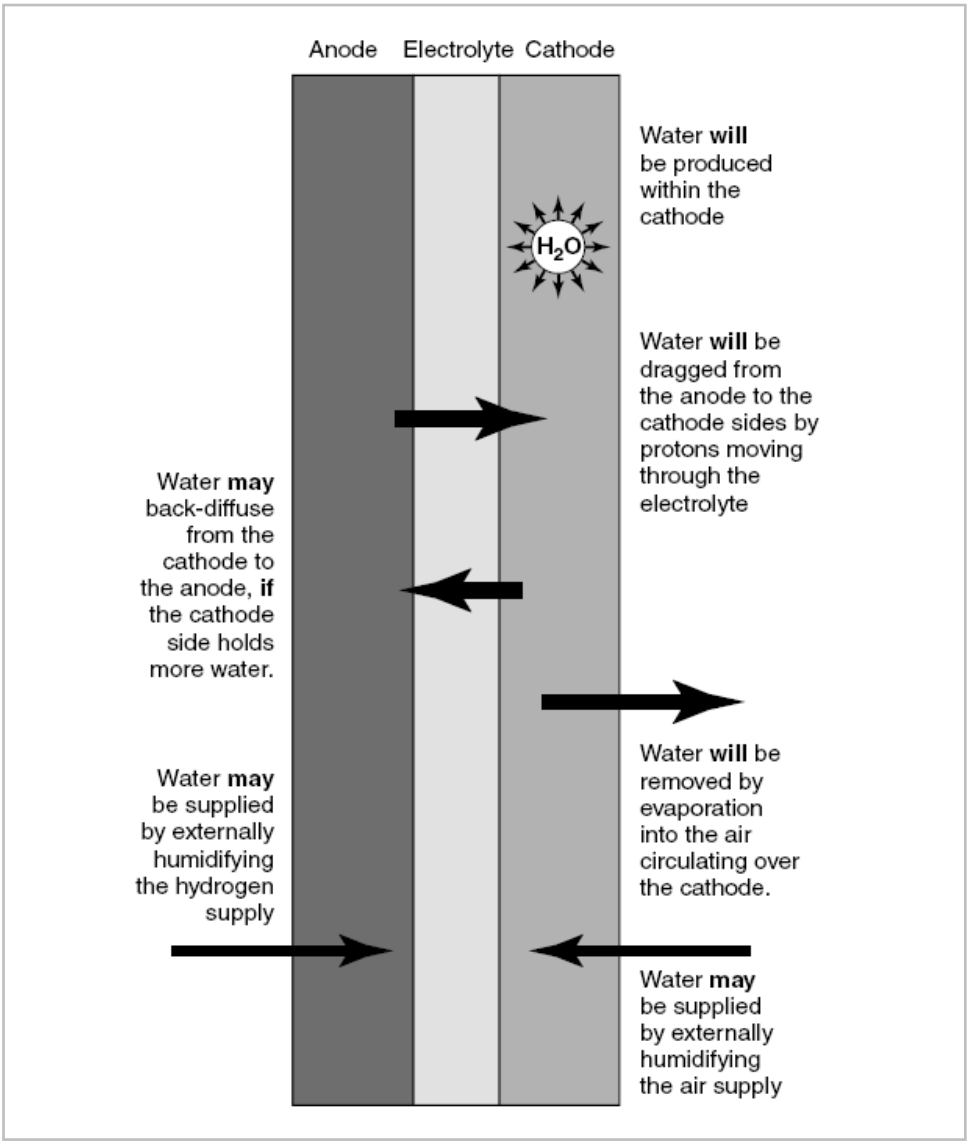

Figure 3.1: Various water movements of water within the MEA (Larminie and Dicks, 2003)

3.2 The microporous layer

In an attempt to determine the function of the MPL, Nam et al. (2009) used environmental scanning electron microscopy to observe the vapour condensation and liquid water breakthrough in the catalyst, microporous and gas diffusion layers of the MEA. It was found that the coarse pore structure of the gas diffusion layer allows for growth of large water droplets but the microporous layer limits droplet growth due to a finer pore structure. Based on the interfacial water droplet morphologies, a physical model was developed for the movement of liquid water across multiple porous layers. The simulation predicts that the MPL reduces the size of interfacial water droplets formed at the CL interface and reduces the number of liquid water breakthroughs (and therefore the saturation level) in GDL. This is illustrated in Figure 3.2 shown below (obtained from Nam et al., 2009).

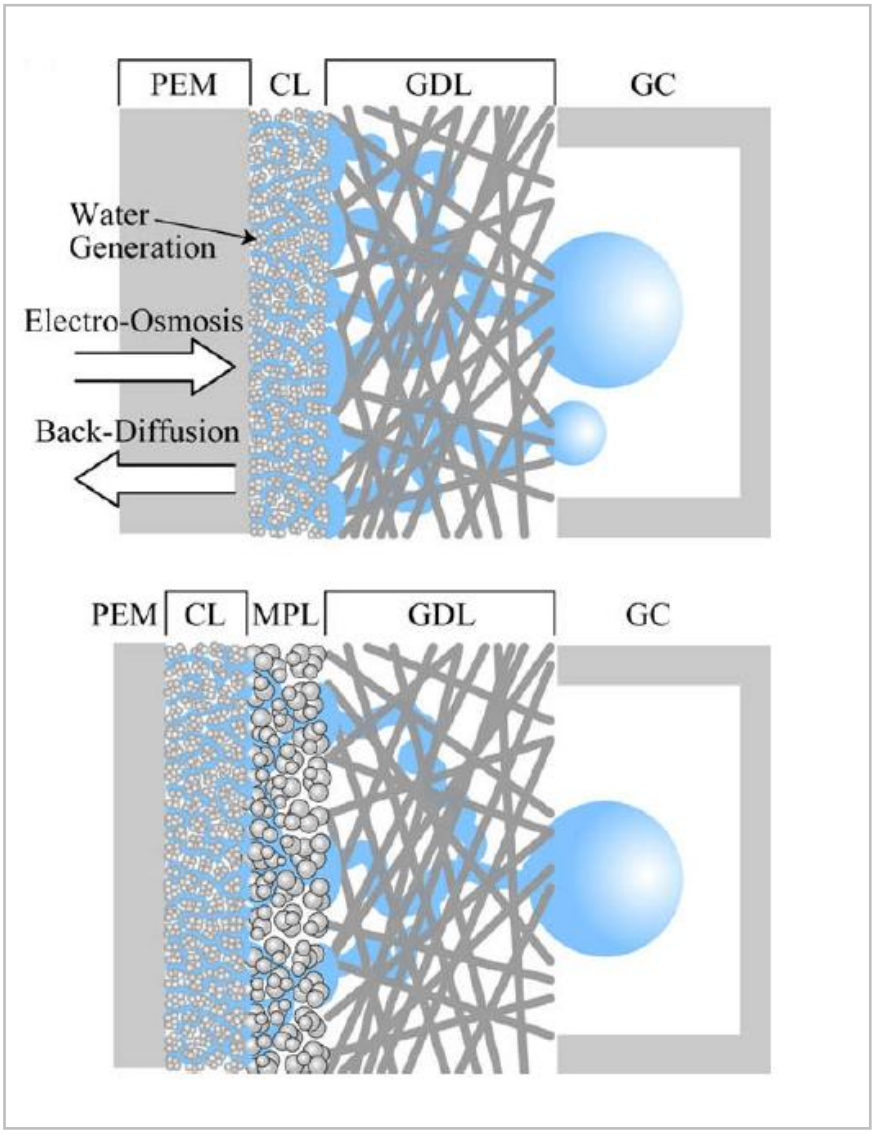

Figure 3.2: Movement of liquid water through the cathode with and without an MPL (Nam et al., 2009)

Related to the work by Nam et al., Gostick et al. (2009) studied liquid water breakthrough at the cathode by measuring water saturation and capillary pressure for GDLs with and without a MPL. They found that the GDL saturation at the point of water breakthrough was reduced from ≈27 % to less than 3 % as a result of the MPL restricting the number of water entry points into the GDL.

More recently Lee et al. (2013) used synchrotron X-ray radiography to observe the through-plane liquid water distributions in an operating PEMFC with and without microporous layer. Conversely to the previous studies, they found that the MPL increases the number of breakthrough locations and suggest that this reduces the saturation level in the GDL and water agglomeration at the catalyst layer/MPL interface (illustrated in Figure 3.3) resulting in improved performance.

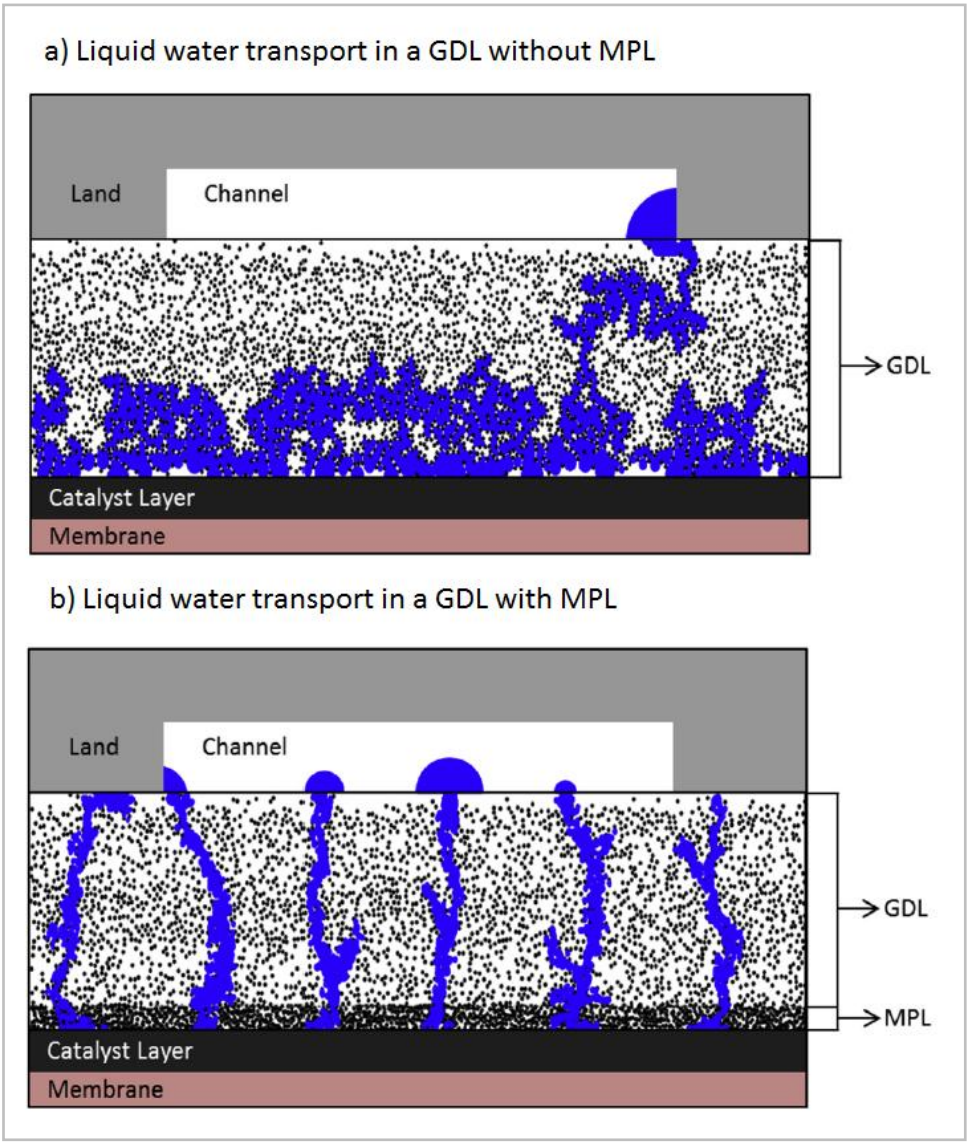

Figure 3.3: Comparison of liquid water transport in a GDL with and without MPL (Lee et al., 2013)

Deevanhxay et al. (2013) used soft X-ray radiography to visualize liquid water accumulation in the MEA with and without MPL during operation. They found that the liquid water accumulates in the GDL under the flow field land/rib both with and without MPL. As illustrated in Figure 3.4, the MPL was shown to act as a buffer between the catalyst later and the accumulated liquid water in the GDL. Based on this result and polarization curve analysis, they conclude that the MPL improves performance by causing a reduction in water accumulation at the catalyst layer/diffusion medium interface.

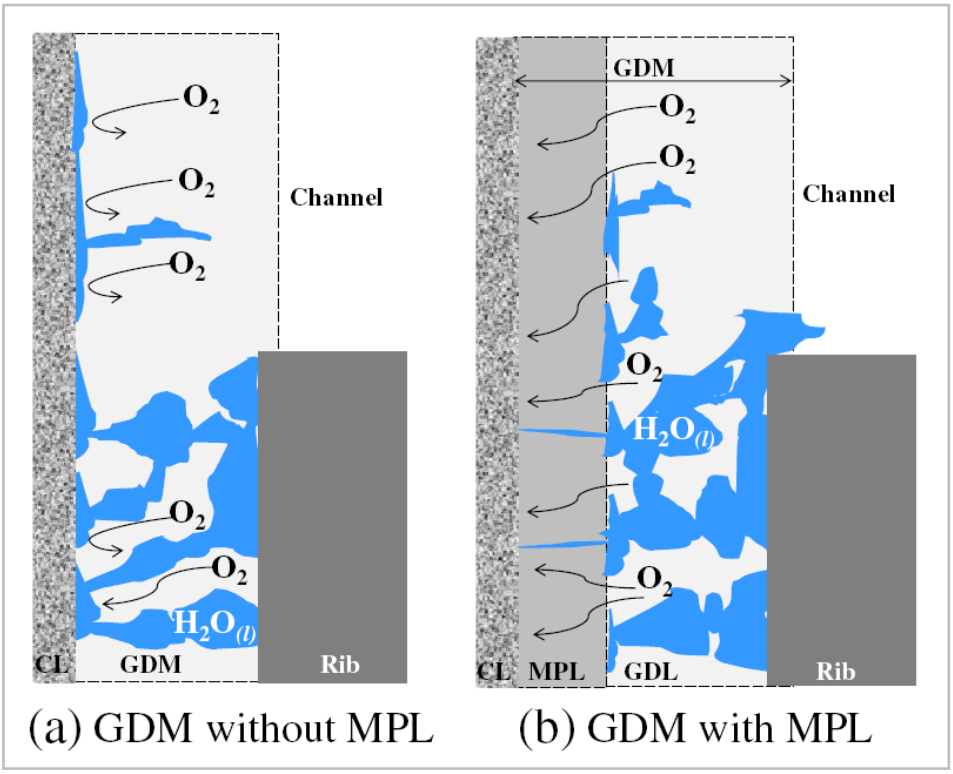

Figure 3.4: Proposed schematic of liquid water accumulation in the cathode GDM (Deevanhxay et al., 2013)

Apart from the fact that the polarization curves measured by Deevanhxay and co-workers are uncharacteristic of hydrogen and oxygen at high relative humidity and stoichiometry (performance is poor and showing signs of high overpotential at relatively low current density cf. Figure 6.21 from this study), one would expect the MPL to increase diffusion resistance. Therefore under similar conditions of water saturation in the GDL, the MEA without MPL should benefit from improved mass transport of oxidant to the catalyst layer. Lee et al., (2013) found that an MEA without MPL performed better than one with MPLs during galvanostatic operation at 0.6 A/cm^2 when using high hydrogen and oxidant stoichiometric ratios. Tseng and Lo (2010) observed that under light and intermediate load conditions, fuel cells with and without MPL show similar performances. Deevanhxay and co-workers show that the MEA with and without MPL have similar (low) levels of water accumulation at 68 ^{o}C at about 0.6 A/cm^2 but the MEA with MPL shows much better

performance at this condition. This suggests that reduced water accumulation is not the only MPL induced factor causing performance improvement.

Wargo et al. (2013a) used a combination of focused ion beam scanning electron microscopy and X-ray computed tomography to analyze the detailed microstructure of the MPL and GDL to determine the contribution of each layer to the transport characteristics of the diffusion medium (DM). They found that the addition of the microporous layer increases DM tortuosity and inhibits diffusion but were unable to elucidate the effect of the MPL on improving water management. Based on the water visualisation of the DM they conclude that an MPL with structural irregularities such as cracks and holes will be more effective in removal of liquid water from the catalyst layer.

Models developed by Weber and Newman (2005) and Pasaogullari et al. (2005) hypothesize that the MPL increases the back diffusion rate of water from the cathode to the anode. Though this assertion is commonly discussed in literature it has not been shown experimentally, with results being either inconclusive or contradictory (Gostick et al., 2009). Atiyeh et al. (2007) investigated the effect of the MPL on water migration through the membrane in the form of the net water drag coefficient (moles of water dragged through membrane from anode to cathode per mole of protons). They used an experimental system whereby the spent gas from the fuel cell was passed through a condenser allowing for all water leaving the system to be collected. The relative humidity of the feed gas was controlled and therefore by measuring the current density (and therefore generated reaction water) a water balance could be performed. Considering the cathode side only, the difference between the sum of the water generated and the water entering with the humidified air and the water leaving (at steady state) will give an indication of the water migrating through the membrane. Therefore, crucial to this investigation is the condition of steady state (i.e. no accumulation of water in the system with time). It is conceivable that the water will gradually accumulate at the interface between the GDL and flow field and, upon reaching sufficiently large size (a slug), be rapidly forced out of the flow field (as liquid water) by the flow of reactant gas. Depending on the rate of this process and the contribution of liquid water to the overall water balance, the steady state assumption may not be valid. Steady state could have been validated by measuring the total amount of water leaving the cell and showing that this was equal to the sum of the amount entering the cell and the water produced by the ORR. Apart from the uncertainty in the condition of steady state, temperature variations contributed significantly to experimental uncertainty in vapour pressure (and therefore relative humidity). Atiyeh et al. found that as a result of measurement uncertainty and inherent performance variability the effect of the MPL on the

movement of water through the membrane was statistically insignificant. That is not to say that there is no effect, just that any effect was masked by the experimental error. The importance of this was not emphasized by Atiyeh et al. and as a result some authors have misinterpreted the result claiming that it was found that the MPL does not affect water drag (e.g. Cindrella et al., 2009, Nishiyama et al., 2011 and Thomas et al., 2014).

Nishiyama et al. (2011) estimated capillary pressures of the MPL and GDL using a pore size distribution model. They concluded that due to the high capillary pressure of the MPL the net water drag from anode to cathode is reduced. The net drag calculated from the PSD model (with consideration of capillary pressure) was compared with measured values using a water balance technique described by Murahashi et al. (2006). Similar to the study by Atiyeh et al. (2007) there was large experimental error associated with the data, making inferences drawn from the model less reliable. Therefore the effect of the MPL on water transport through the membrane is unclear (Gostick et al., 2009).

Thomas et al. (2014) inserted insulated platinum wires (cf. Figure 3.5) to measure local interfacial temperature between the diffusion media and the CCM during MEA assembly for GDLs with and without MPLs to investigate the effect of the MPL on heat transfer. They conclude based on temperature measurements and polarization curve analysis that the presence of the MPL provides a thermal resistance which increases the electrode temperature locally, improving vapour phase water removal. However it is not clear whether the addition of the platinum wires (which are about 7 times thicker than GDL fibres) affects the integrity of the MEA and therefore produces results which are not applicable to an unmodified MEA. Particularly the contact of the GDL with and/or without the MPL with the wires may alter the interfacial contact resistance or cause non-uniform contact between layers. An indicator of whether the modification has a significant effect is to perform high frequency (ohmic) impedance measurements and compare against an unmodified MEA which was not done in their study. The MEAs used by Thomas and co-workers are very similar to those used in this study but the polarization curves for GDL without MPL show erratic behaviour at high current densities (at high RH operation) which is not seen with the MPL coated GDL and is not typically observed at these conditions (cf. Figure 6.27 and Figure 6.28; Kitahara et al., 2010). Another interesting result from the polarization curves of Thomas et al. is that the performance of the MEA with MPL at $T_c = 62.5\ ^oC > T_a = 57.5\ ^oC$ is identical to that of the conditions of $T_a = 62.5\ ^oC > T_c = 57.5\ ^oC$ both of which perform better then at $T_a = T_c = 60\ ^oC$ in the 0.2 to 0.8 A/cm^2 range suggesting a non-linear effect of temperature profile on MPL efficacy.

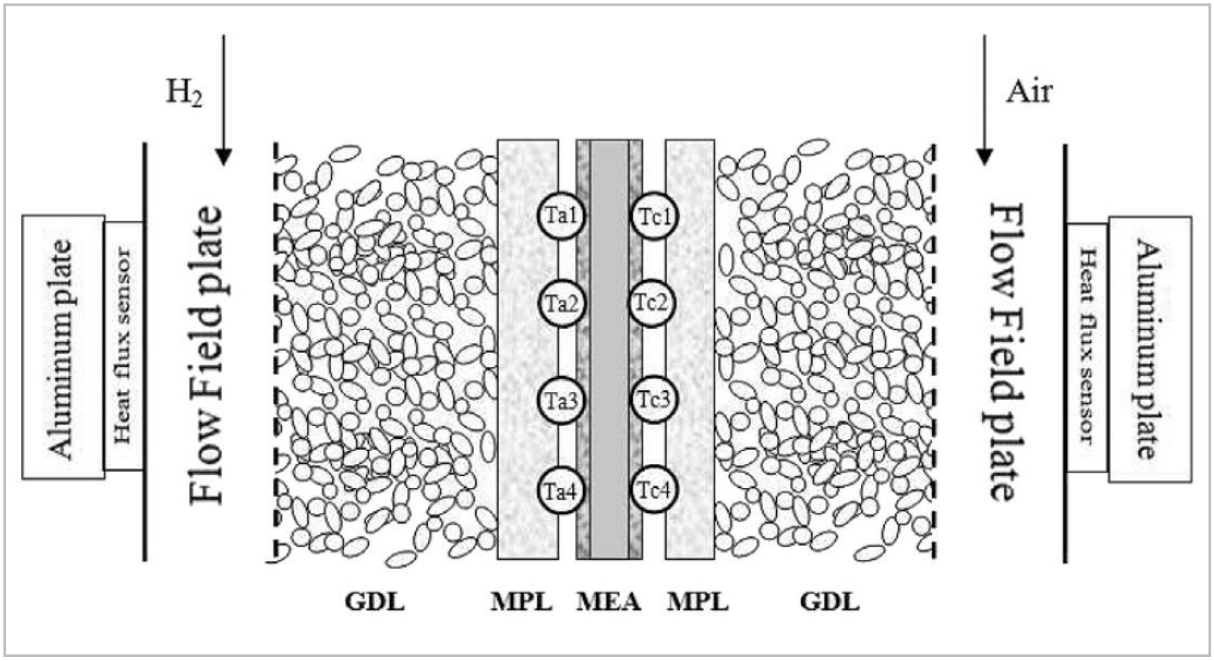

Figure 3.5: Placement of wires for interfacial temperature measurements (Thomas et al., 2014)

Optimization of the MPL for improved efficacy has been studied by a number of researchers. Particularly the pore structure, thickness and water wetting characteristics have been investigated. It has been reported that the properties of the anode MPL have an insignificant effect on PEMFC performance relative to the cathode side MPL (Tanuma and Kinoshita; Ahn et al 2011; Ramasamy et al 2008). As such, MPL studies primarily focus on the cathode side of the PEMFC. Therefore unless otherwise stated, the cathode MPL will be referred to as simply the MPL in the following discussion.

There is a dynamic relationship between the thickness, pore structure and water wetting properties of the MPL. Tseng and Lo (2010) found that reducing the thickness of the MPL also reduced the average pore size. Papers by Park et al. (2008) and Park and Popov (2009) both showed the dynamic relationship between PTFE content in the MPL and GDL and average pore diameter. Park et al. found that increasing the PTFE content reduces average pore diameter and porosity of the microporous layer.

As any one of the physical properties of the microporous layer can significantly affect PEMFC performance, the relationship between them should be kept in mind. When investigating or comparing the effect of a change of a single MPL property the other properties must be carefully controlled and/or characterized in order to correctly interpret and explain the performance results. However, due to the dynamic relationship between the MPL properties careful control is challenging possibly leading to ambiguous performance results.

3.2.1 Microporous layer thickness

Due to the small pore size in the MPL, Knudsen diffusion is an important porous diffusion mechanism during low pressure PEMFC operation (Pant et al., 2012; Chan et al., 2012). Therefore it may be concluded that it is desirable to have an extremely thin MPL to reduce the path length for diffusion to improve mass transfer of reactants to the catalyst layer. However there are a number of other factors associated with MPL thickness which affect mass transfer efficacy. Many research groups have found there to be an optimal MPL thickness, however the value for this thickness and the reasons for justifying optimal effectiveness vary.

Pasaogullari and Wang (2008) argue that as the MPL thickness is increased the overall liquid permeability is reduced resulting in an increase in liquid pressure across the MPL and higher GDL saturation. Their model for two phase transport across multi-layer diffusion media predicts that for the MPL to be efficacious it must be thinner than 50 µm. They propose that the thinner the MPL the better the water removal from the catalyst layer. Other researchers have found there to be an optimal MPL thickness (Hiramitsu et al., 2010; Tseng and Lo, 2010; Kitahara et al., 2010; Qi and Kaufman 2002; Paganin et al., 1996).

Paganin et al. (1996) varied MPL thickness (Vulcan XC-72 10 wt % PTFE) and showed that fuel cell performance reaches a maximum for an MPL thickness of 50 µm. They suggest that a very thin MPL does not provide a smooth enough surface to reduce contact resistances and that a thicker MPL causes mass transfer limitations due to the lengthened diffusion distance. Kitahara et al. (2010) measured MEA performance at high and low humidity operation for changing MPL thickness with a fixed total thickness of the porous diffusion medium (GDL + MPL) of 250 µm. Both mean flow pore diameter in the MPL and PTFE content were fixed at 3 µm and 20 wt % respectively. Under high humidity operation the thinnest MPL (90 µm) gave the best performance at high current density operation. They conclude that decreasing the MPL thickness (penetrated into the GDL substrate) enhances in-plane permeability which promotes the discharge of water from the GDL. This is contrary to the simulations of Nam et al. (2009) and observations by Gostick et al. (2009) who suggest that low in plane permeability of water is desirable to decrease the GDL saturation at liquid breakthrough.

Tseng and Lo (2010) investigated the effects of physical characteristics of the GDL and MPL on fuel cell performance under high humidity operation. It was found that an MPL of thickness 84 µm gave better MEA performance than thinner (38 µm) and thicker (136 µm) MPLs. They conclude that an extremely thin MPL inhibits mass transfer due to reduced pore

size whereas a thick MPL increases electronic resistance due increased amount of (non conductive) PTFE. It is unclear why pore structure should change significantly with MPL thickness and furthermore whether the results by Tseng and Lo (2010) discussed above should be attributed to MPL thickness or pore structure or a combination of both. The same argument can be applied to any research into thickness optimization which does not carefully characterize consider the effect of changing pore size distribution.

It is clear that there exists an optimal MPL thickness however the function of the MPL is not well established and therefore the reasons as to why an extremely thin MPL hinders efficacy are not conclusive.

3.2.2 Microporous layer pore structure

Knudsen diffusivity, the thermodynamics of phase change and capillary flow are all functions of pore size and geometry**.** As such, the porous structures of both the GDL and MPL are among the most important factors influencing the flow of liquid water and reactant gas in the MEA (Pasaogullari and Wang, 2004).

Kong et al. (2002) used Li_2CO_3 as a pore forming agent in an attempt to vary MPL pore structure. PEMFC performance was compared for MPLs with pore former loadings of 0, 3, 5, 7 and 10 mg cm^{-2}. It was found that a loading of 7 mg cm^{-2} gave the best performance. They argue that relatively large pores (macro-pores) provide effective pathways for diffusion of reactant gas, however if the macro-pore volume is too large the electric conductivity of the electrode is reduced. Therefore there exists an optimal ratio of macro-pore to micro-pore volume. Tang et al. (2007a) used NH_4Cl as a pore former in the MPL slurry to increase both the average pore size and porosity of the MPL. Based on performance results, they conclude that large pores facilitate transport of liquid water whereas smaller pores are required for gas diffusion. Chun et al. (2010) also used an ammonium salt as a pore forming agent (along with heat treatment) to control MPL structure. They found that using the pore forming agent contributed to the formation of more pores in the MPL and that drying the MPL at high temperature (150 °C) increased the volume of macro pores and decreased the volume of micro pores. The MPL dried at low temperature (80 °C) gave best PEMFC performance under high relative humidity operation. Based on this result it was concluded that micro-pores (<100 nm) are more efficient at water removal than meso-pores (0.1-5 µm) and macro-pores (>5 µm).

More recently, Chun et al. (2013) fabricated a porosity-graded MPL using thermal expandable graphite (TEG). Unlike conventional pore formers TEG does not decompose during pore formation. Instead it expands by a factor of two when heated, resulting in the

formation of pores in the MPL. The gradient direction in porosity was from the catalyst layer/MPL interface (smallest pores from 10 wt % TEG) to the MPL/GDL interface (20 wt % TEG). The porosity gradient MPL performed better than uniform porosity MPLs (of 0, 10 and 20 wt % TEG) at high current density indicating improved water removal ability. This is in agreement with simulations by Zhan et al. (2007) who predict that the larger the porosity gradient in the GDL the better the gas diffusion.

Kitahara et al. (2010) showed that the mean pore diameter in the porous diffusion medium (PDM) has a significant effect on PEMFC performance. A change in the mean pore diameter of the PDM from 1 to 3 μm resulted in about a 50 % increase in fuel cell power density at 0.6 V operation. They propose that the MPL reduces saturation of the catalyst layer and that pore diameter should be small enough to prevent back transport of water from the substrate to the electrode but not too small such that gas permeability and therefore water vapour transport from the catalyst layer are significantly reduced.

Chen et al. (2008) showed that MPLs fabricated by dry layer preparation performed better than wet layer prepared MPLs. In their study, meso-pores are defined as pores being in the size range of 0.5-15 μm and micro-pores and macro-pores are those pores which are smaller and larger than meso-pores respectively. The improved performance of dry layer prepared MPLs is attributed to a higher proportion of hydrophobic meso-pores which have a high capillary pressure and therefore remain free of liquid water thus improving gas phase mass transport. Tseng and Lo (2010) found that MPL coated GDLs with an increased pore size (larger fraction of pores in the 4 to 18 μm due to increased baking time) performed better than those with smaller pores which they attributed to higher gas permeability.

3.2.3 Microporous layer water wetting characteristics

It is well established that adding hydrophobic PTFE to the GDL improves PEMFC performance at high current density under operation with humidified feed gas (Chang et al., 2011; Ramasamy et al., 2008). As one would expect, the addition of PTFE is also applied to the microporous layer and again results in improved performance.

Park et al. (2008) investigated the effect of PTFE content in the MPL on PEMFC performance at high relative humidity operation. They found that increasing the amount of PTFE resulted in an increased resistance to water flow in the GDL (due to reduced pore size and increased hydrophobicity in the MPL). A PTFE content of 20 wt % gave the best fuel cell performance by which was inexplicably attributed to a reduction in the saturation of the catalyst layer and GDL.

Chen et al. (2008) found that a PTFE content of 30 wt % in a dry layer prepared cathode MPL gave best PEMFC performance at high relative humidity operation. This was attributed to a combination of water wetting characteristics and pore structure with hydrophobic meso-pores improving gas transport. Tseng and Lo (2010) found that the PTFE content in the MPL affected the pore structure and that 40 wt % PTFE resulted in the best PEMFC performance under high relative humidity operation. However the performance results for the different PTFE content MPLs were very similar, and therefore due to possible MEA variance the result is not convincing.

According to Latorrata et al. (2014) PTFE is not the only polymer capable of effectively imparting hydrophobic properties on the gas diffusion media. They added three different fluorinated polymers (perfluoroalcoxy, fluorinated ethylene propylene (FEP) and fluorinated polyurethane) to the GDL and in-house fabricated MPLs and compared the resulting MEA electrochemical performances at low and high cathode relative humidity. It was found that the MEA containing FEP experienced reduced mass transfer limitations and improved performance relative to the other MEAs at both high and low relative humidity. This was attributed to the superhydrophobic properties of the FEP gas diffusion media. It should be noted that the performance results were not substantially different (especially at high relative humidity) and due to the lack of polymer content optimisation and quantification of MEA variance, conclusive statements on the efficacy of the different polymers cannot be made with certainty.

Common to the majority of the above analyses is the use of externally humidified reactant gas. It is commonly believed that extra humidification of reactant gases is essential for a PEMFC operating above 60°C (Larminie and Dicks, 2003). However there are a number of benefits associated with not using additional humidification as will be discussed in the following section.

3.3 Low humidity PEMFC operation

Leakage or impurities would compromise the effectiveness of external humidification, which could significantly reduce fuel cell performance. Therefore a PEMFC system without external humidification could potentially be more reliable. Additionally, operating a fuel cell system without an external humidification system is less costly and simpler to implement.

Reducing the amount of water entering the fuel cell lowers the risk of flooding at high current density operation reducing mass transfer limitations. Chen et al. (2008) found that a wet layer prepared MPL (30 wt % PTFE) produced a larger PEMFC limiting current at low cathode relative humidity than at high relative humidity. Flooding at the anode side of the

PEMFC can also cause carbon support degradation due to reactant starvation (Yang et al., 2012). Therefore by reducing the degree of water accumulation in the MEA both improved performance and durability are possible.

As highlighted by Larminie and Dicks (2003), apart from externally humidifying the reactant gas entering the fuel cell, the humidity can be increased by lowering the operating temperature (which would increase ohmic and activation losses), lowering the air flow rate (which would reduce cathode performance) or increasing the operating pressure (which would require a compressor) yet all of these methods have negative consequences. Alternatively, it has more recently been shown that the use of a microporous layer in the MEA significantly improves fuel cell performance when operated under dry conditions (Chen and Chang 2013; Tanuma and Kinoshita, 2012; Kitahara et al., 2012; Ahn et al., 2011). Therefore, instead of high reactant gas humidity operation, internal water management via the MPL may prove a preferable method of achieving adequate membrane saturation.

Ramasamy et al. (2008) conducted a detailed investigation of macro and micro-porous layer interaction in PEMFC under wet and dry conditions. It was observed that PTFE content in the macro-porous GDL has a much lower effect on PEMFC performance under dry condition operation. This suggests that the optimal water wetting characteristics of an MPL for use under wet conditions may be different from that of dry condition operation.

Ahn et al. (2011) compared the performance of an optimized cathode hydrophilic MPL with a commercial MPL (20 wt % PTFE) under both wet and dry conditions. The hydrophilic MPLs (10 wt % nafion) performed better than the commercial MPLs under both conditions with the most significant improvement in performance occurring at high current density under dry conditions. This result was attributed to more efficient water removal from the catalyst layer by the hydrophilic MPL improving reactant mass transfer to the catalyst surface. Similarly, Tanuma and Kinoshita (2012) also found that a hydrophilic MPL performed better than a commercial hydrophobic MPL (10 wt % PTFE Freudenberg-NOK) under both wet and dry conditions using pure oxygen as an oxidant. Tanuma and Kinoshita (2012) showed that the compared MPLs had a significantly different pore size distribution highlighting the fact that neither research group attempted to control pore structure. Therefore the performance results of these studies can not necessarily be solely attributed to the effect of hydrophilicity in the MPL. Additionally testing with pure oxygen mitigates mass transfer limitations at high current density and therefore the effect of the MPL to improve water management in the GDL is not investigated under these conditions.

More recently Chen and Chang (2013) found that MPL composition and PTFE loading both affect performance at low air inlet relative humidity operation. For a fixed (acetylene black) carbon loading of 1.5 mg cm^{-2} in the cathode MPL, a PTFE loading of 30 wt% gave the highest peak power density at low (<40 %) air RH operation. Additionally, the effect of changing the MPL composition was investigated and it was found that a 30 wt % Black Pearls 2000 (with acetylene black) with a total carbon loading of 1.0 mg cm^{-2} and a PTFE loading of 30 wt% gave best performance at low air RH. The optimal composition and PTFE loading for low RH operation were different to those at high RH loading and therefore it was concluded that optimal MPL properties depend on the inlet air RH during operation.

There has also been work on the effect of dual layer MPLs of different hydrophilic/hydrophobic properties on PEMFC performance. Kitahara et al. (2012) compared the effect of dual layer hydrophobic (substrate side)/hydrophilic (catalyst layer side) MPL with single layer hydrophobic and hydrophilic MPLs. They found the dual layer MPL gave the best PEMFC performance under relatively dry conditions (cathode RH=0, anode RH=60 %) which was attributed to the hydrophobic MPL preventing dry out of the water retained by the hydrophilic MPL therefore conserving humidity in the catalyst layer. Chun et al. (2011) found that a dual layer hydrophilic (substrate side)/hydrophobic (catalyst layer side) gave better PEMFC performance than a single hydrophobic MPL and a dual layer hydrophobic/hydrophilic MPL (as was investigated by Kitahara et al. (2012)) under low relative humidity (50 % anode and cathode) operation. It was suggested that the internal hydrophilic MPL retains water and humidifies the air diffusing to the catalyst layer and in so doing prevents membrane dry out.

3.4 MPL characterization using X-ray computed tomography

In recent years the improvement in X-ray Computed Tomography (XCT) equipment has allowed for the analysis of the MEA structural characteristics at low-micron to sub-micron resolutions. Of particular interest to this study is the use of µCT for the detailed analysis of the physical characteristics of the gas diffusion medium.

James et al. (2012), Gao et al. (2013), Ostadi et al. (2011) all used X-ray tomography to analyse the three dimensional structure of the GDL to predict fluid transport characteristics.

Pfrang et al. (2013) used µCT to identify the MPL and segment it from the GDL. The difficulty with isolating the MPL is that it is of similar composition to the GDL (predominately carbon) and therefore has similar ‘grey values’. Therefore simple grey-level thresholding as is normally used for segmentation (cf. Figure 2.5) is unsuitable. As illustrated by Figure 3.6, Pfrang and co-workers found that by using a sophisticated method of diffusion filtering and

grey-level thresholding the GDL, MPL, PTFE and air could be effectively segmented for isolated analysis.

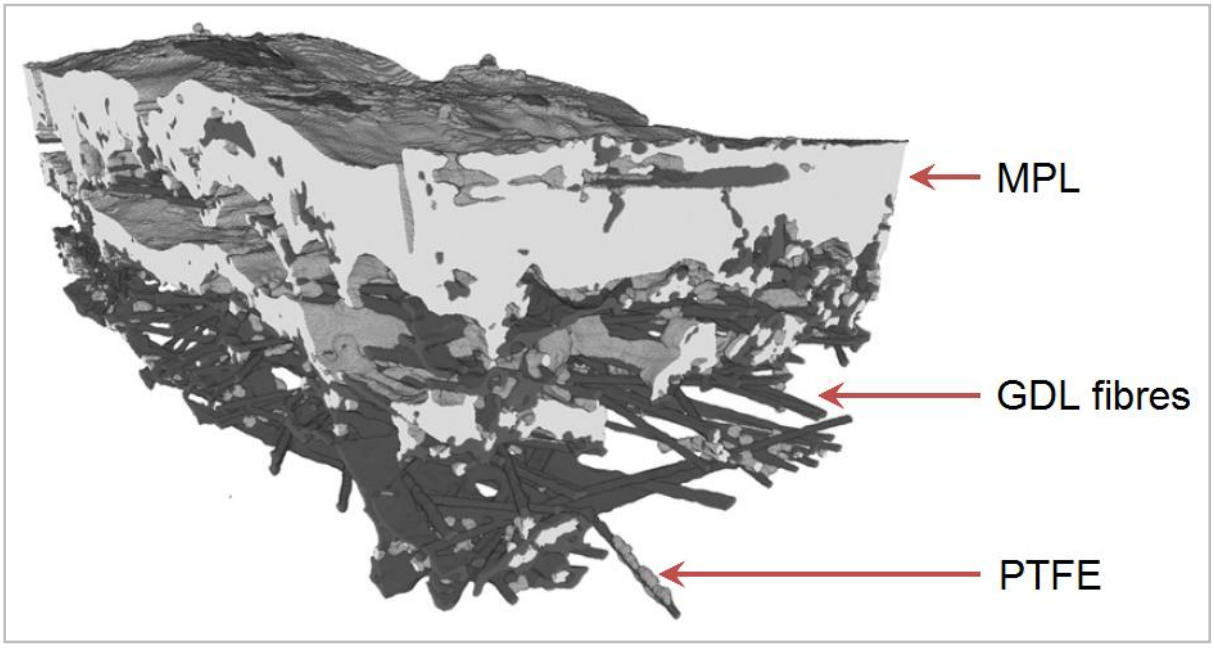

Figure 3.6: 3D reconstruction of the GDL/MPL from Pfrang et al. (2013)

Wargo et al. (2013b) used nano-scale XCT and focused ion beam nanotomography to capture and analyse the 3D microstructure of the MPL including porosity, pore connectivity, tortuosity, structural diffusivity coefficient, and chord length and compared the results against other experimental data. They found that the porosity result from nano-XCT was a very good match to the experimentally measured value and that in general the nano-XCT technique gave data which better reflects the microstructure and structure-related transport properties of the tested MPL sample.

4 Objectives of this study

In summary, it has been demonstrated that the incorporation of a microporous layer improves PEMFC performance at both high relative humidity (at high load) and low relative humidity operation. Due to the many factors influencing PEMFC performance, it is likely the MPL serves a number of roles in reducing polarization losses. However few of these roles have been thoroughly elucidated and as a result, optimal MPL physical characteristics are not based on theory. Due to this lack of theoretical basis, the explanations of optimal properties found experimentally are varied and sometimes contradictory.

It is evident that there is a strong relationship between pore size distribution, thickness and ionomer content in the MPL and therefore investigating each property individually is challenging. Particularly, pore structure is a key parameter and should be carefully controlled when investigating the effect of thickness and water wetting properties on PEMFC performance. Additionally it is a challenge to isolate the specific effect of the MPL from the effect of the GDL on water management.

Conventional porous diffusion media characterization methods (SEM and MIP) are destructive and have limitations which may impact on the accuracy of the measurements. X-ray computed tomography is a relatively new technique which has the potential to overcome these limitations.

The two key questions arising from the literature are; how can the specific effect of the MPL be reliably correlated to PEMFC performance and what is the individual effect of each structural property of the MPL on PEMFC performance? The primary objective of this study is to develop a methodology for the fabrication, characterization and correlation of physical properties of the MPL with PEMFC single cell performance.

Before investigating the effect of varying MPL properties on MEA performance, the variation in the fixed MEA components must be quantified to allow for statistically significant results. The doctor blade method will be used to deposit MPL inks of different composition onto GDL substrate and the physical properties of the MPL and GDL measured using mercury intrusion porosimetry, scanning electron microscopy and X-ray microscale computed tomography. The correlation of these physical properties to MEA electrochemical performance will then be addressed in detail.

The methodology developed in this study can be used to investigate the individual effects of MPL properties on PEMFC performance which will provide the basis for a better theoretical understanding of the role(s) of the MPL at both high and low relative humidity operation.

5 Experimental

The following section provides a detailed description of the experimental method used for this research. This includes evaluation and validation of test station accuracy, details of electrochemical testing of MEAs, fabrication of the MPL and characterization of the porous diffusion media.

Equipment and materials used in this study were either commercially available or accessible at either the University of Cape Town, University of the Western Cape or Stellenbosch University.

5.1 Gas diffusion layer characterization

Prior to MPL fabrication, GDLs from a number of commercial suppliers were characterized to quantify the variation in areal weight, porosity and pore size distribution. Areal weight variations will be a function of sample size, with smaller samples showing larger variation. Therefore samples of the size used for this study were weighed to estimate the variation in mass. Five 25 cm^2 samples of Sigracet® 25BA, Sigracet 25BC and Freudenberg® H2315 I6 were measured using a high precision analytical balance (Mettler Toledo XS104 repeatability=0.04 mg) to quantify the variation in areal weight. A further five samples of each type of GDL were then analysed using mercury intrusion porosimetry (Autopore IV 9520 Automatic Mercury Porosimeter) to determine variations in porosity and pore size distributions.

5.2 Microporous layer fabrication and characterization

MPLs were fabricated using the doctor blade method. A viscous ink slurry containing deionised water (resistivity above 5 MΩ.cm @ 25 ^{o}C), Triton X-100, carbon black (Vulcan® XC72R) and 60 wt% PTFE solution (DuPont™ Teflon® PTFE TE-3859) were coated onto a 25 x 9 cm SGL 25BA GDL at a blade height of 100 µm and speed of 7.5 mm/s. The coated area extended the length of the GDL and had a width of about 7 cm. Figure 5.1 shows the doctor blade setup and a freshly coated GDL.

After coating, the GDL was dried at 100 ^{o}C for one hour to remove water and then baked and sintered at 350 ^{o}C for an additional hour to remove Triton X-100 and disperse the PTFE.

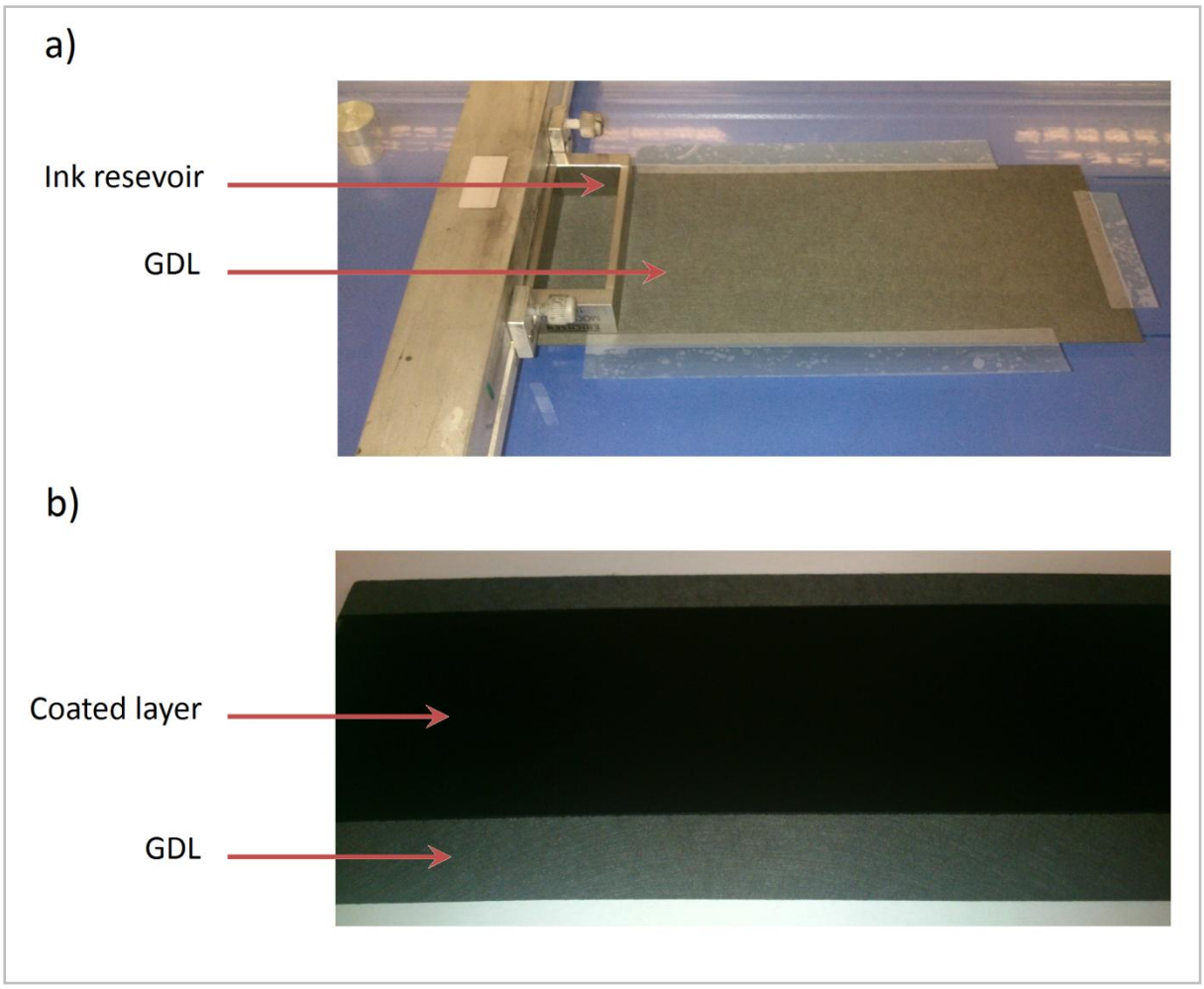

Figure 5.1: Doctor blade process showing GDL before (a) and after (b) ink coating

The exact glass transition temperature of PTFE (the point at which PTFE will become molten and disperses through the MPL layer) will vary depending on the source of PTFE used. To determine the glass transition temperature of DuPont™ Teflon® PTFE TE-3859 and to validate the baking conditions used to remove the surfactant, thermal gravimetric analysis (TGA) combined with single differential thermal analysis (SDTA) were performed using a Mettler Toledo TGA/sDTA851e.

In an attempt to modify MPL thickness, two different ink compositions were used and coated at a blade height of 100 µm. The two ink compositions are shown in Table 5.1. The water and Triton-X100 were added to 50 ml beaker and then the carbon powder was slowly added whilst continuously stirring the mixture to allow the carbon to enter the solution. The ink was then homogenized at 8000 rpm for 30 minutes using a Silverson L5T mixer. The PTFE solution was then added to the ink which was then further homogenised at 500 rpm for 10 minutes. Mass measurements of added components were obtained using a Mettler Toledo XS104 analytical balance.

Table 5.1: MPL ink compositions for doctor blade deposition

Ink recipe 1 (11.9 solids wt%, 20 wt% PTFE*)	
Component	Mass (g)
Carbon	1.992
Triton X-100	3.986
Water	13.510
PTFE solution	0.664
Total	20.152
Ink recipe 2 (14.9 solids wt%, 20 wt% PTFE*)	
Component	Mass(g)
Carbon	1.991
Triton X-100	3.991
Water	9.350
PTFE solution	0.664
Total	15.996

*relative to carbon weight

A Nova NanoSEM™ electron microscope was used to locally measure in-house fabricated MPL thickness (cf. Section 6.1.3). The MPL coated GDL and a cutting blade were submerged in liquid nitrogen for two minutes and then the GDL was cut cross-sectionally and mounted using a glue resin. The MPL was scanned at magnifications between 800 and 1000 times.

Similar to the GDL characterization, in-house fabricated MPLs were also analysed by mercury intrusion porosimetry (Autopore IV 9520 Automatic Mercury Porosimeter) to determine the pore size distributions. These results were compared against commercial MPLs from SGL 25BC and Freudenberg H2315 I3 C1.

5.2.1 X-ray micro computed tomography

A GDL (SGL 25BA) with an 11.9 wt % solids ink MPL and an MEA containing a 14.9 wt % solids ink MPL at the cathode were each scanned using X-ray computed tomography. From these results a procedure was developed to measure the thickness distribution across the MPL. The system used was a General Electric Phoenix L240 with NF180 additional X-ray source. The NF180 tube was used at a voxel resolution of 2 µm and the X-ray source was set to 60 kV and 240 µA. 2000 images were recorded at 500 ms per image. A detector shift was activated to minimize circular ring artefacts, and the sensitivity of the detector was increased to twice its normal value. Reconstructed volumes were analysed using VGStudioMax 2.2 at the Stellenbosch University CT Scanner Facility.

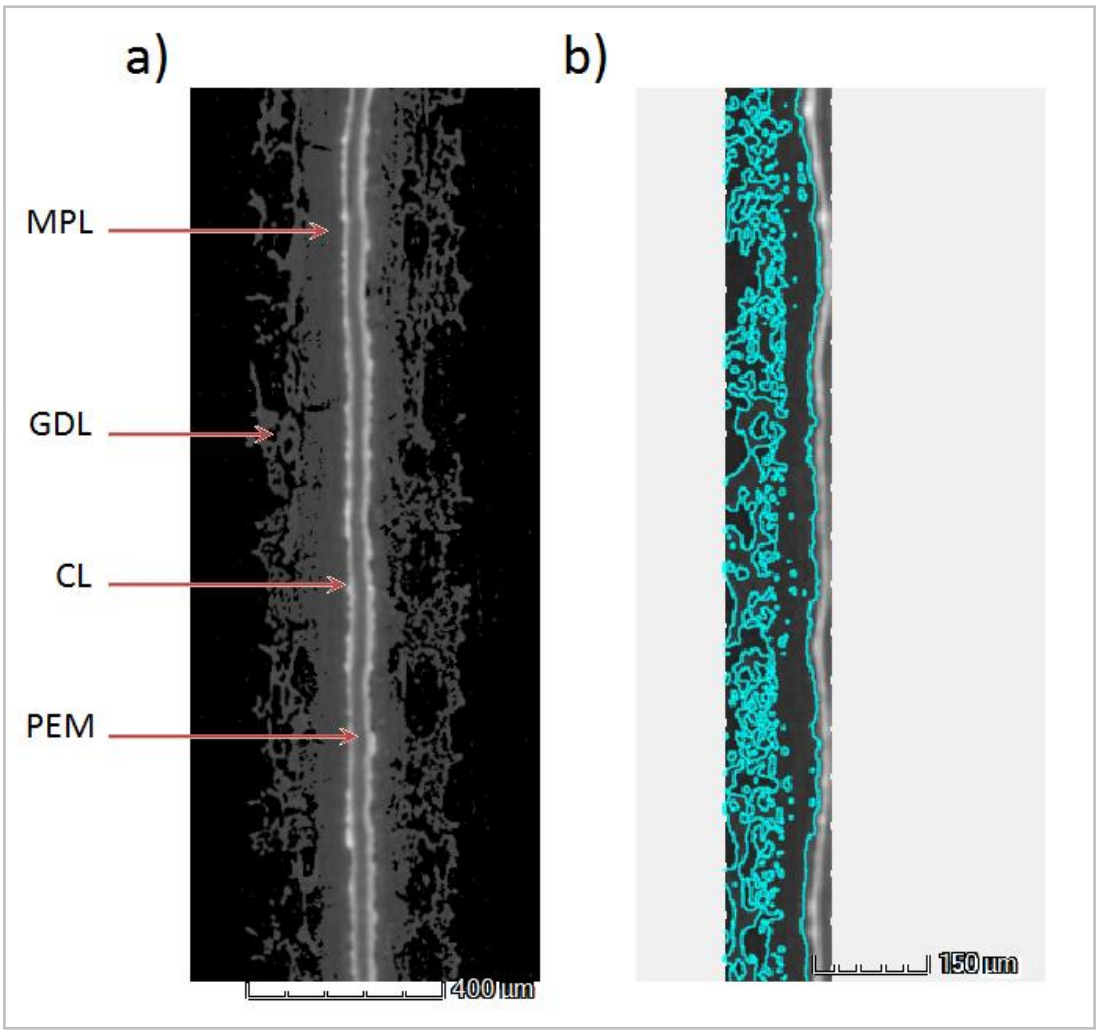

Figure 5.2: a) 2D X-ray CT raw image of MEA and b) section of surface fit to GDL/MPL subsection

Figure 5.2 shows a 2D image of an MEA with grey-level thresholding from low density (black) to high density (white). The low density void spaces appear black and the catalyst layer (with relatively dense platinum) appears light grey. The MPL and GDL due to their similar composition have similar densities and so both appear dark grey. Figure 5.2b shows a 2D section of the one half of the MEA with a surface fit which captures all of the MPL and part of the GDL.

Using this surface a wall thickness analysis was performed using the Wall Thickness Analysis tool add-on module VGStudio MAX 2.2. An orthogonal line is extended from one surface about a user specified value. The end point of the measurement line is the opposite surface. The smallest distance between the two surfaces defined the calculated wall thickness. An illustration of this procedure is shown in Figure 5.3 below.

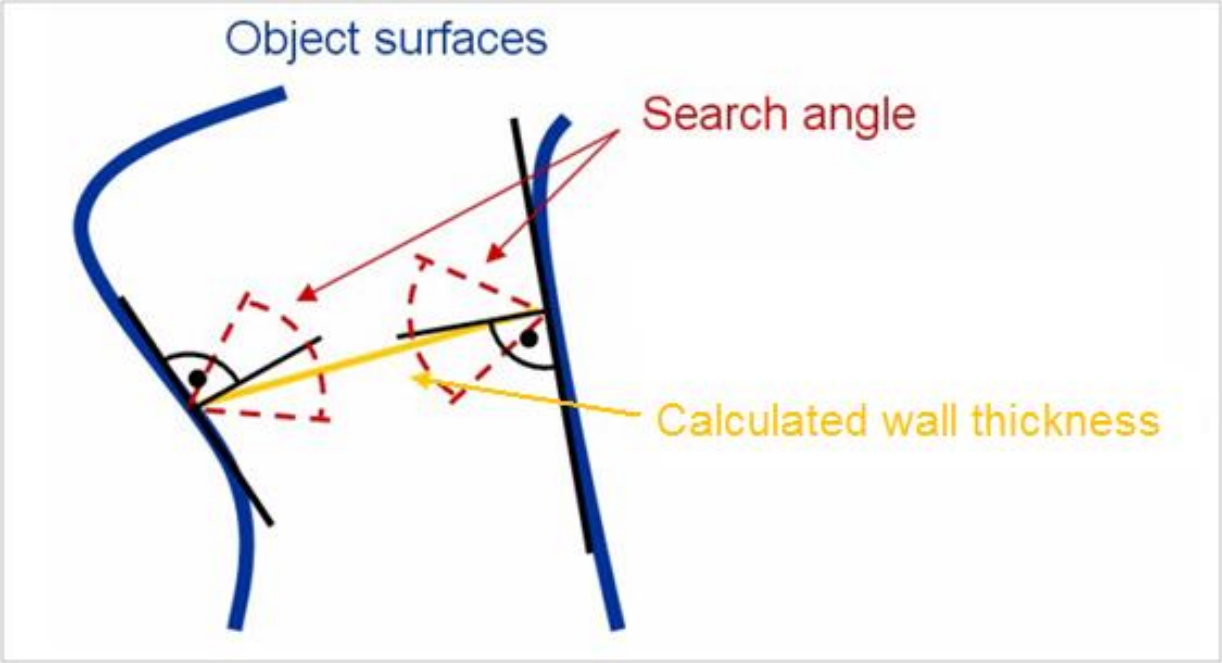

Figure 5.3: VGStudio MAX thickness analysis procedure

The analysis tool allows the user to specify the wall thickness interval of interest and the minimum (volume) size for a component to be listed as a result. Using Advanced mode reduces gaps in the analysis at the cost of increased computation time. Advanced mode was used for all thickness analyses in this study. Additionally a thickness range of 0 to 80 µm, a search angle of 30 degrees and minimum volume of 20 voxels were selected.

Figure 5.4 to Figure 5.7 show the application of this method to measure through-plane 2D thickness of the MPL. The catalyst layer is rendered in red using simple grey-level thresholding and the distinction between the MPL and GDL fibres due to different characteristic thicknesses is clear.

The thickness analysis tool (VGStudioMax 2.2) produces a histogram of the thickness distribution for the defined surface fit to the sample. In order to capture all of the MPL, the tolerance setting for the surface fit is relatively low. As a result of this, a surface fit to the MPL will always include some of the GDL fibres and CCM as shown in Figure 5.4 and Figure 5.6 (the CCM is shown in red). In general, the GDL fibres characteristic size is smaller than the MPL thickness, but there is a degree of overlap due to thin regions in the MPL as shown in Figure 5.8. This figure also shows a small peak at 2 µm thickness which is due to a portion of the CCM captured due to volume sectioning and the surface fit.

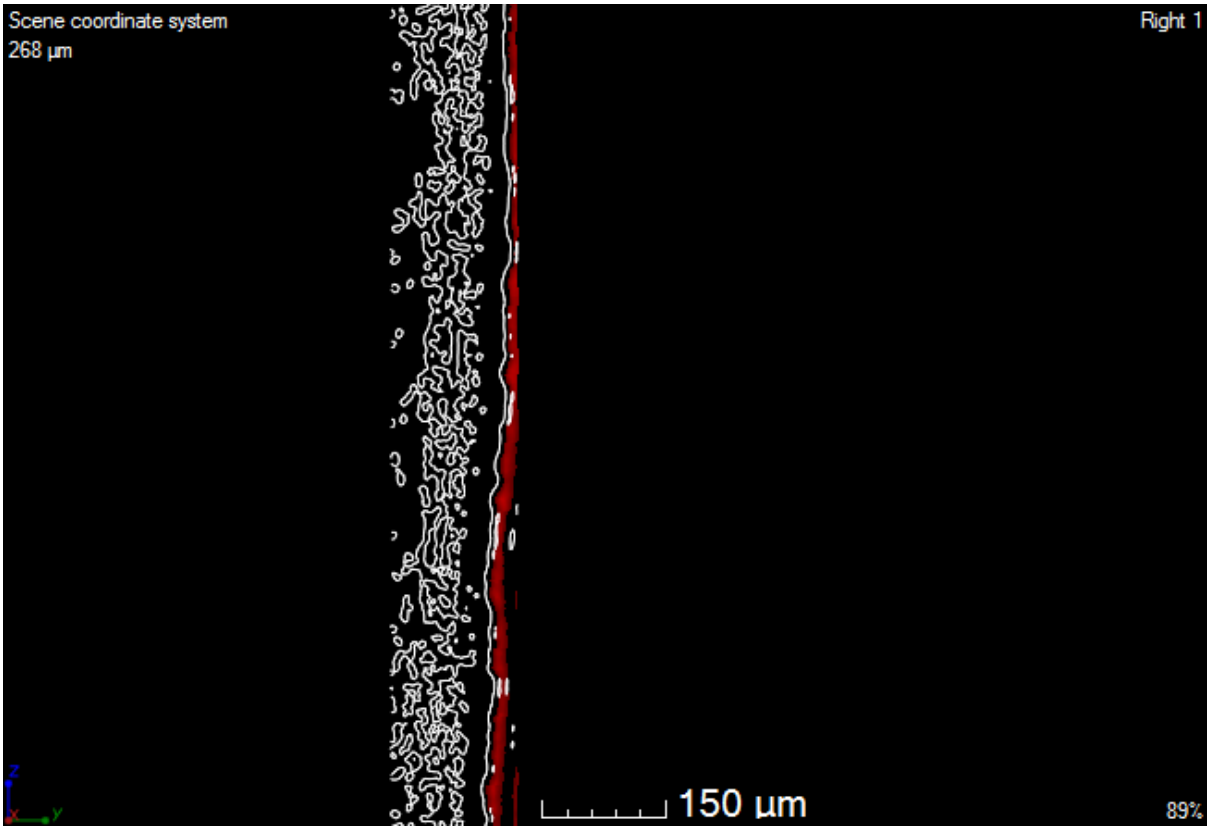

Figure 5.4: Through plane cross-section along z-axis with Pt render (in red) and MPL/GDL surface fit

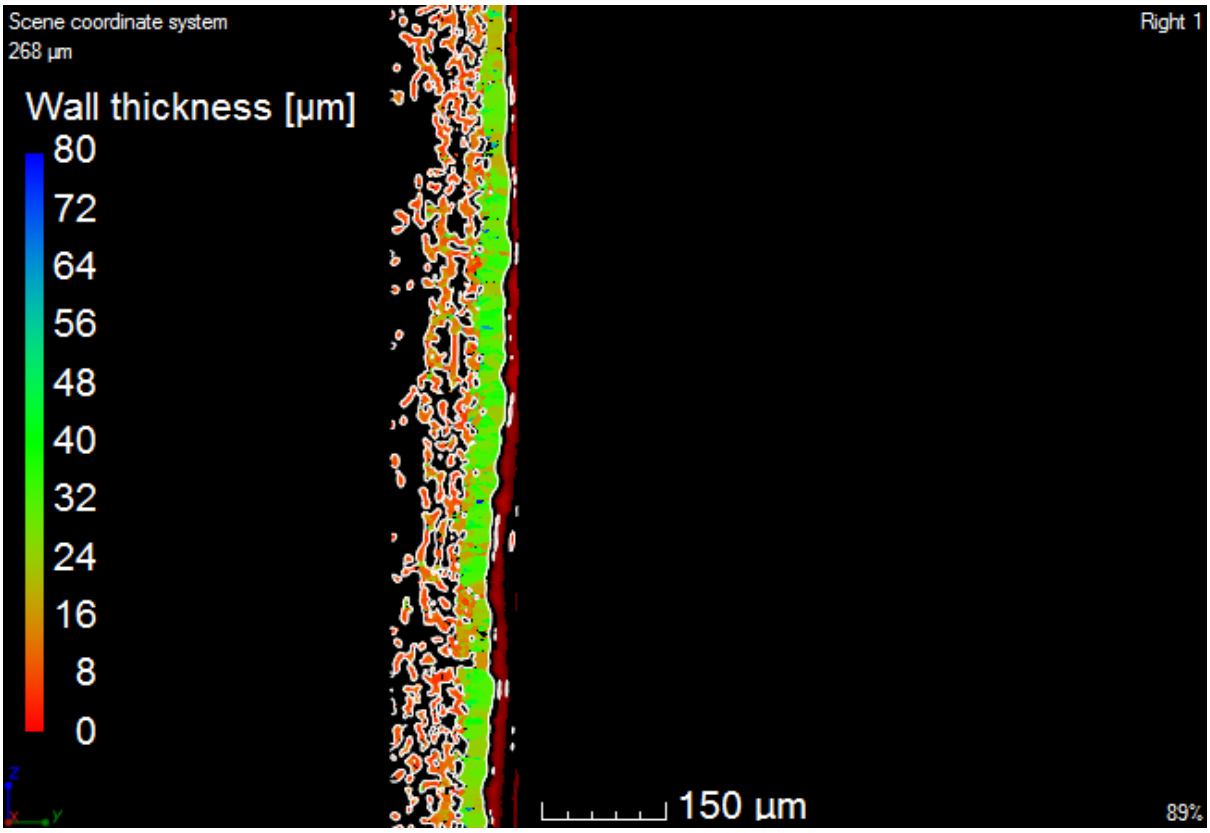

Figure 5.5: Thickness analysis 1 showing distinct layers

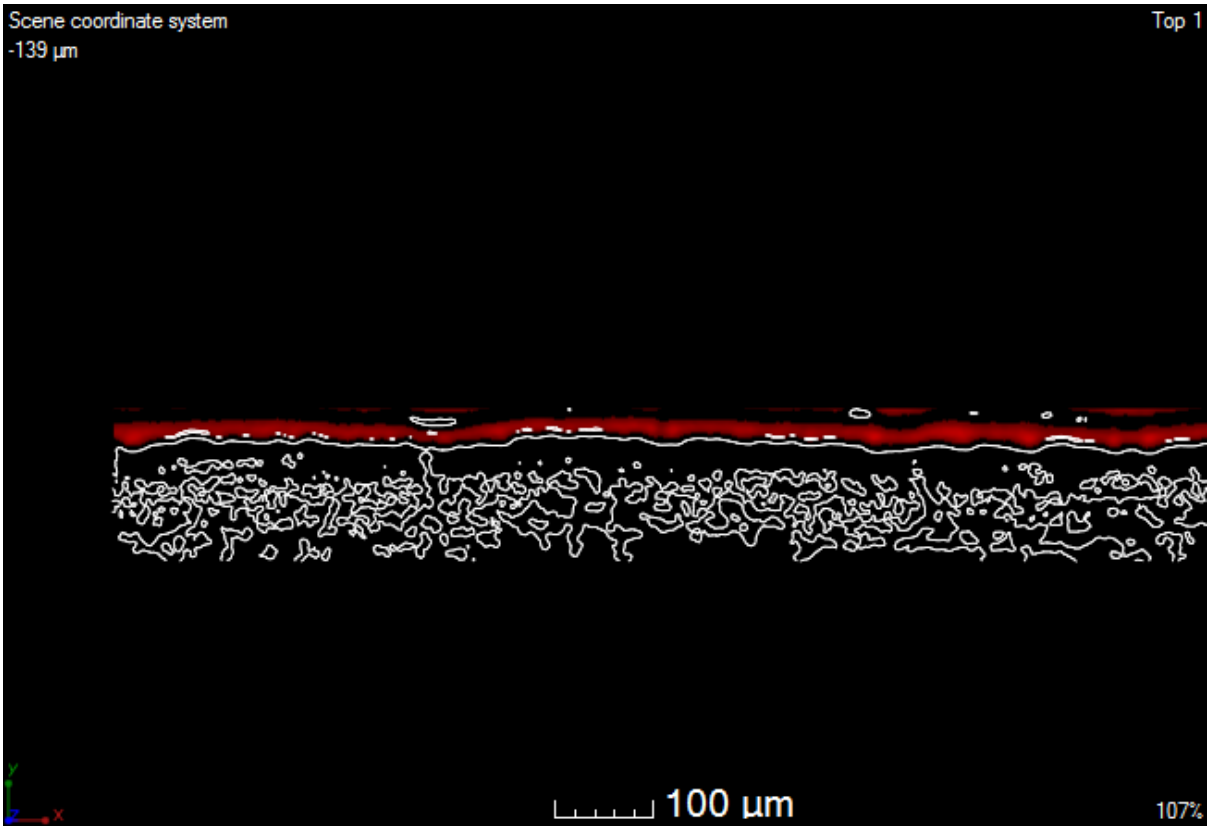

Figure 5.6; Through plane cross-section along x-axis with Pt render (in red) and MPL/GDL surface fit

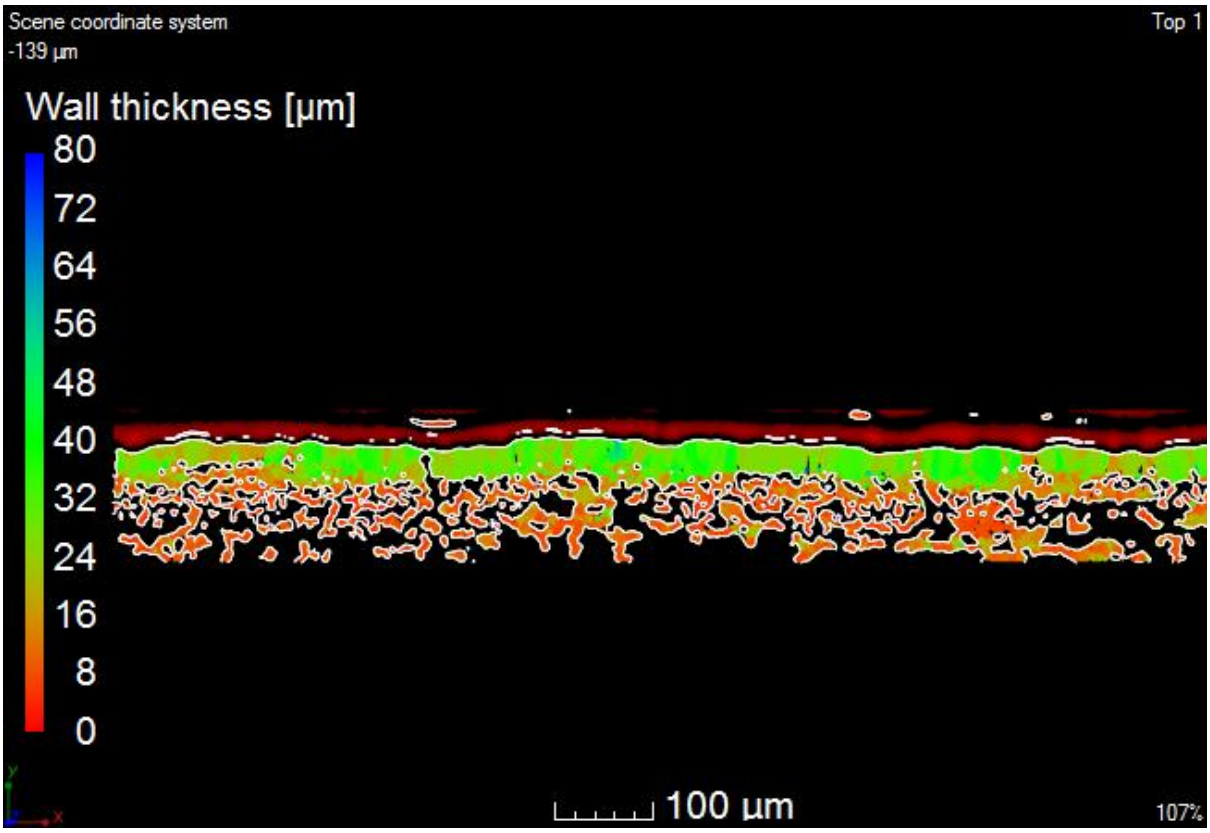

Figure 5.7: Thickness analysis 2 showing distinct layers

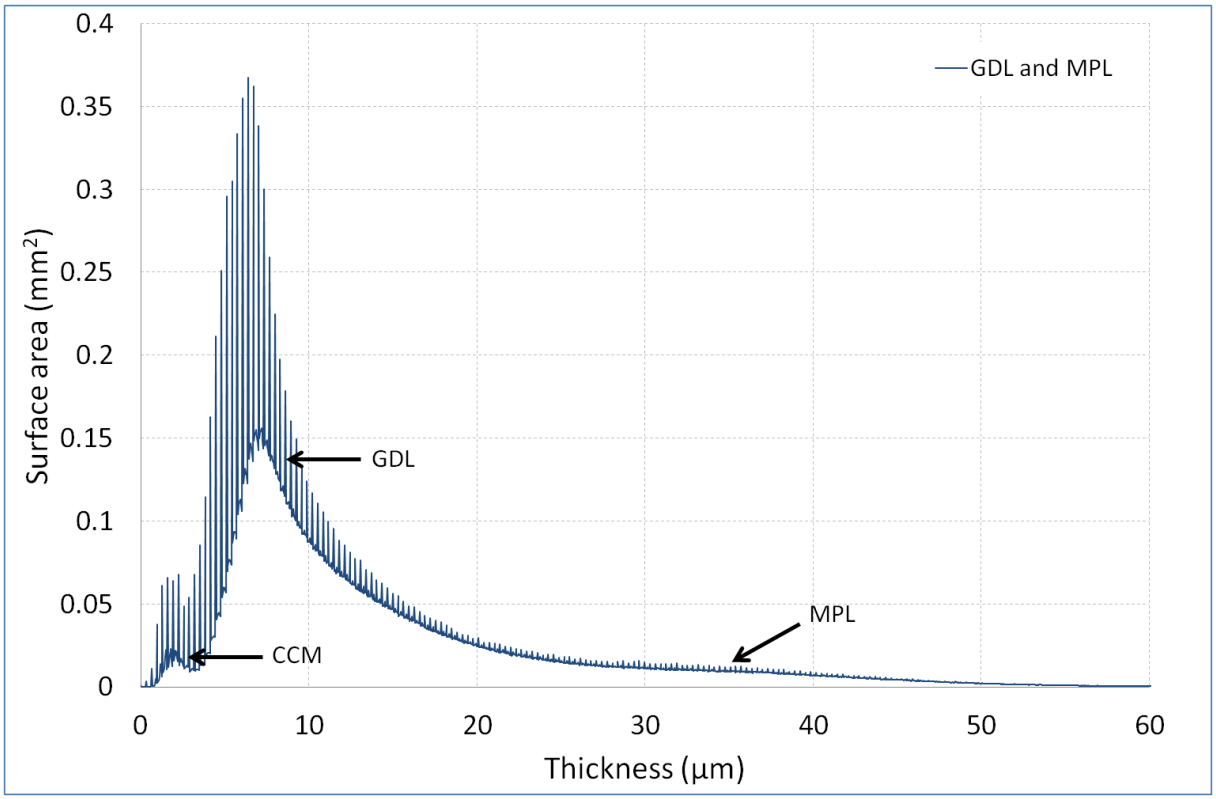

Figure 5.8: Thickness analysis of surface fit to MPL section including GDL and CCM regions

In order to isolate the MPL thickness distribution, a second thickness analysis is performed on a sample subsection with the exact same surface fit but only containing the GDL fibres (Figure 5.9). This representative thickness distribution for the GDL can then be scaled and subtracted from the original thickness analysis histogram (Figure 5.10). In this way the thickness distribution of the MPL can be quantified as shown in Figure 5.11.

This procedure was applied to 5 samples from an MEA (shown below in Figure 5.12) containing an in-house fabricated MPL (from 14.9 solids wt% ink) to quantify the thickness distribution across the MPL. Each sample was approximately 2.5 x 9 mm. Discussion of the results of this analysis is presented in Section 6.1.4.

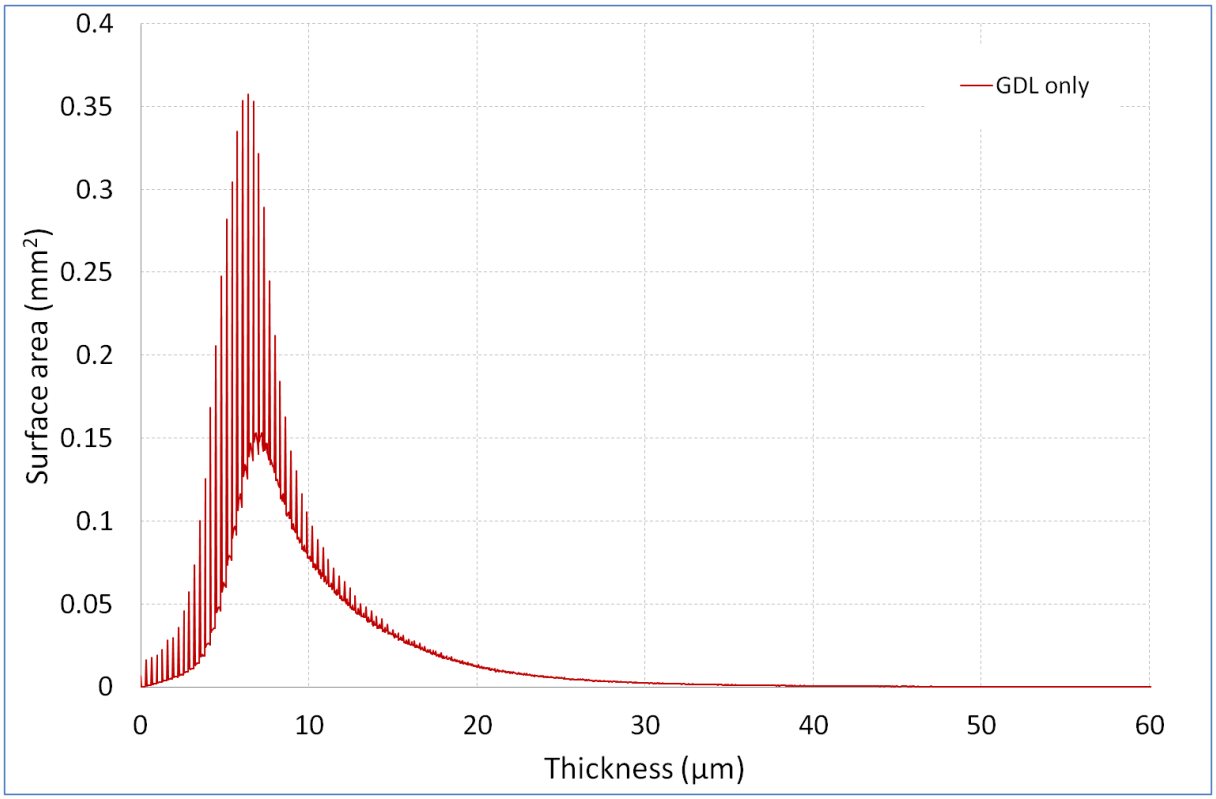

Figure 5.9: Scaled thickness distribution of subsection contacting GDL fibres only

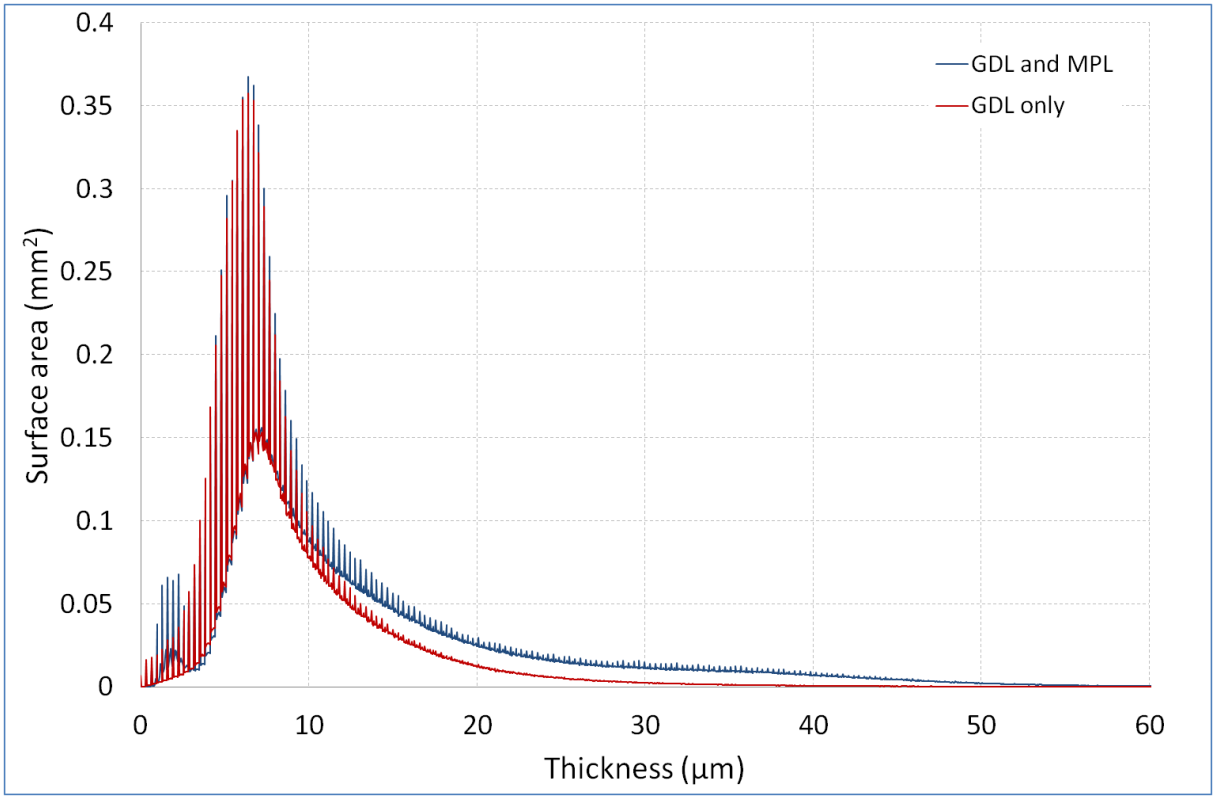

Figure 5.10: Overlaid thickness distributions of GDL/MPL/CCM and GDL only

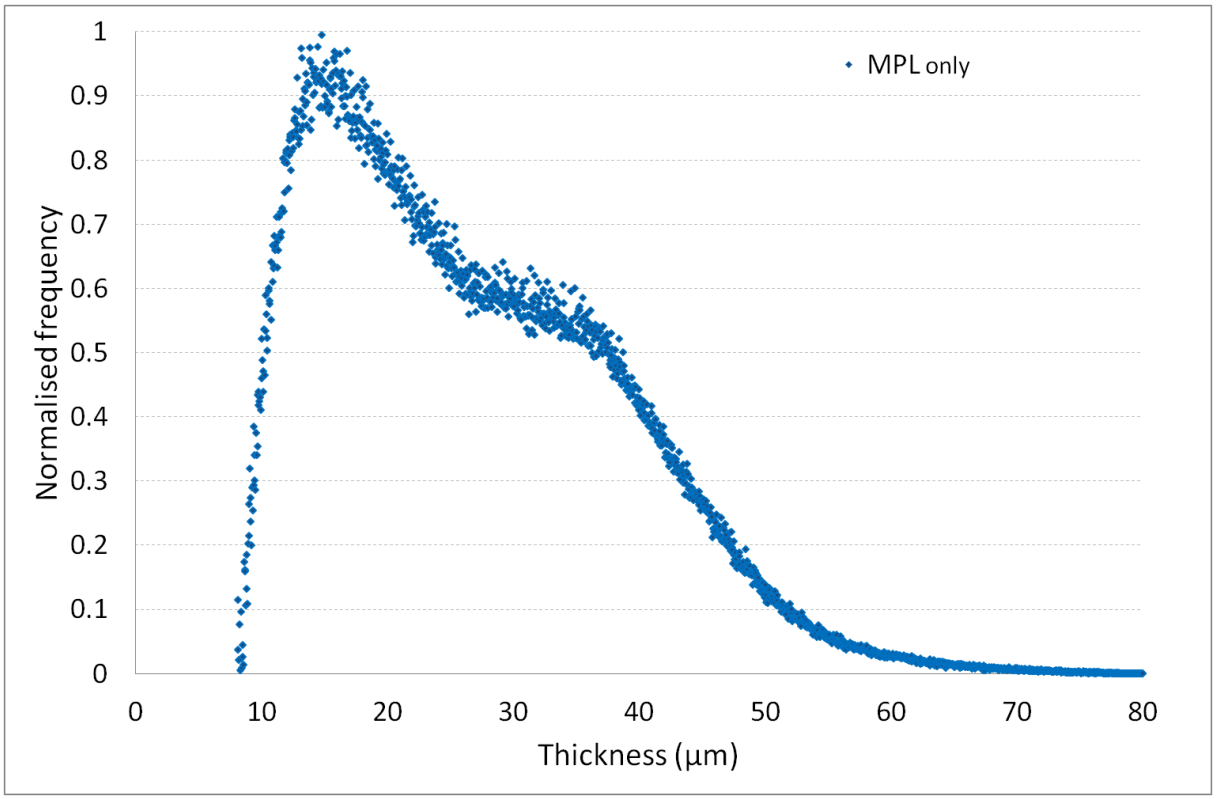

Figure 5.11: Thickness distribution of MPL only after subtraction of GDL overlap

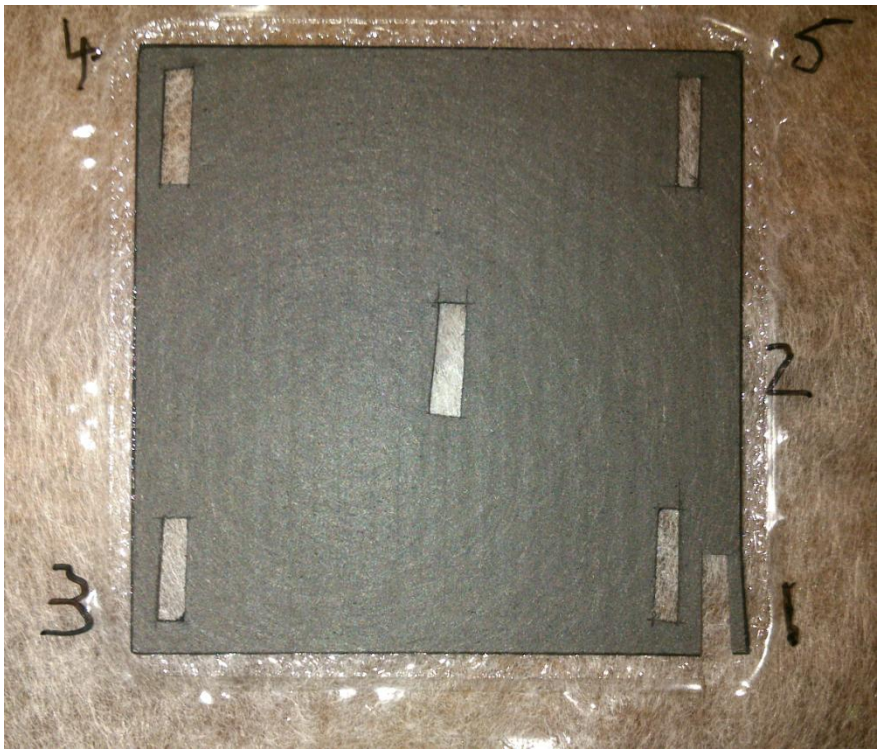

Figure 5.12: MEA sampling with 14.9 wt % ink MPL coating on SGL 25 BA at cathode

5.3 Cell materials and assembly

Ion Power DuPont® NAFION® NR-211 CCMs and Sigracet® SGL 25BC, SGL 25BA and Freudenberg H2315 I6 GDLs were used for MEA assembly and testing. Advanced PEMFC test stations (FuelCon Evaluator-C) linked to balticFuelCells single cell quickCONNECT fixtures (FC 25/100) with 25 cm^2 active area and 5-fold serpentine flow fields were used for all MEA testing.

Prior to placement of an MEA into the test cell, the flow fields and heating plates were cleaned with isopropanol and lint-free cloth.

The separate MEA components were carefully placed to ensure good alignment of the layers upon cell closure as illustrated in Figure 5.13. No hot-pressing was used. The cell was then placed inside the cell fixture pressure unit which consists of a pneumatic actuator allowing for a continuously controlled and easily adjustable cell contact pressure.

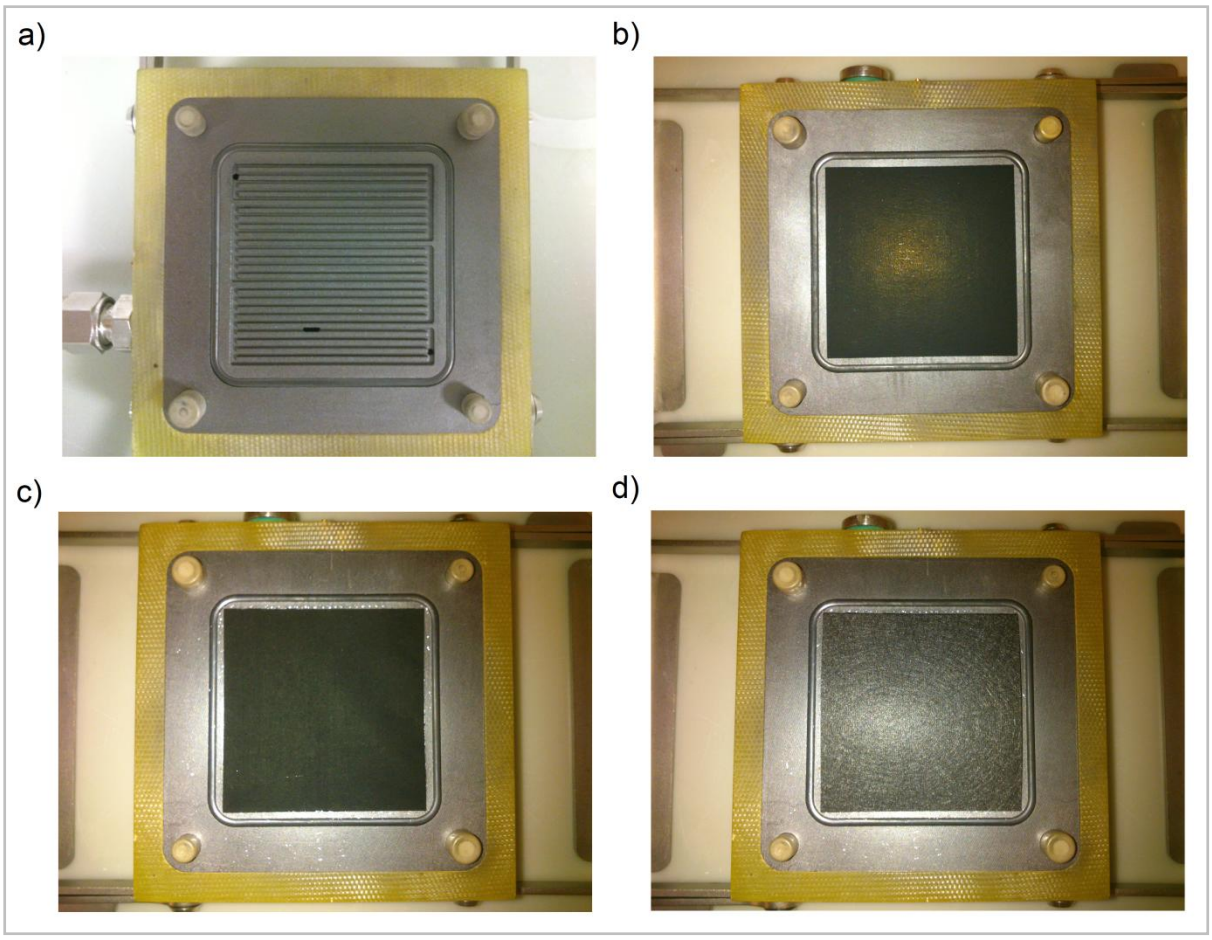

Figure 5.13: a) 5-fold mixed serpentine flow field and placement of b) anode GDL c) CCM and d) cathode GDL

5.4 Test station evaluation

Prior to data collection the system was rigorously tested to ensure reliability. Particular important aspects that were addressed were temperature and relative humidity control and contamination mitigation. As a final validation an MEA was tested across two different test stations to ensure precise (and accurate) data generation. Testing conditions A-E are given in the Appendix Table A.3.

5.4.1 Contamination mitigation

It is expected that successive polarization curves (PCs) should improve until the membrane is fully conditioned whereby stable performance should be observed (Cuccaro et al., 2008). Repeat polarization curves are shown in Figure 5.14. It was also observed that there was rapid and continual performance loss during galvanostatic operation resulting in the suspicion that there was some form of contamination entering the system.

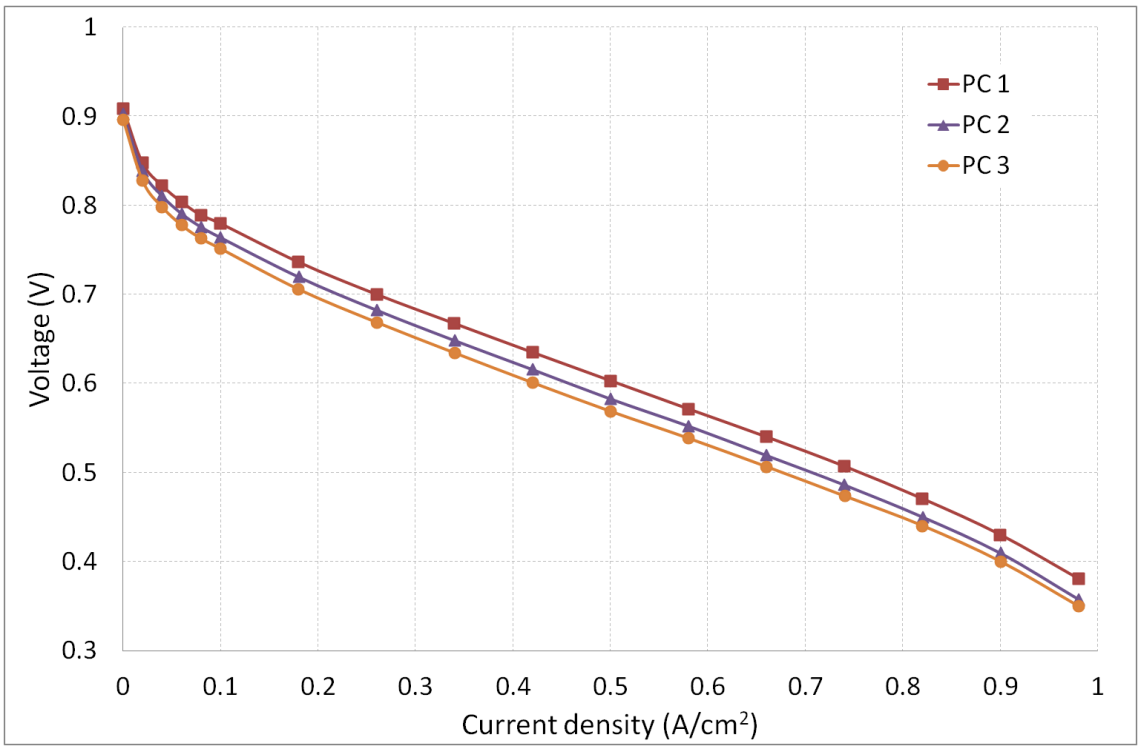

Figure 5.14: Repeat polarization curves at Condition A showing performance loss

The original gas supply to the system was from a hydrogen generator (Proton energy systems Hogen® S Series 2) and an air compressor (Atlas Copco SF 8 FF WorkPlace Air System™). It was decided to switch to high purity hydrogen and synthetic air from cylinders (Air Products South Africa). However, this did not resolve the issue and so the test cell was connected directly to the gas supply through glass bubblers at ambient temperature (by-passing the test station).

The successive polarization curves for the bypass system are shown in Figure 5.15. It was found that with each successive PC, the performance improved and stabilized after three repeats implying a fully conditioned MEA state. In particular the activation overpotential decreased with each successive load sweep. It was therefore concluded that either the contaminant was entering the supply gas during delivery from the cylinder to the cell, or that the impurity was in the humidification water. The entire water delivery system was cleansed with chlorine solution and the bubblers were completely drained and refilled with high resistivity (>8 Mohm.cm2) deionised water. Stable performance was then observed as shown by the repeat polarization curves in Figure 5.16.

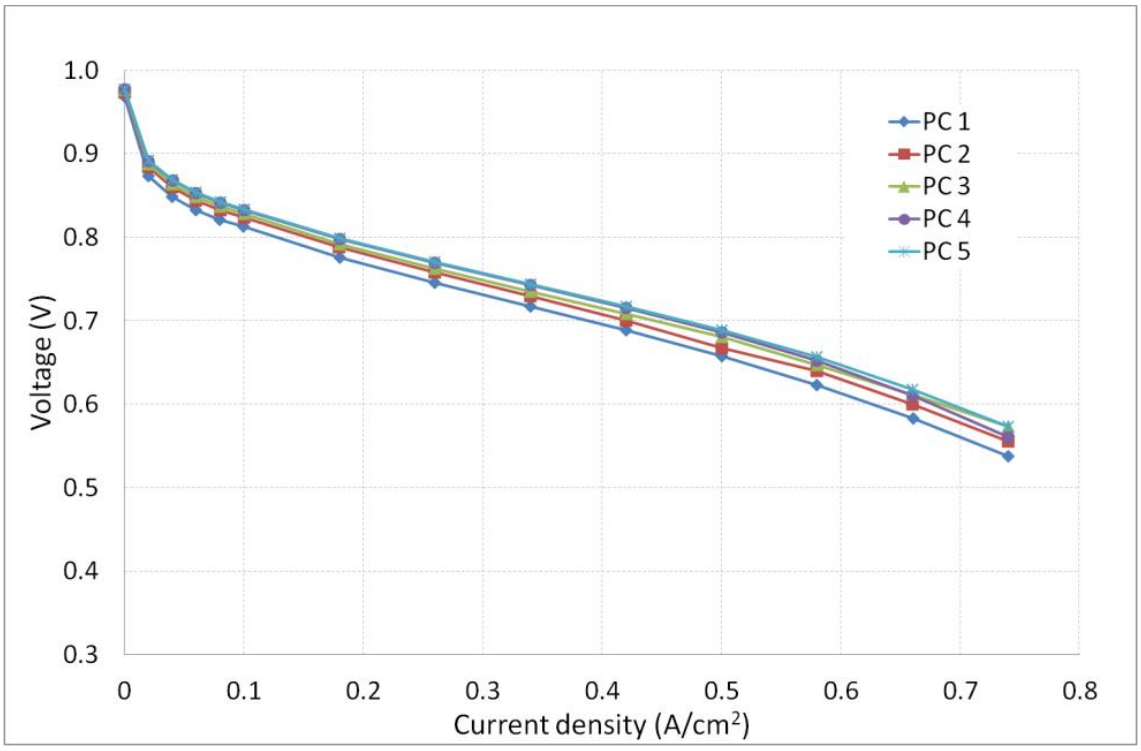

Figure 5.15: Polarization curves for bypass-system at Condition B showing performance improvement

To test precision of electrochemical testing, a cell was assembled and tested under identical set point conditions across two FuelCon test stations. A comparison of the performance results is shown in Figure 5.17. There was less than 15 mV performance difference between the test results up to a current density of 0.74 A/cm^2. It was therefore concluded that the electrochemical test system produces data with good precision and reproducibility.

High purity hydrogen, air and oxygen from gas cylinders were used for all electrochemical testing in this study. Additionally before each test the bubblers were drained completely and refilled with deionised water.

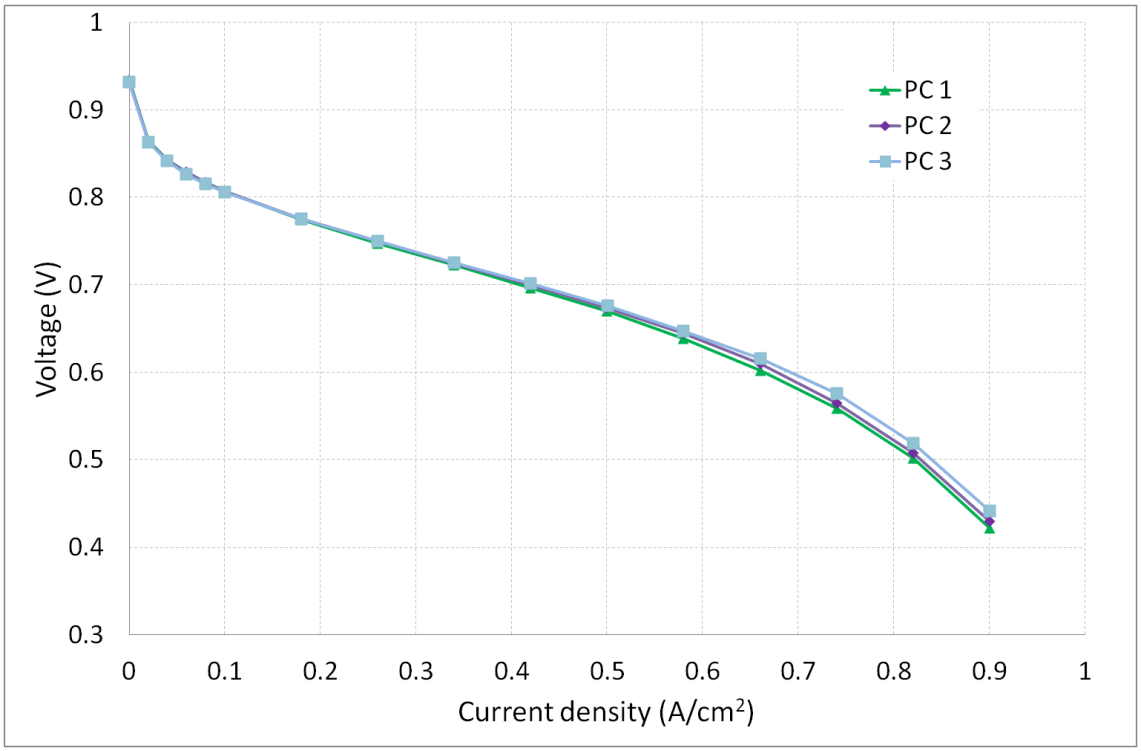

Figure 5.16: Repeat polarization curves at Condition C after system cleanse showing stable performance

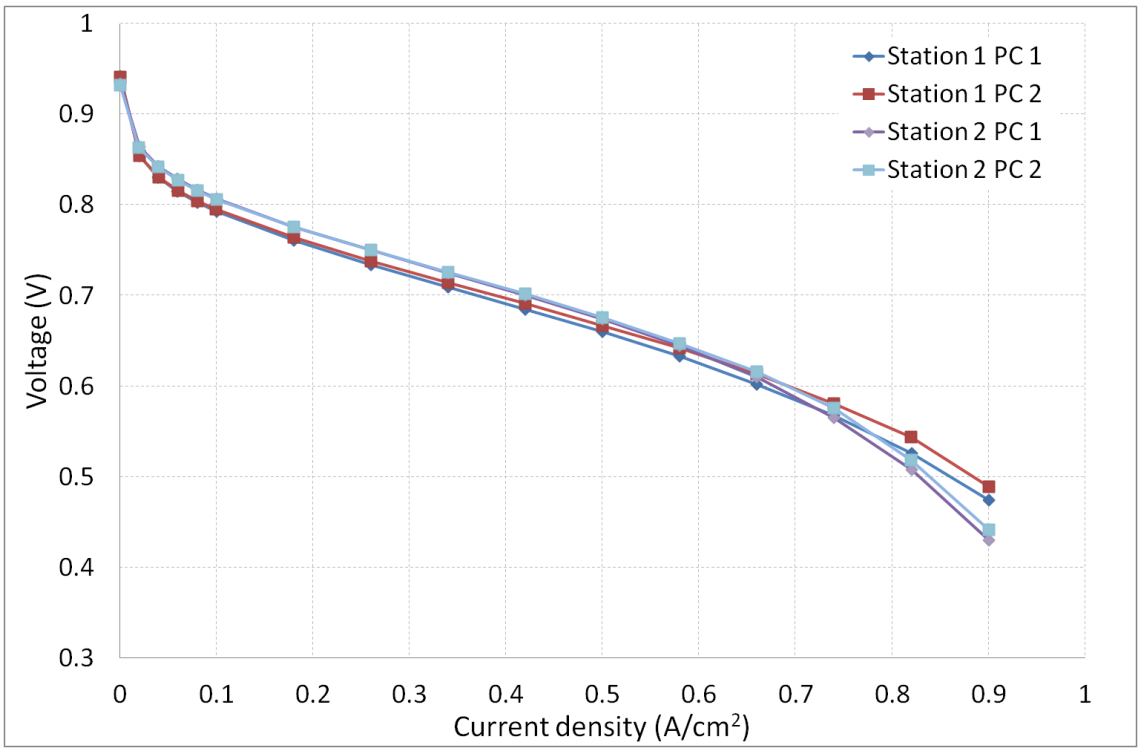

Figure 5.17: Precision testing at Condition C across two test stations using the same MEA and test cell

5.5 Electrochemical testing

VBScript automated test procedures were used extensively in this study to improve control and efficiency of test procedures. Standard procedures for polarization curve and EIS analysis as discussed by Cooper et al. (2005) and USFCC (2006) as well as additional safety and operational considerations were incorporated into each of the scripts. Specific procedures such as leak testing, conditioning and polarization curve analysis were arranged into modular libraries to improve script management and generalization. The following sections will describe additions to the standard procedures with justification.

5.5.1 VBScript automated testing procedures

The user interface as shown in Figure 5.18 allows for operation and manual control of test processes. The “Tags” e.g. T901 can be used to modify process variable set points either manually or using a script command.

The libraries written for this study performed the following functions:

- Cell compression
- Leak testing
- Bubbler drainage and refill
- Heating
- Cyclic conditioning
- Polarization curve analysis
- EIS analysis
- Shut down (return to ambient conditions)

The cell compression library gradually increases the cell contact pressure to a user specified value. The leak test library measures pressure drop over 5 minutes for a pressurized system and informs whether there is a leak at either the cathode or anode based on a comparison to the USFCC (2006) standard. The bubbler drain and refill library activates manual level control and then opens the bubbler drain valves until the vessel is empty (based on level indicators). The bubbler is then refilled to the middle water level indicator and automatic level control reactivated.

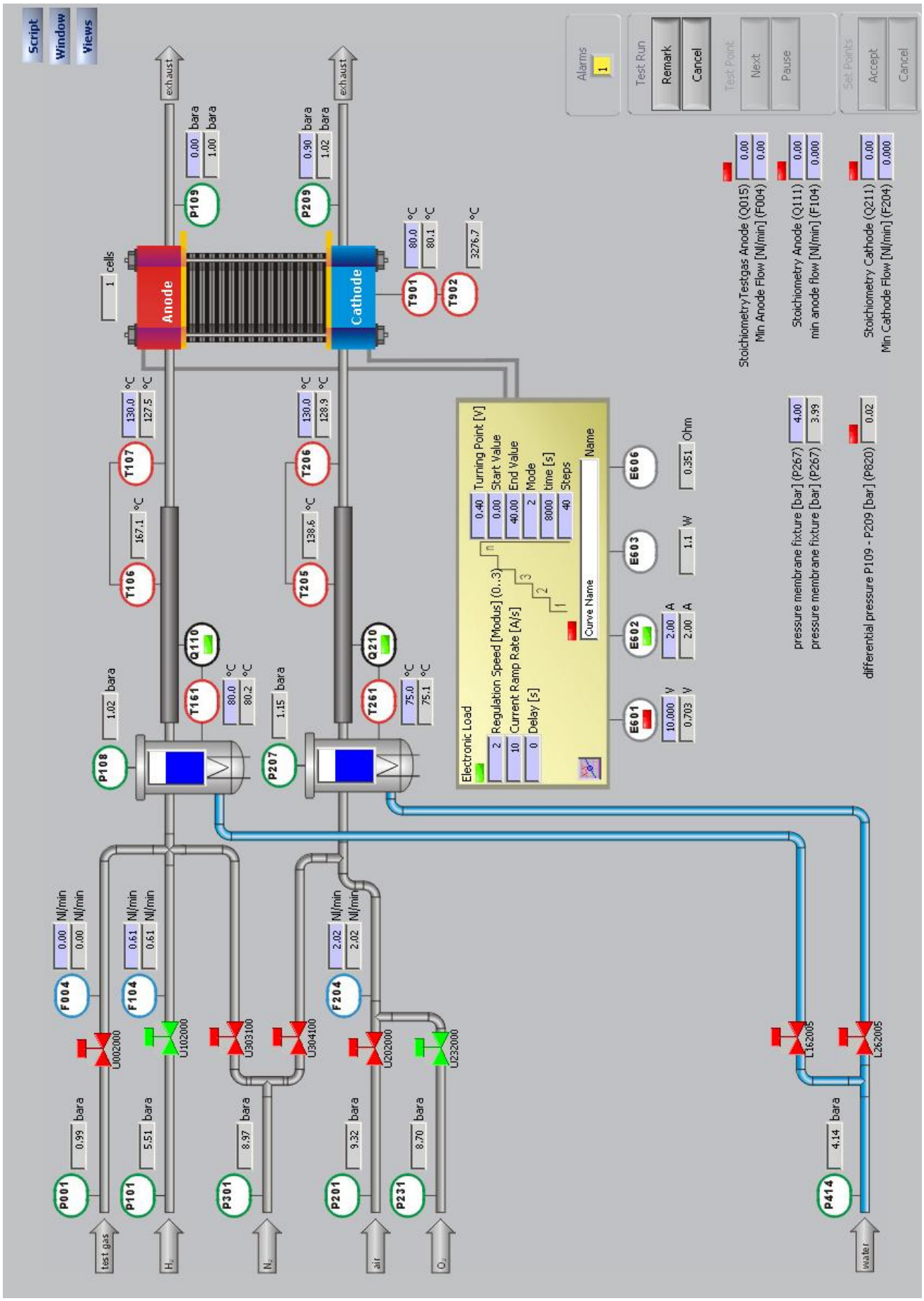

Figure 5.18: Screenshot of FuelWork user interface showing Tag identifiers for process variables

The heating library heats and pressurizes the fuel cell system in a controlled manner and activates humidification. The anode and cathode inlet temperatures are automatically set to 40 ^{o}C higher than the cell temperature to prevent condensation in the supply line. The conditioning library activates hydrogen and air flow and sets the user defined flow rates in a controlled manner to prevent over heating of the supply line. The MEA is then cycled between 0.3 V (holding for 10 minutes) and 0.8 V (for 30 seconds) a number of times defined by the user. After each cycle, a high frequency resistance measurement (at 10 kHz) is performed and the current and real impedance written to Excel. In this way the conditioning of the MEA can be monitored to confirm stable performance prior to testing.

The polarization curve library has been generalized to allow for flexible testing. The user can specify the number of polarization curves to measure for air and/or oxygen, the activation and ohmic region current increment step sizes, the stabilization time period at each point, the number of repeat voltage measurements, whether to use constant gas flow or stoichiometric load following, whether to perform HFR measurements and finally the minimum voltage limit and the maximum current limit for the analysis. Additionally the user can select the option of temperature equilibration whereby the actual cell temperature is compared with the set point temperature after a current set point change and if the difference is larger than a user specified tolerance an additional wait period is initiated to facilitate temperature equilibration. Cell temperatures, voltage and current measurements at each point are written to an Excel file in a convenient format for the user. The polarization curve library and sample data output are included in Appendix B to exemplify the VBScript libraries written for this study.

The electrochemical impedance spectroscopy library performs an EIS measurement at user specified current density and flow rate with either air or oxygen at the cathode. Procedures are included to ensure temperature equilibration when performing EIS at high current densities. The impedance frequency and real and imaginary components are all written to an Excel file for convenient data analysis.

Finally a shut down library was written to mitigate MEA damage when returning to ambient conditions and to purge the system of residual reactant gases. The script follows the oxygen consumption shut down strategy as described by Oyarce et al. (2014). Once the oxygen is depleted from the catalyst layer, both anode and cathode are purged with humidified nitrogen. The bubbler and cell temperatures are then reduced to ambient conditions with the cell temperature always slightly higher than that of the bubbler to prevent condensation and excessive MEA dry-out. Finally all gas valves are closed and the cell is decompressed upon user acknowledgement. Using the above libraries, a full suite of tests lasting a number

of days can be performed with the user only having to be present for the cell assembly and leak test at the start. The script written to perform the electrochemical testing is included in Appendix B.2 Single cell testing script.

5.5.2 Operating conditions and analyses performed

A script was written to compress the cell, perform an automated leak test, condition the MEA and then measure polarization curves and EIS at both low and high relative humidity.

The cell was compressed to a contact pressure of 4.8 bar and all leaks at both cathode and anode were less than 0.035 bar over 5 minutes for all tests. The MEA was conditioned at low relative humidity for 12 cycles between 0.8 V for 30 seconds and 0.3 V for ten minutes at a constant flow rate of hydrogen and air at stoichiometries of 2 @ 1 A/cm^2. Following each cycle a HFR measurement was taken at 10 kHz to monitor membrane hydration. After conditioning polarization curve and EIS analysis were performed at the same humidity. During polarization curve measurement the current was increased by 0.02 A/cm^2 in the activation region where the drop in voltage is rapid and 0.08 A/cm^2 in the ohmic region where the voltage drop is approximately linear. The assumed transition region between activation and ohmic regions was fixed to ensure data points across tests could be used for statistical analysis of performance variations. Following the low RH test, the MEA was then reconditioned (using the same procedure as before) at high relative humidity and the polarization curve and EIS analysis repeated. The conditions for the low and high relative humidity tests are given as fold out pages in Appendix A (Table A.3) as Condition D and E respectively. The parameters for the polarization curve and EIS analysis were the same for both humidity conditions and are also tabulated in Appendix A. The total duration of a single test run was approximately 48 hours.

5.6 MEA electrochemical variance testing

Six repeat electrochemical test procedures (at the conditions described in Section 5.5.2) were performed on different MEAs to quantify variance. For each test, Ionpower NR211 CCMs with SGL 25BC at the anode were used. At the cathode, SGL25BA, SGL25BC or Freudenberg H315 I6 was used as diffusion media. Both SGL 25BA and Freudenberg I6 are carbon paper substrates without MPL. SGL 25BC is effectively SGL 25 BA substrate with an MPL. The sample size is small and the type of distribution unknown for the MEA performances and therefore parametric statistics are not strictly valid. However it is found that twice the value of the estimated standard deviation is a useful descriptive statistic and will be used as error margins on plots of experimental variance.

6 Results and discussion

This section presents the experimental results along with a discussion of the findings from MPL fabrication, PDM characterization and variance testing of the electrochemical performance of MEAs with different porous diffusion media at the cathode.

6.1 MPL fabrication and PDM characterization

The results validating the MPL fabrication method are shown below in Section 6.1.1. This is followed by PDM characterization using MIP showing variability in pore structure of commercial GDLs and comparing in-house fabricated MPLs to commercial products. The final investigation of MPL fabrication compares the results of MPL thickness measurement by conventional SEM and a novel method using X-ray µCT. Lastly, electrochemical performance variance results for MEAs with different GDLs at the cathode are presented and discussed in Section 6.2.

6.1.1 TGA and SDTA analysis

Figure 6.1 shows the result of TGA analysis on an MPL coated SGL 25BA GDL dried at 100 ^{o}C. The boiling point of Triton X-100 is approximately 270 ^{o}C (AMRESCO, 2011) and unmodified carbon black thermally decomposes above 500 ^{o}C. From the figure it is seen that at around 20 minutes of running time the surfactant begins to leave the MPL and is completely removed in under 10 minutes at 350 ^{o}C. The other components of the GDL/MPL are thermally stable up to 500 ^{o}C.

Single differential thermal analysis (SDTA) on DuPont Teflon PTFE TE-3859 is shown in Figure 6.2. The symbol ΔT represents the difference between the actual temperature of the sample in the thermo gravimetric analyzer and the model reference temperature. During a sample phase change, energy is absorbed with no change in temperature which results in a more negative value for ΔT. Therefore Figure 6.2 shows that the glass transition temperature of PTFE TE-3859 is between 320 and 340 ^{o}C which is in agreement with product specification literature.

From the TGA/SDTA results it can be concluded that the MPL heat treatment procedure described in Section 5.2 will completely remove surfactant and disperse PTFE without degrading the carbon in the GDL and MPL.

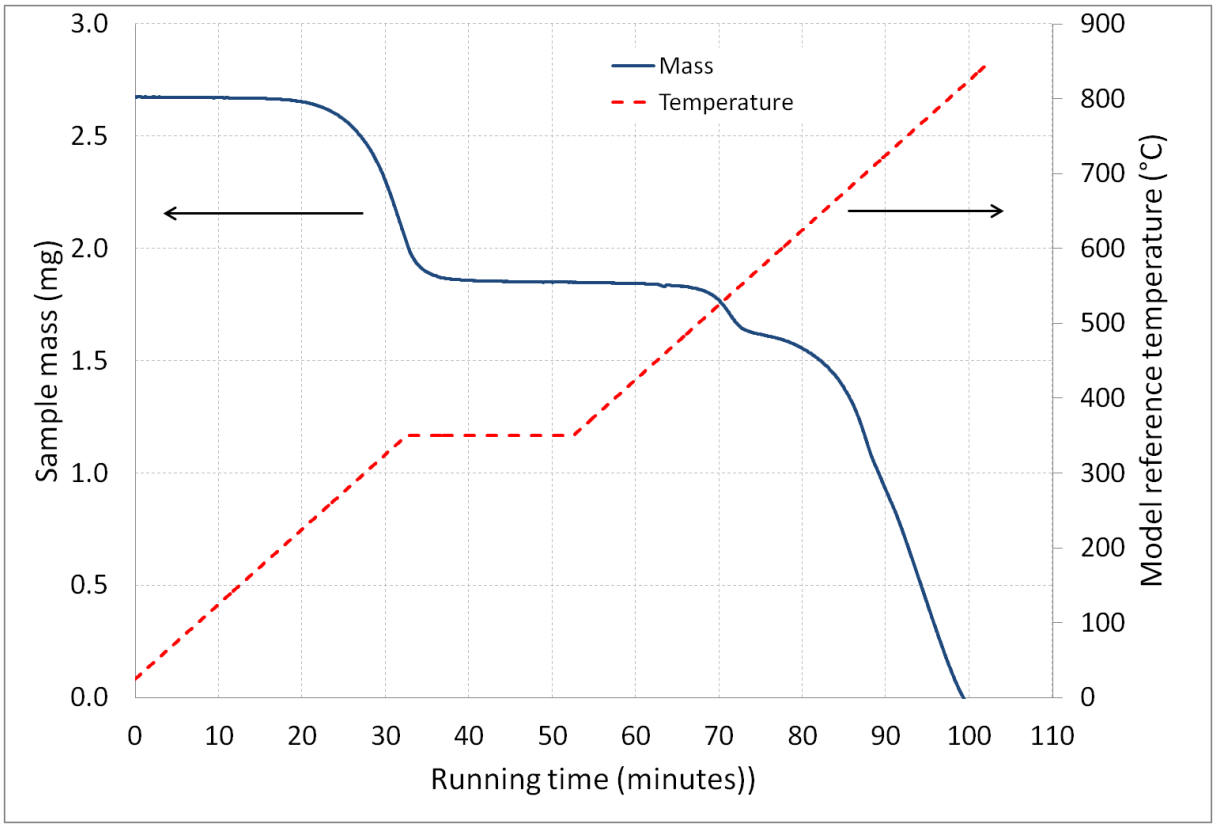

Figure 6.1: TGA analysis of MPL coated GDL showing loss of surfactant and decomposition of carbon

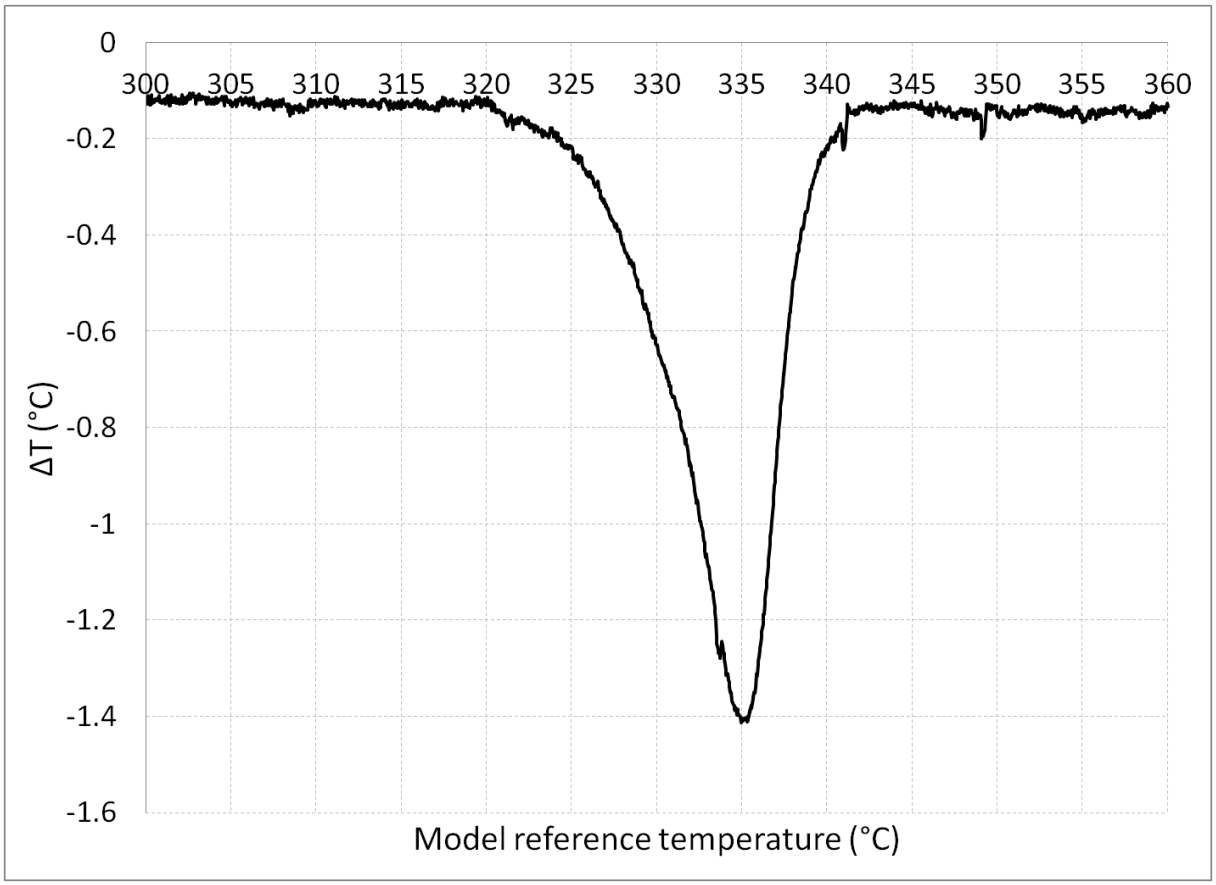

Figure 6.2: SDTA analysis of DuPont Teflon PTFE TE-3859. Ramp rate=2 °C/min

6.1.2 Pore structure and areal weight analysis

Figure 6.3 compares the pore structure between two in-house fabricated MPLs (coated on SGL 25BA substrate) and two commercial MPL coated GDLs measured by mercury intrusion porosimetry (MIP) with the incremental intrusion volume normalised with respect to sample area. Measured areal weights are given in Table 6.1 and Table 6.3. The micropore volume of the 14.9 wt% MPL is larger than that of the 11.9 wt% MPL due to the increased MPL thickness (cf. Section 6.1.3) resulting in a larger MPL volume per unit mass of sample. Freudenberg I3C1 has a notably different GDL pore structure than the other samples and both SGL 25BC and Freudenberg I3C1 have a higher proportion of small pores (< 0.3 µm) than the in-house MPLs.

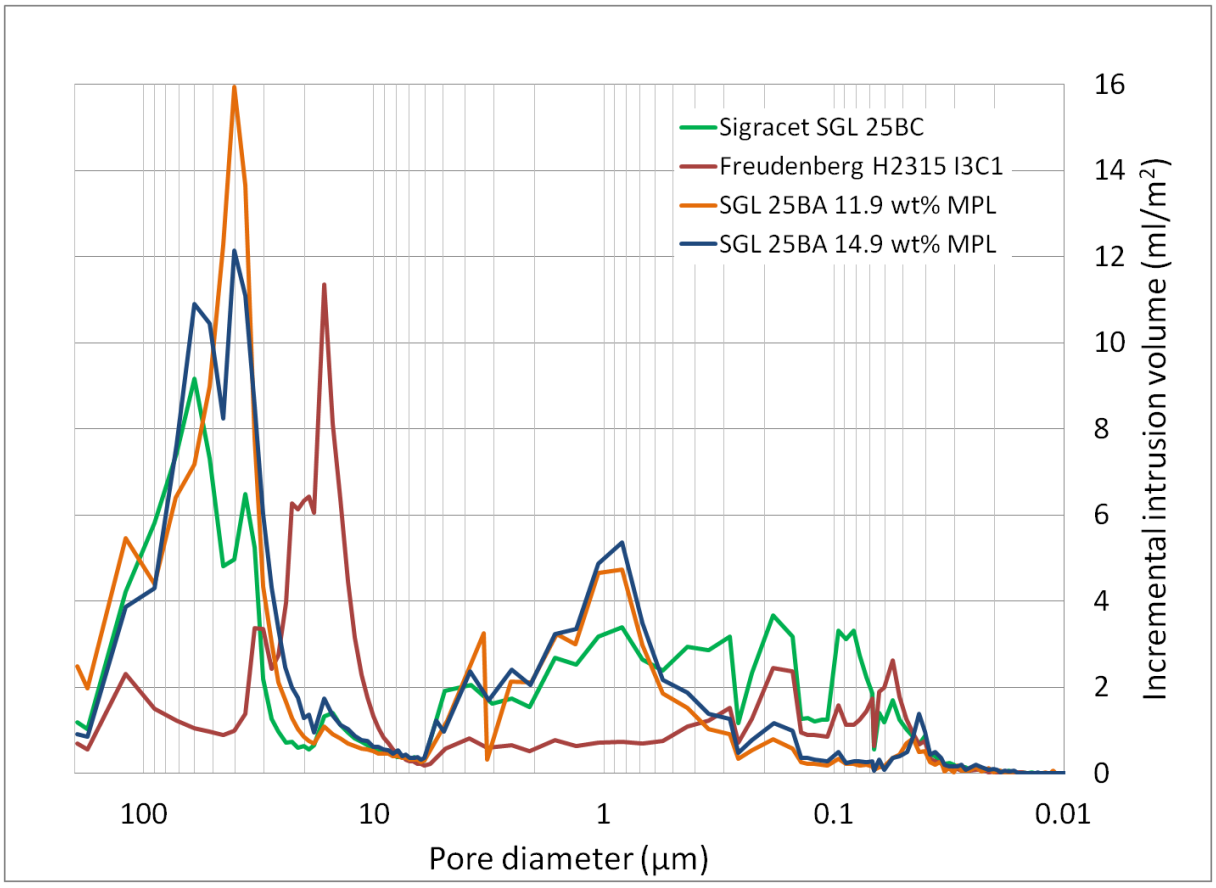

Figure 6.3: Pore size distribution comparison of in-house MPLs with commercial products

Even though the two in-house fabricated MPLs have significantly different thicknesses, the pore structure is very similar. Subsequently, by testing these two MPLs electrochemically in an MEA with all other components carefully controlled, it may be possible to analyze the individual effect of MPL thickness on performance.

Figure 6.4, Figure 6.5 and Figure 6.6 show repeat MIP analyses on Freudenberg H2315 I6 (without MPL), SGL 25BA and SGL 25BC respectively to quantify the variance in the pore

structure for commercial samples with and without MPLs. Both SGL 25BA and Freudenberg H2315 I6 show relatively small variation in pore structure. SGL 25BC shows larger variation, particularly in the macro-porous region (d_p > 30 µm). By comparing the pore size distributions of the in-house fabricated MPLs and SGL 25BC in Figure 6.3 (which both use SGL 25BA as substrate) with uncoated SGL 25BA (Figure 6.5) it seems that the presence of the MPL modifies the measured pore size distribution in the macro-porous region.

Table 6.1: Areal weight measurements of 25 cm^2 Freudenberg I3C1 and in-house MPL coated SGL25BA

Freudenberg I3C1		SGL 25BA (11.9 wt% ink)		SGL 25BA (14.9 wt% ink)	
Sample	Mass (mg)	Sample	Mass (mg)	Sample	Mass (mg)
1	289.6	1	154.7	1	176.2
2	307.7	2	158.4	2	181.1
3	360.1	3	158.4	3	171.7
4	299.0	4	156.8	4	183.5
5	312.8	5	154.1	5	171.9
6	296.9	6	161.6	6	186.2
Areal weight (g/m^2)	124 ± 20	Areal weight (g/m^2)	62.9 ± 2.2	Areal weight (g/m^2)	71.4 ± 4.9

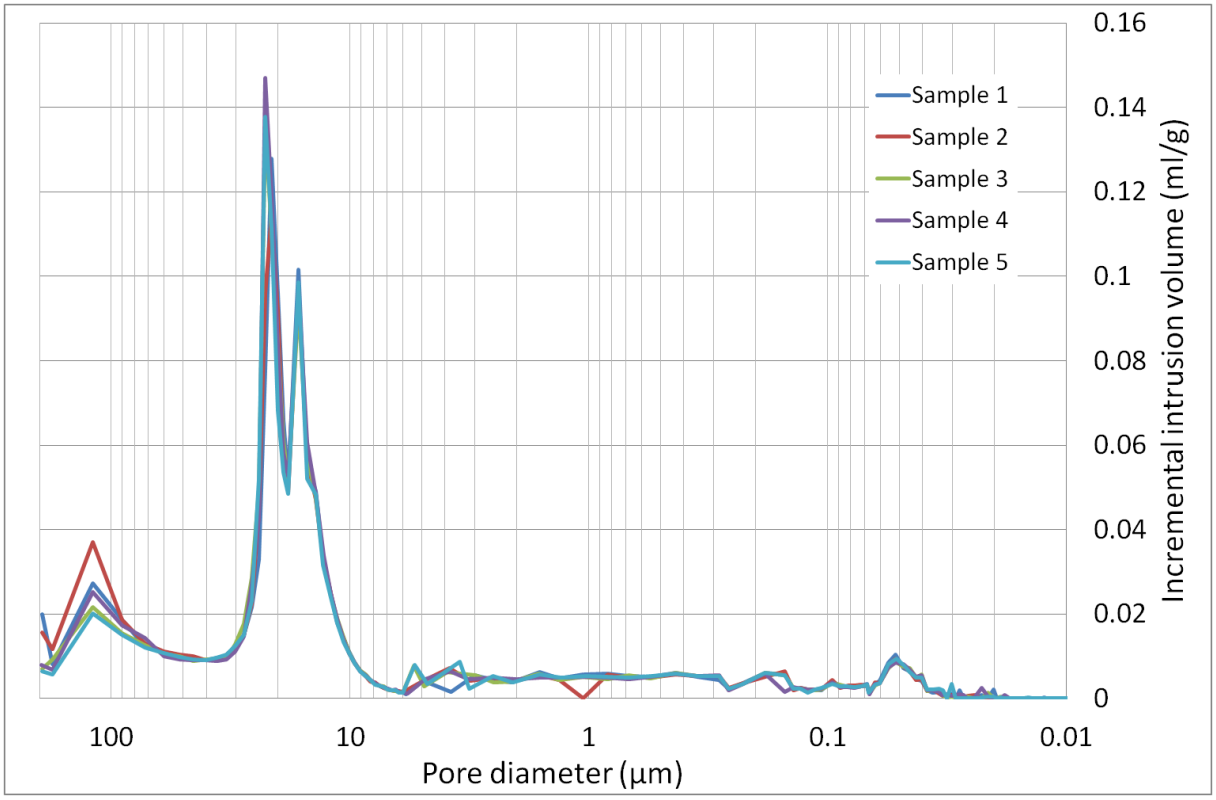

Figure 6.4: Pore size distribution of repeat 25 cm^2 samples of Freudenberg H2315 I6

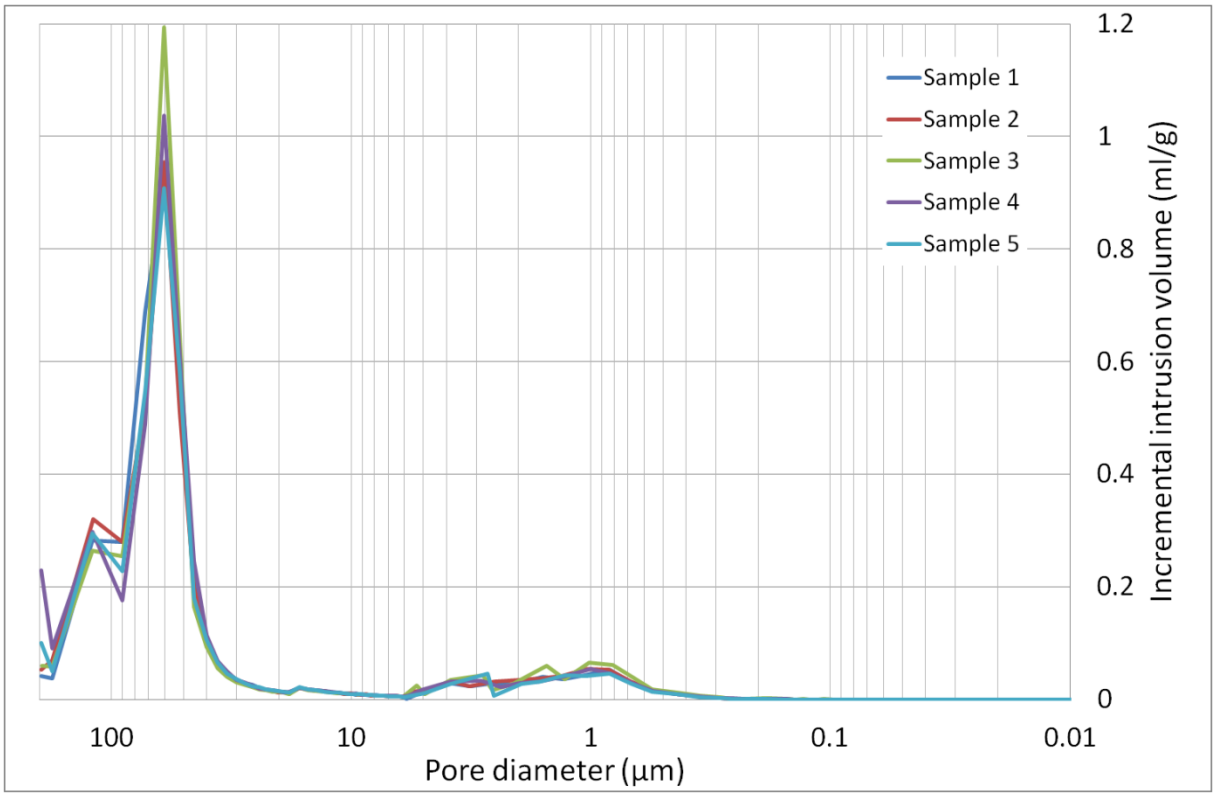

Figure 6.5: Pore size distribution of repeat 25 cm^2 samples of SGL 25BA

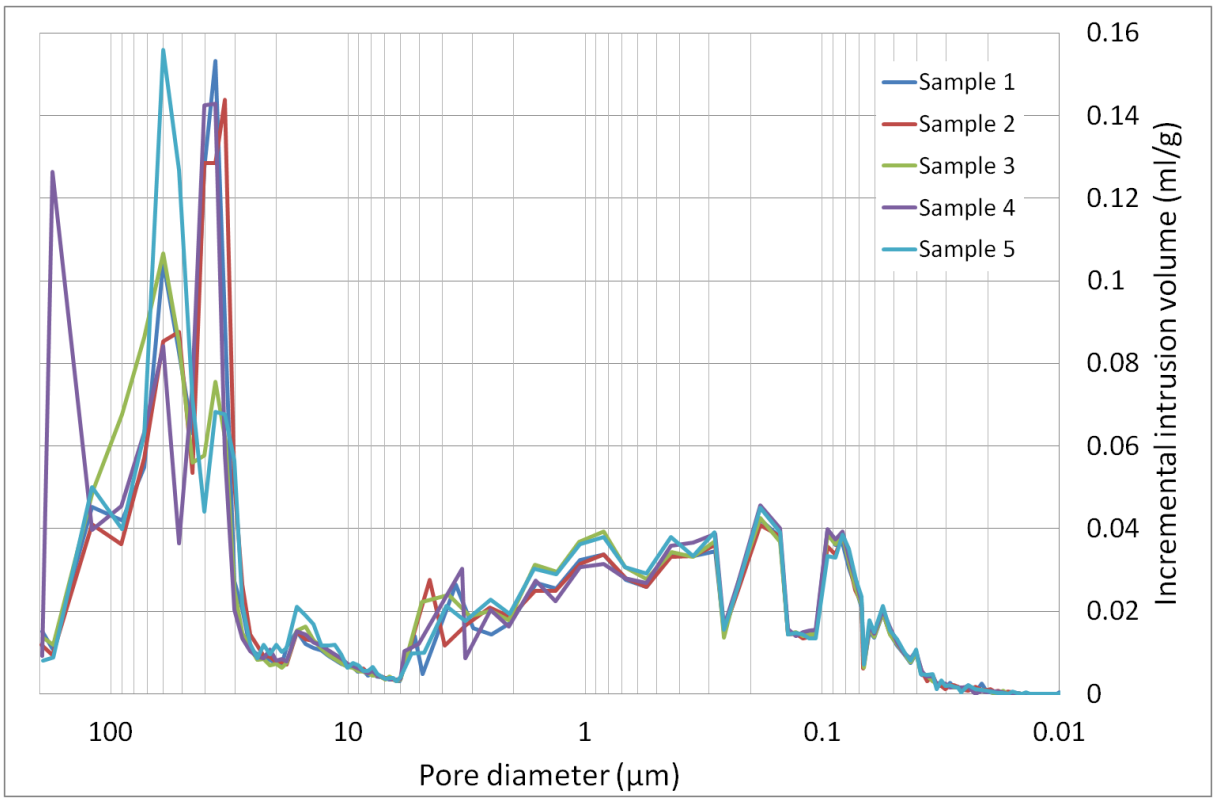

Figure 6.6: Pore size distribution of repeat 25 cm^2 samples of SGL 25BC

The following table summarizes the variation in porosity and (volume based) median pore diameter from the MIP analysis:

Table 6.2: Microstructure variation across commercial GDL samples

	Freudenberg H2315 I6		SGL 25BA		SGL 25BC	
Sample	ε (%)	$\tilde{d}_p$ (μm)	ε (%)	$\tilde{d}_p$ (μm)	ε (%)	$\tilde{d}_p$ (μm)
1	44.6	21.13	51.8	70.01	44.6	28.36
2	45.3	21.62	50.8	69.17	45.0	28.82
3	43.9	21.09	52.6	67.85	43.0	14.18
4	44.4	21.28	52.0	68.14	44.7	21.13
5	42.2	20.82	51.4	70.77	43.9	14.78
Average	44.1 ± 2.3	21.19 ± 0.59	51.7 ± 1.3	69.2 ± 2.5	44.2 ± 1.6	21 ± 14

The median pore diameter is most sensitive to meso- and macro-porous variation due to the relatively large associated volumes. Table 6.2 quantitatively shows that the variation in large pores (GDL pores) is small for SGL 25BA and Freudenberg H2315 I6 but relatively large for SGL 25BC. This suggests that the MPL may modify the measured pore structure of the GDL in a variable manner. The porosity variation is small across all measured samples.

The variation in areal weight for SGL 25BA, SGL 25BC and Freudenberg H2315 I6 were measured from ten random 25 cm^2 samples with the results tabulated below.

Table 6.3: Areal weight measurements of 25 cm^2 commercial GDL samples

Freudenberg I6		SGL 25BA		SGL 25BC	
Sample	Mass (mg)	Sample	Mass (mg)	Sample	Mass (mg)
1	295.2	1	94.8	1	222.3
2	297.2	2	96.2	2	220.0
3	300.2	3	96.3	3	220.5
4	293.9	4	95.5	4	220.8
5	297.8	5	96.7	5	224.4
6	302.7	6	96.0	6	220.3
7	296.6	7	95.1	7	223.0
8	293.6	8	94.5	8	225.0
9	298.4	9	93.3	9	229.0
10	301.6	10	93.1	10	229.4
Areal weight (g/m^2)	119.1 ± 2.5	Areal weight (g/m^2)	38.06 ± 0.99	Areal weight (g/m^2)	89.4 ± 2.8

The specified areal weights for SGL 25BA and SGL 25BC are 40 ± 10 and 86 ± 10 g/m^2 respectively. Both these values are in good agreement with the measured values. The following equation relates areal weight, porosity and thickness:

$$\rho\bar{x}(1-\varepsilon) = A_w$$

Where ρ is the real density of the solid component of the GDL, $\bar{x}$ is the average GDL thickness, ε is porosity and A_w is the areal weight. Therefore, assuming a constant real density, for a fixed porosity and areal weight the average thickness is fixed and calculable.

The density of carbon (either in the form of fibres or carbon black powder) is between 1.7 and 2.2 g/cm^3 and the density of PTFE is about 2.2 g/cm^3. Therefore the real density of GDL (with or without MPL) should also be between these values. Using the above equation for commercial specifications for thickness and areal weight, the porosity of SGL 25BA should be between 88 % and 90 % and that of SGL 25BC should be between 78 % and 83 %. The porosity values found from MIP are significantly lower than this and give non-realistic density values. El-kharouf et al. (2012) measured porosities of 66.2 % and 36.5 % for SGL 25BA and SGL 25BC respectively. These values also fall outside the range of realsitic porosities based on the commercial specifications for the materials. Both the areal weights and thicknesses of the samples measured in this study are in close agreement with commercial specifications and therefore it can be concluded that not all of the void space is filled during porosimetry analysis, resulting in an underestimate of porosity for the samples.

6.1.3 Scanning electron microscopy MPL thickness measurements

Figure 6.7 shows a SEM cross section and thickness measurement of SGL 25BA GDL coated with an MPL of ink composition 1 (cf. Table 5.1). Figure 6.8 shows the same analysis applied to an MPL fabricated from ink composition 2.

During analysis it was evident that the freeze-fracture method used for sample preparation caused some deformation of the MPL along the cross-section and isolating a region for an accurate thickness measurement was challenging. Comparing the two measured cross-sectional MPL thicknesses, increasing the solids wt% of the MPL ink from 11.9 to 14.9 approximately doubled the final MPL layer thickness. It should also be noted that it is not always easy to distinguish between the MPL and PTFE within the GDL and therefore the degree of penetration of the MPL into the GDL is difficult to measure.

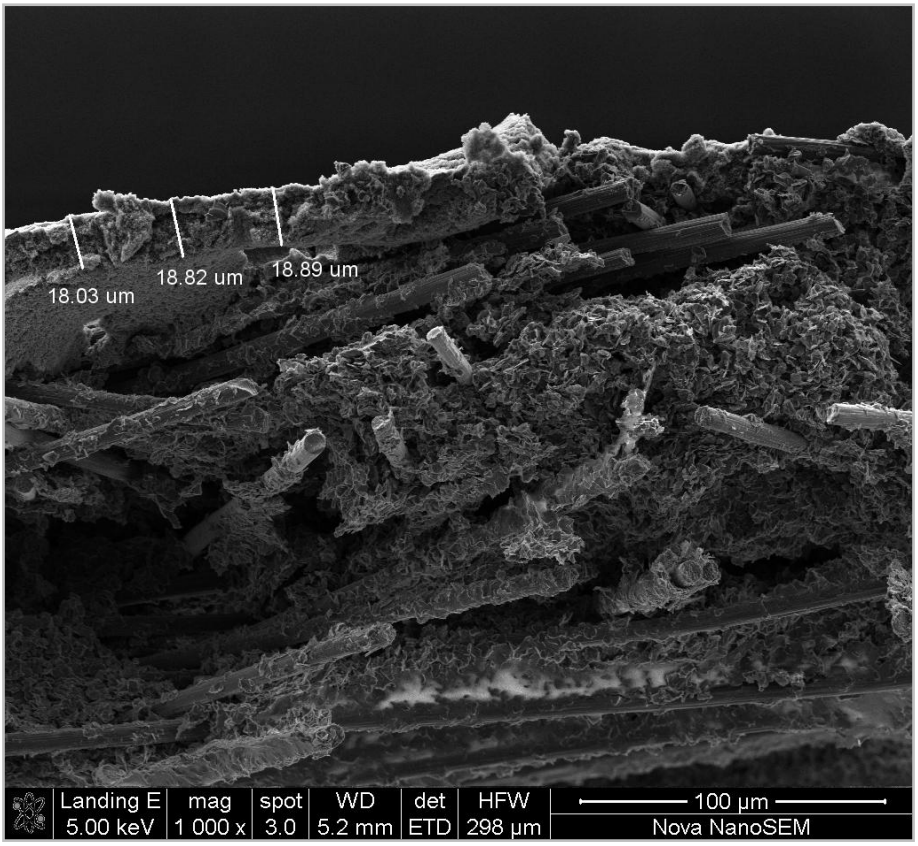

Figure 6.7: SEM image of 11.9 solids wt% MPL prepared by freeze-fracture

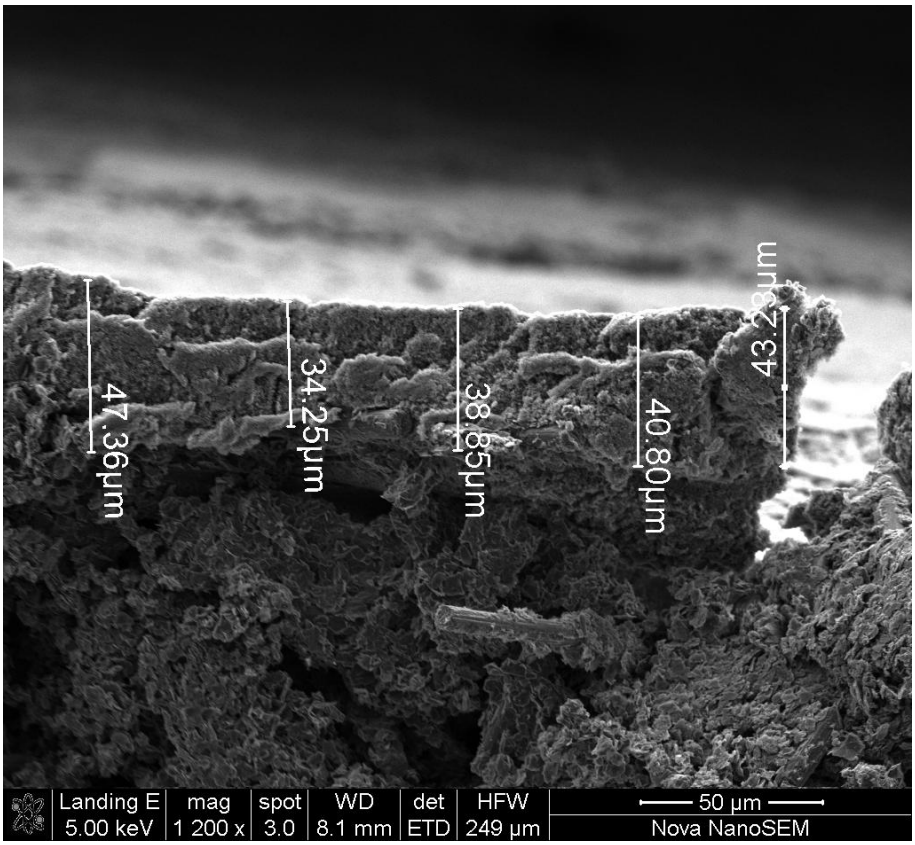

Figure 6.8: SEM image of 14.9 solids wt% MPL prepared by freeze-fracture

6.1.4 Computed tomography MPL thickness analysis

Figure 6.9 shows a 3D volume rendering of a scanned SGL 25BA GDL coated with an MPL fabricated using 11.9 solids wt % ink (composition 1). Also shown is the colour coded thickness analysis result for the sample. Qualitatively it seems the average thickness is in the vicinity of 20 microns (cf. the SEM image in Figure 6.7) but it is also clear that there is a relatively large distribution of thicknesses across the sample. Additionally the topography of the MPL is influenced by the substrate structure and the fibres are visible on the surface.

Figure 6.10 shows a similar 3D volume image with thickness measurement for the MPL fabricated from ink composition 2 (14.9 solids wt %). This MPL was extracted from a sample of an MEA using the procedure described in Section 5.2.1. Again it is clear that even with the thicker MPL there is a range of thickness distributions. Five samples from a 25 cm^2 MEA were scanned after electrochemical testing and the thickness distributions of the MPLs in each sample quantified. These distributions are plotted in Figure 6.11 to Figure 6.15.

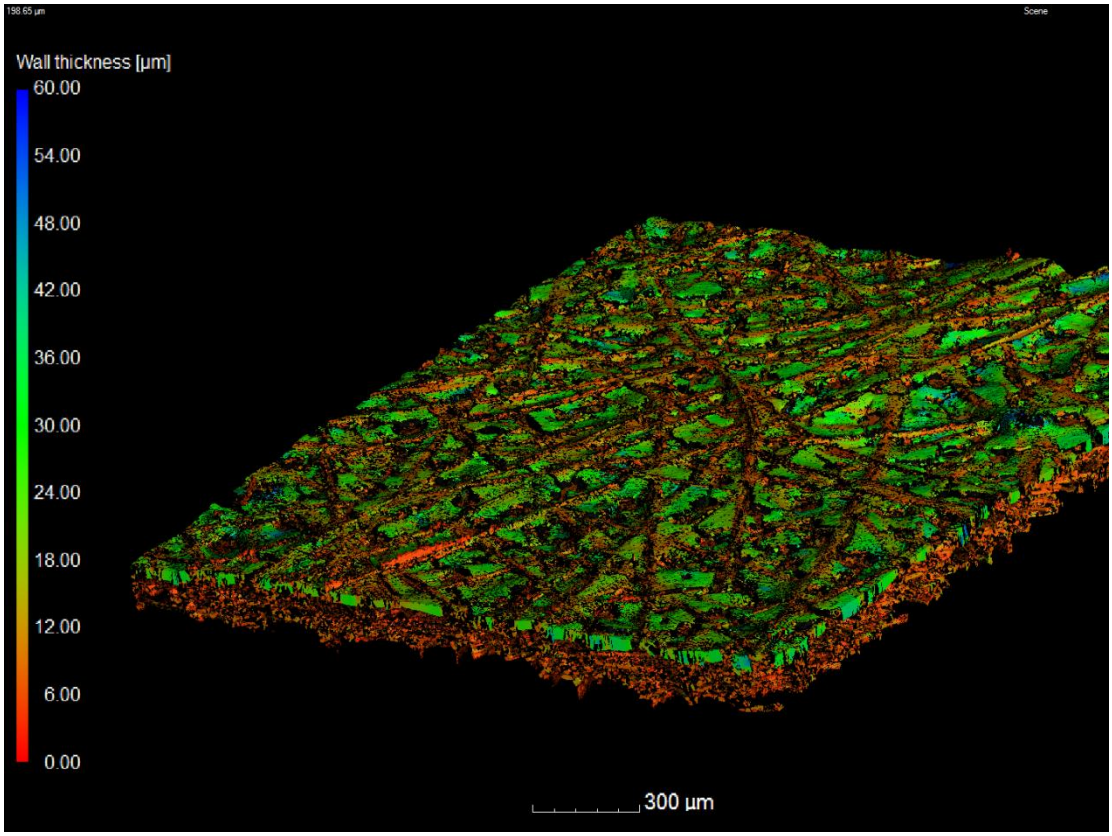

Figure 6.9: X-ray µCT 3D volume rendered image of (11.9 solids wt% ink) MPL with thickness analysis

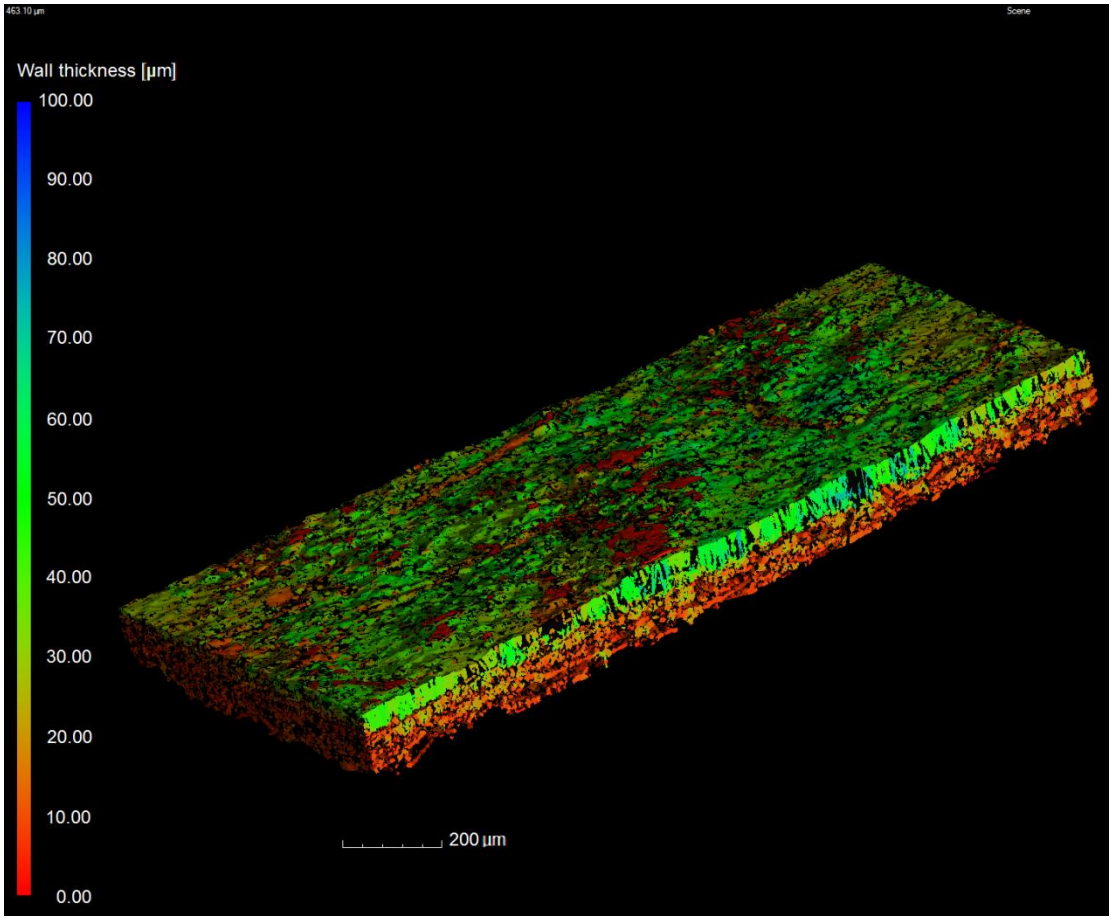

Figure 6.10: X-ray µCT 3D volume rendered image of (14.9 solids wt% ink) MPL virtually extracted from MEA

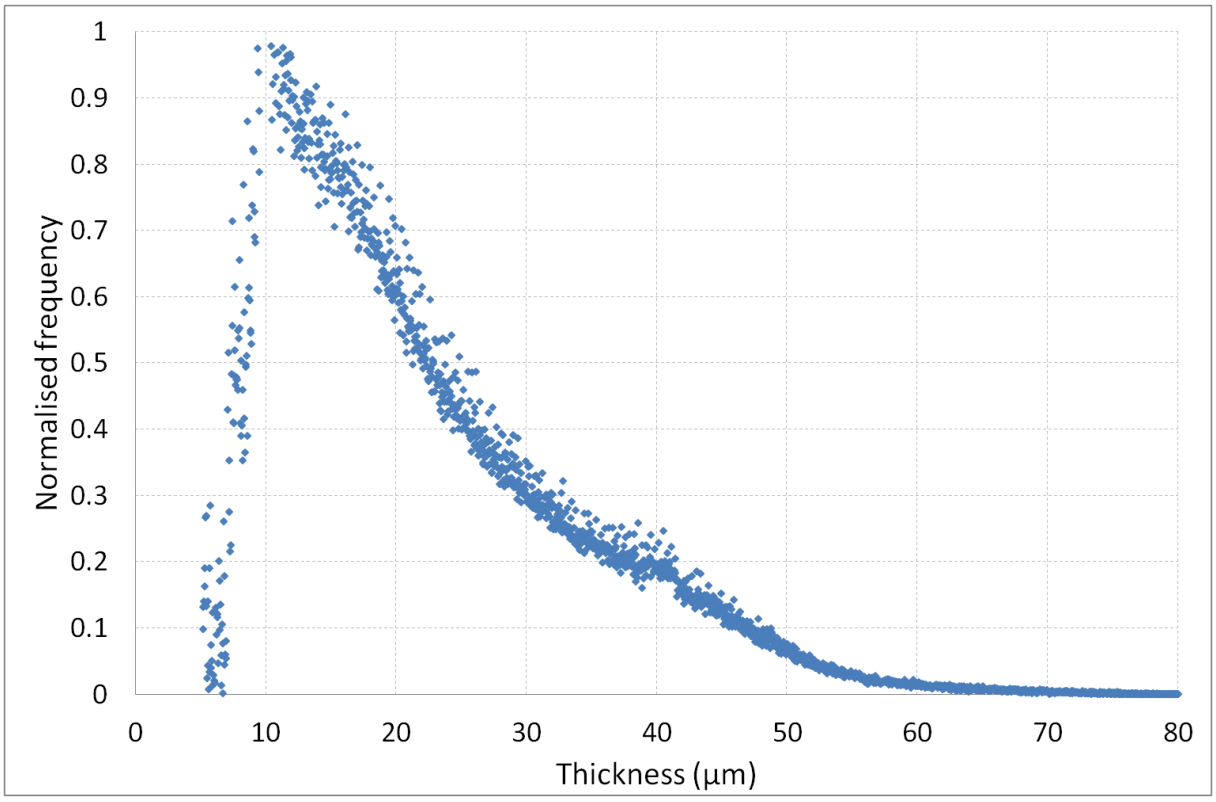

Figure 6.11: MPL thickness distribution MEA sample 1

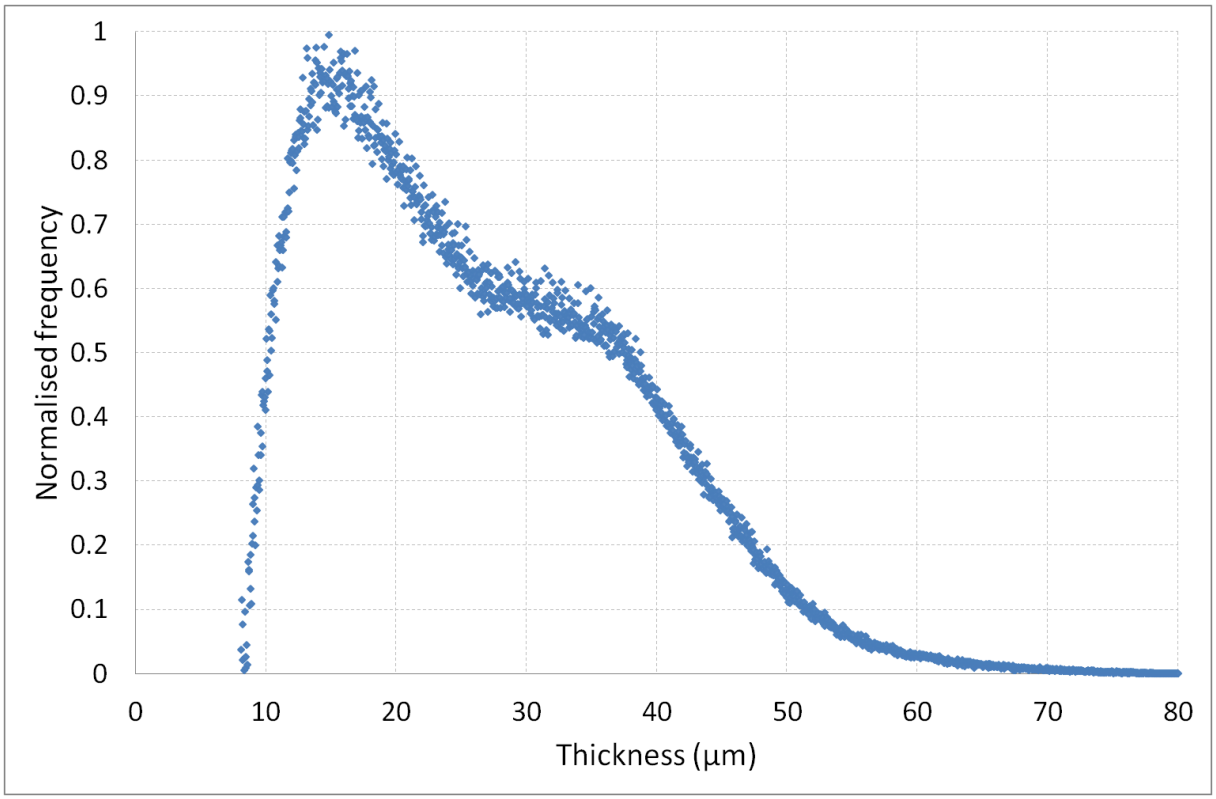

Figure 6.12: MPL thickness distribution MEA sample 2

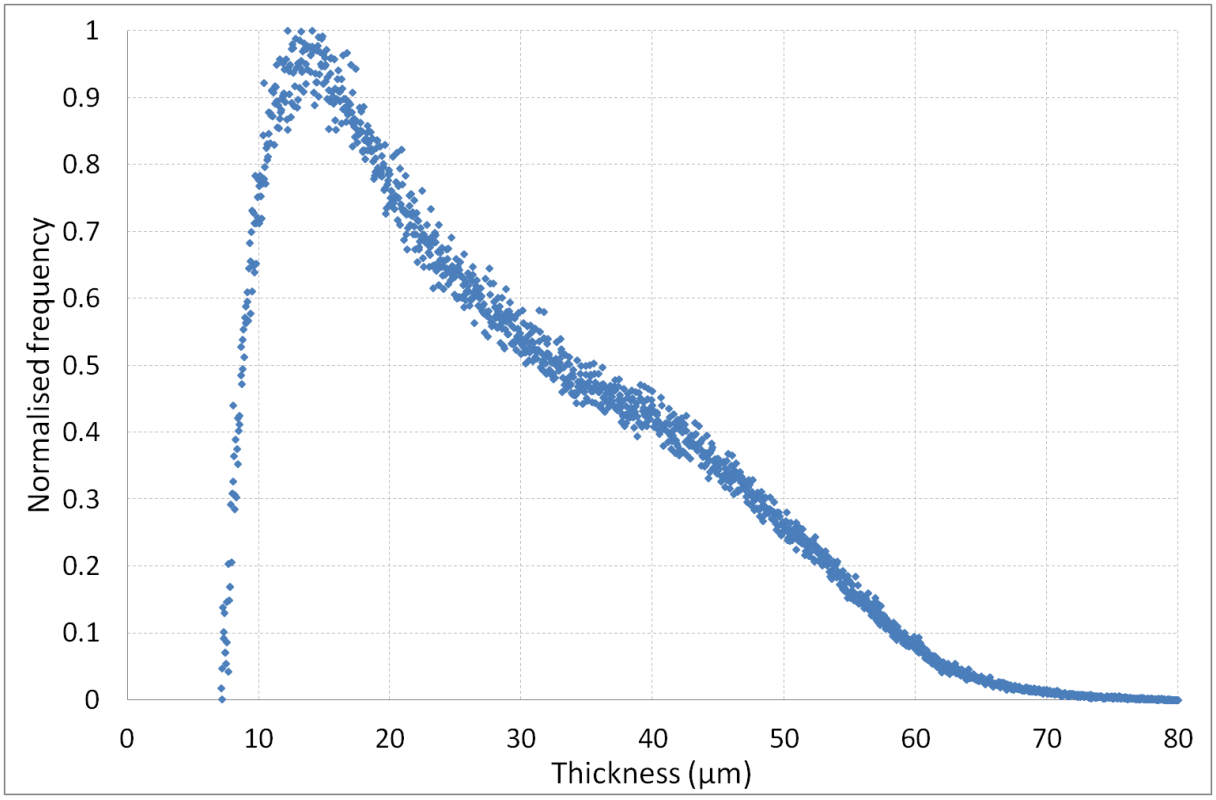

Figure 6.13: MPL thickness distribution MEA sample 3

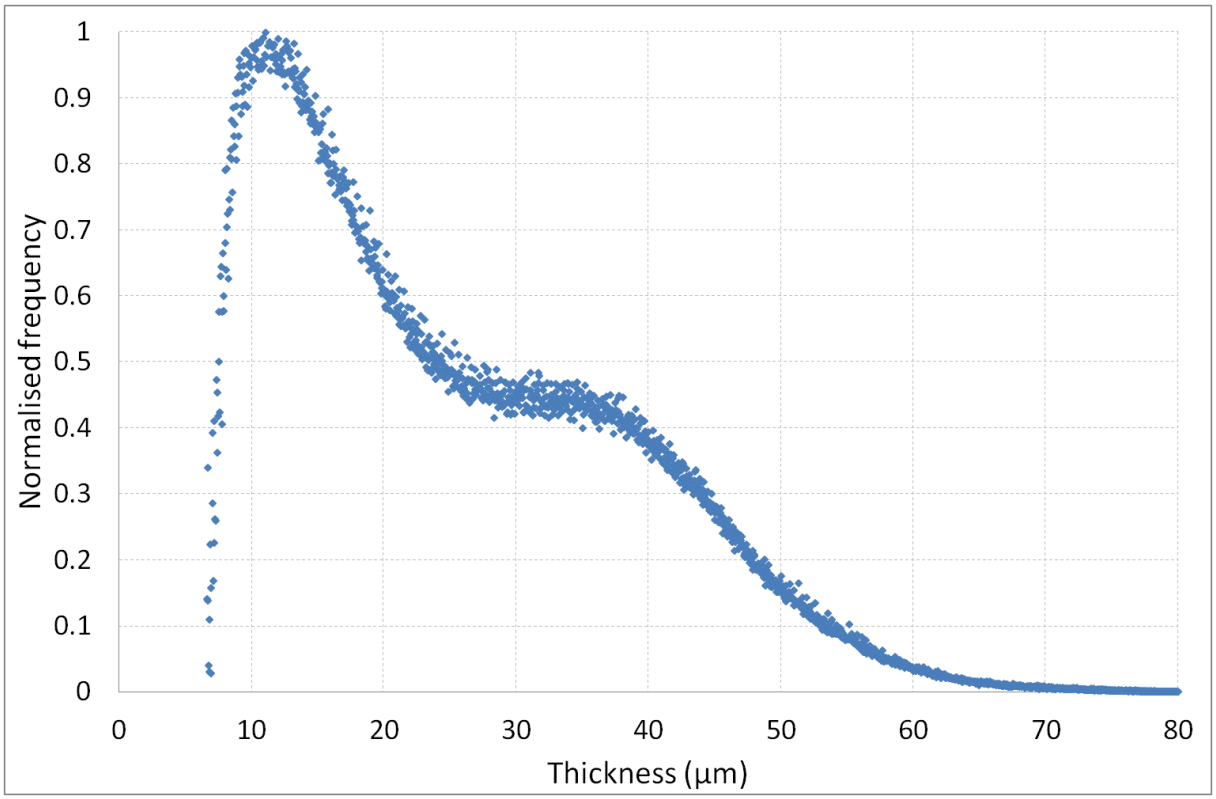

Figure 6.14: MPL thickness distribution MEA sample 4

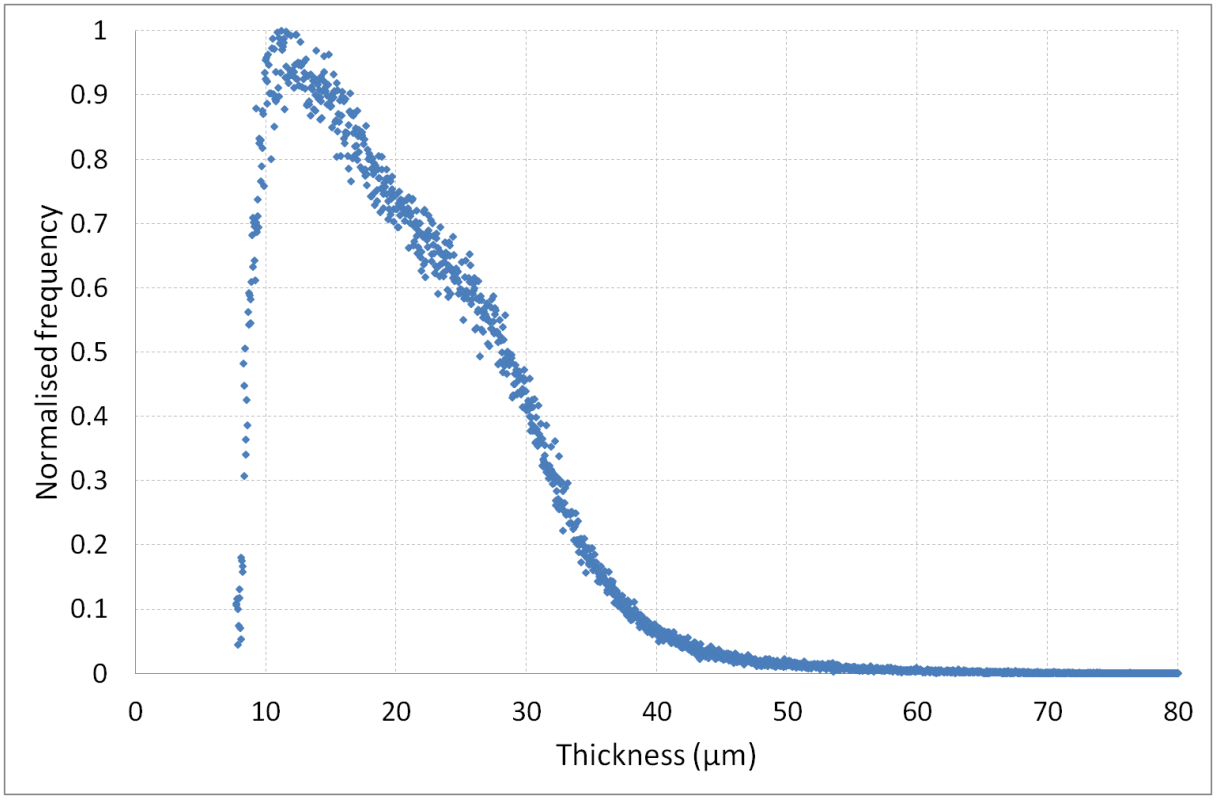

Figure 6.15: MPL thickness distribution MEA sample 5

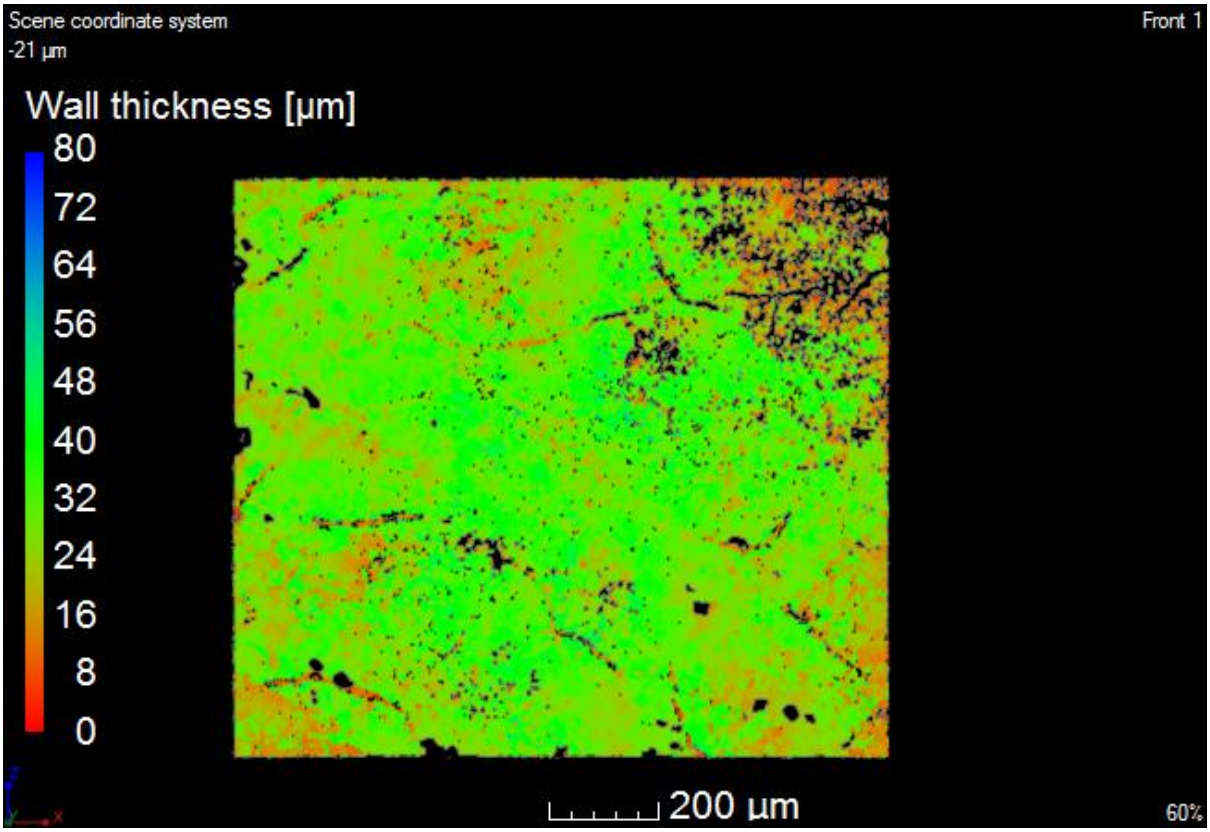

Figure 6.16: In-plane cross section of MPL (MEA sample 2) showing thickness distribution

From the MPL thickness distribution plots it is evident that MPL thickness follows an overlapping bimodal distribution with the major mode being about 15 µm and the minor mode varying between 25 and 35 µm. The thinner regions of the MPL are associated with samples 5 and 1 (cf. Figure 5.12) which are from the same side of the MEA. This may be due to the deposition or drying treatment of the MPL during fabrication.

Figure 6.16 shows an in-plane cross-section of an MPL sample to better visualise the thickness distribution. Black regions are caused by thin MPL areas and non-ideal alignment of MPL relative to z-axis because it is not perfectly flat. The thin and thick regions are distributed over the entire surface.

Based on these results, µCT analysis of the MPL is able to provide more detailed MPL thickness information than conventional SEM measurements. In this case the technique was destructive as samples had to be small (about 20 mm^2) to maximise the resolution of the scan. However, (nano) CT equipment does exist which can achieve sub-micron resolutions with much larger sample sizes. Therefore it is possible to non-destructively scan and analyse an entire 25 cm^2 MEA in a similar manner.

6.2 Electrochemical performance

Figure 6.17 shows a typical conditioning process during the MEA variance testing component of this study. The fresh MEA benefits from a substantial improvement in performance as a result of the conditioning at low relative humidity. There is a corresponding decrease in ohmic resistance with performance improvement, implying that membrane hydration is improving with each conditioning cycle. The performance and ohmic resistance level out after 11 cycles at low RH.

The ohmic resistance at high relative humidity conditioning is substantially lower than that a low relative humidity and does not change significantly during the conditioning process. This suggests that the original conditioning and electrochemical tests at low relative humidity prepare the MEA for rapid conditioning at high relative humidity.

Repeat polarization curves were measured to validate that the MEA was fully conditioned (and therefore giving stable performance). All polarization curves measured in this study gave highly precise repeat results as exemplified by Figure 6.18 to Figure 6.21 and therefore it can be concluded that the conditioning procedures were effective. The precision also suggests a well controlled system and equilibrated oxidant flow when changing between air and oxygen.

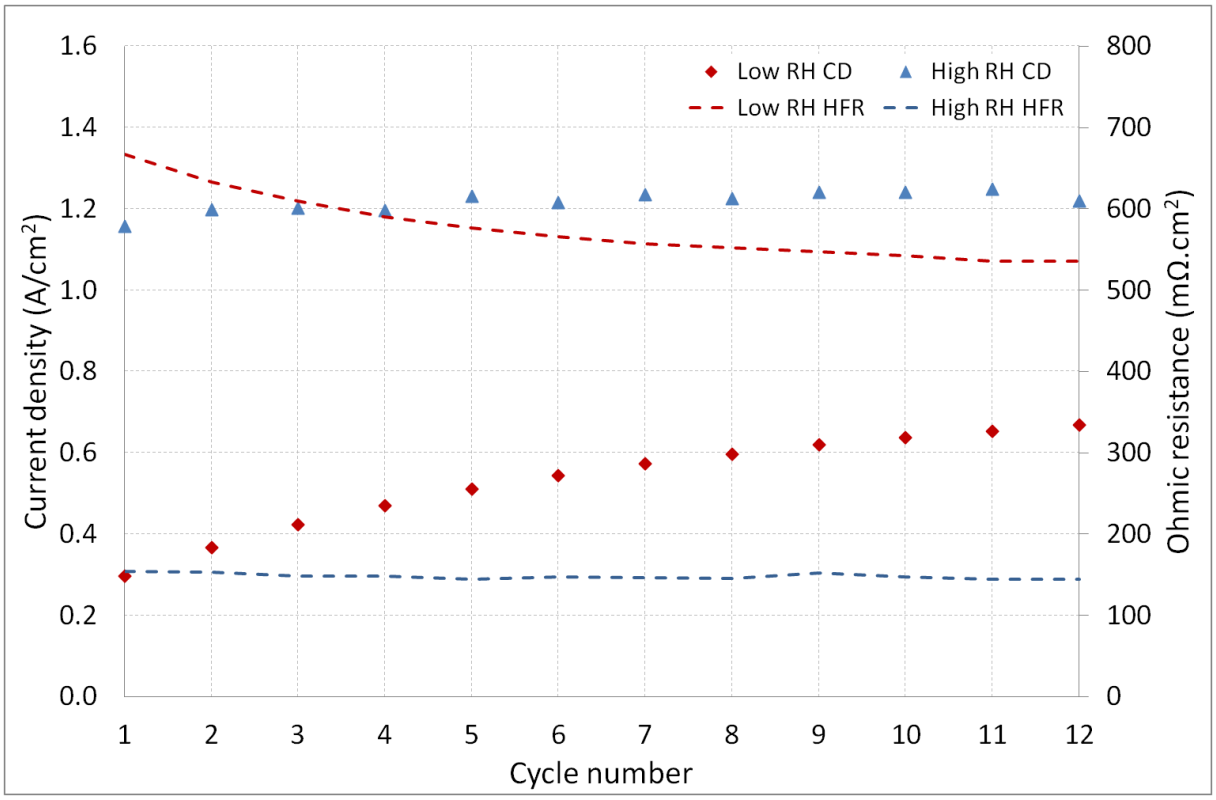

Figure 6.17: Conditioning MEA with Freudenberg H2315 I6 at cathode. Condition D and E

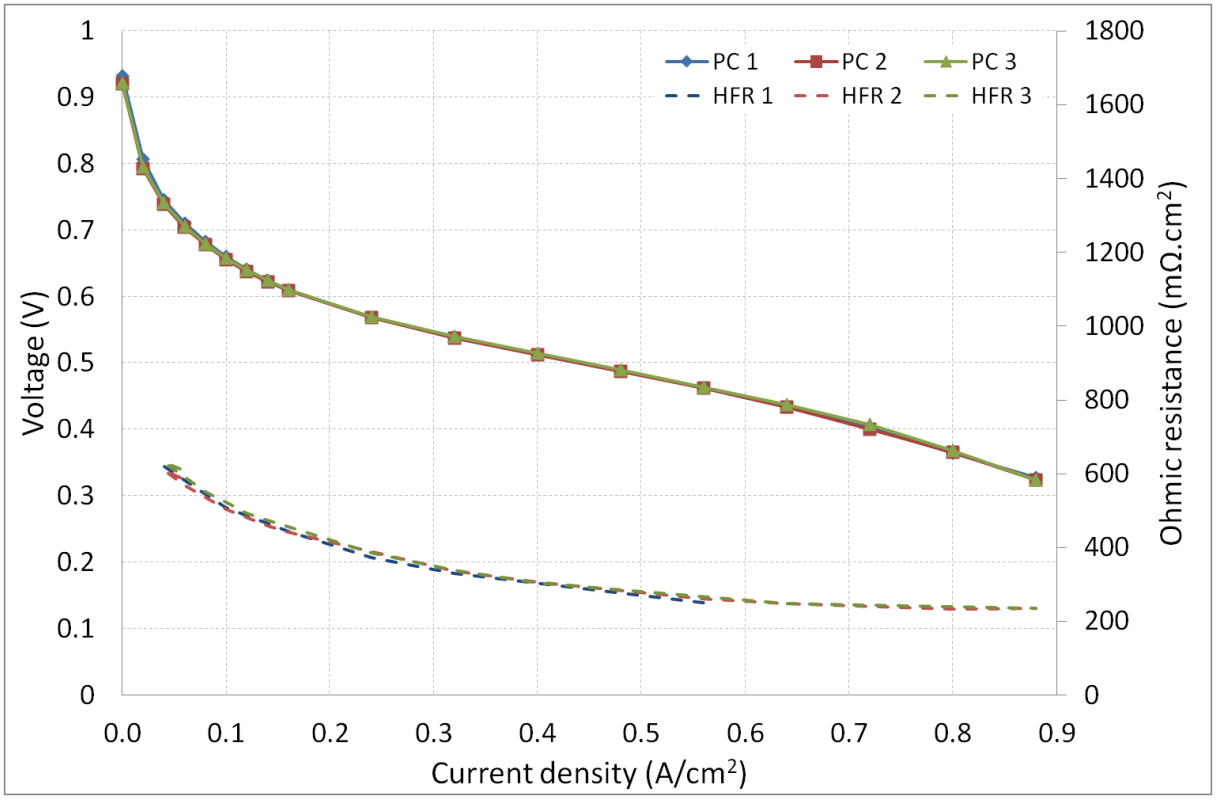

Figure 6.18: Repeat polarization curves with air showing stable performance. SGL 25BC Condition D

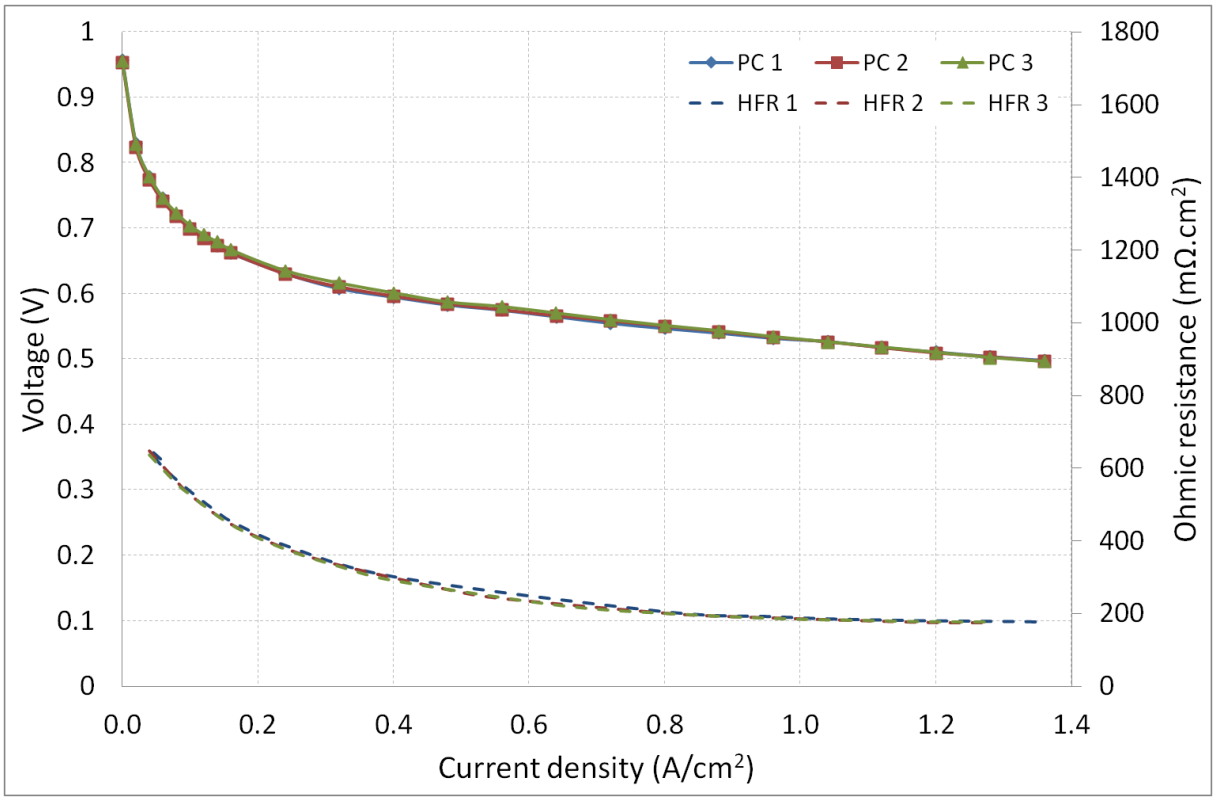

Figure 6.19: Repeat polarization curves with oxygen showing stable performance. SGL 25BC Condition D

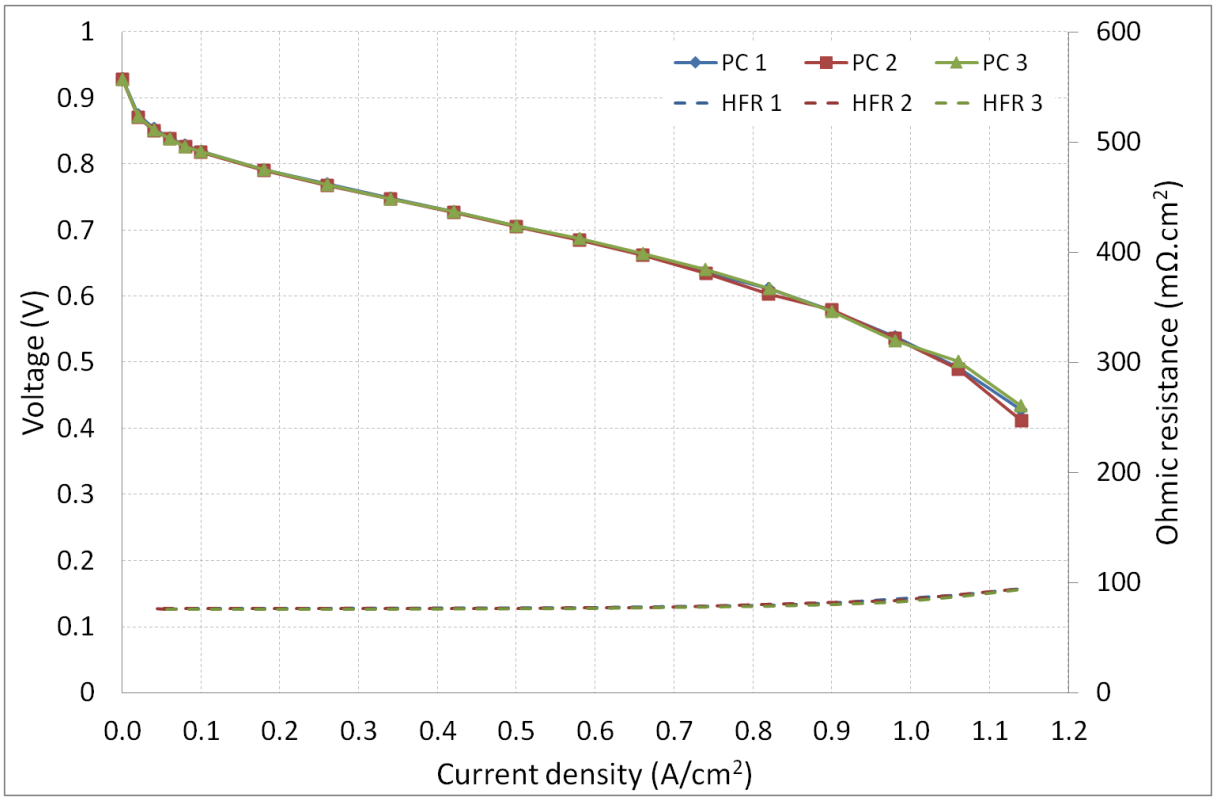

Figure 6.20: Repeat polarization curves with air showing stable performance. SGL 25BC Condition E

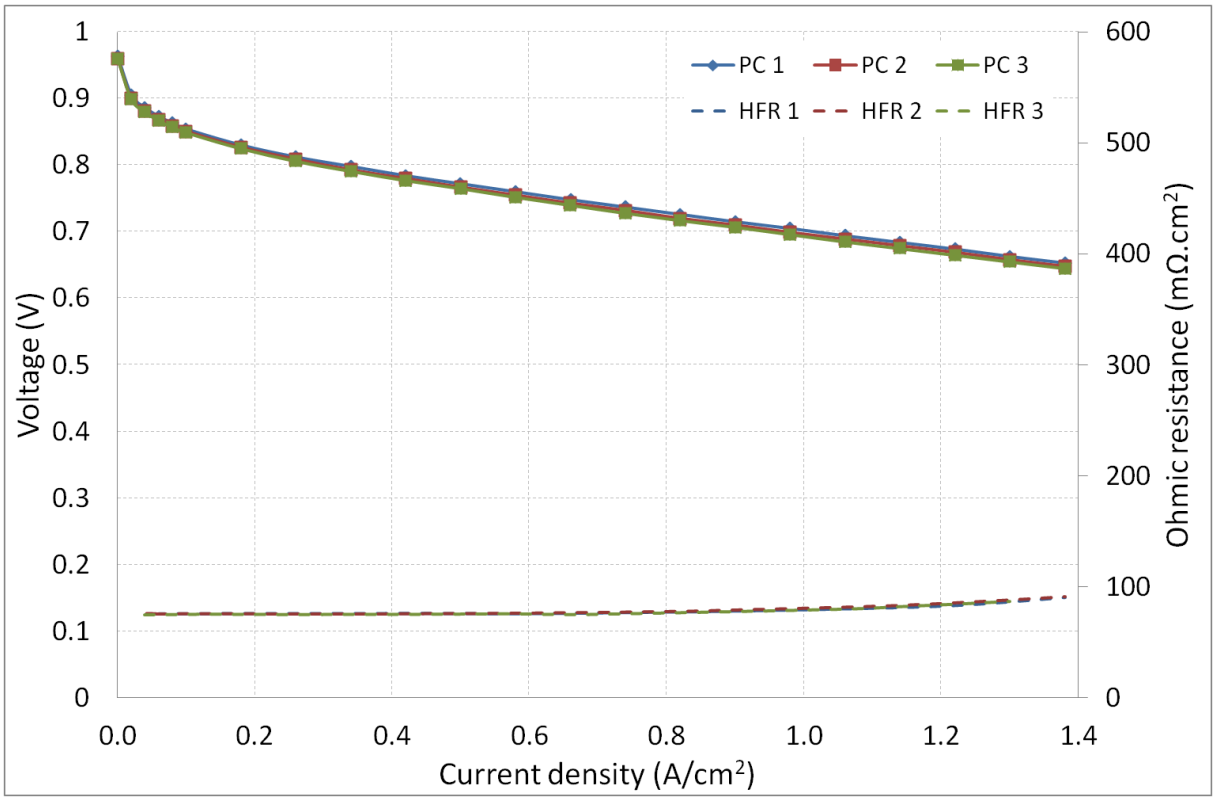

Figure 6.21: Repeat polarization curves with oxygen showing stable performance. SGL 25BC Condition E

6.2.1 High relative humidity testing with oxygen

In this study a 'run' is defined as an electrochemical test with a different assembled MEA with identical components. Figure 6.22 to Figure 6.24 show repeat runs of MEAs with different GDLs at the cathode, quantifying performance variance at high relative humidity operation with oxygen (Condition E in Table A.3 on the fold out page in Appendix A). At these conditions, both membrane hydration and mass transfer are favourable, and for low to moderate current density operation (where the risk of flooding is low) the effect of the GDL variations should be minimal. However the GDL may still affect contact resistance and water accumulation in the catalyst layer but it is unlikely the GDLs will offer variable electronic resistance because of the low variation in porosity and thickness shown in Section 6.1.3.

The ohmic resistance measurements across all three different GDLs were almost identical (apart from the single outlier for Run 5 SGL 25BA) indicating that the membrane hydration, contact resistances and conductivity of the fuel cell components were uniform across all tests at this condition. As such, any performance variation is likely a result of the catalyst layer behaviour during operation. Table 6.4 shows measured charge transfer resistances (CTR) obtained from the high frequency arc of EIS spectra as shown in Figure 6.25 for the different MEAs. There is a direct relationship between the polarization curves and the impedance spectra obtained for each MEA as can be seen by comparing the charge transfer resistances and the polarization curves for each run. The lower polarization curve for Freudenberg H2315 I6 Run 2 (Figure 6.22) has a correspondingly larger CTR.

Freudenberg H2315 I6 GDL showed the lowest performance variance from repeat testing which suggests that there is minimal variance in the Ion Power NR-211 CCMs. Omitting the outlier for SGL 25BA (Run 5), SGL 25BC shows the largest variation in performance across runs. This suggests that the MPL has variable efficacy across repeated runs and may hinder the integrity of the three phase boundary due to water management or resistance to mass transfer. This is supported by the fact that the variance increases with current density.

It is important to note that (regardless of the cause) there is variation at the benign condition of high RH operation with oxygen which intensifies under non-ideal operating conditions (as will be shown in the Sections to follow). The variation is not so large that it would be obvious from single measurement that there is an uncharacteristic result and therefore repeat measurements are critical to identify outliers and to statistically prove the significance of results. Such an analysis is shown in Section 6.2.4 to test the effect of the MPL on PEMFC performance at low RH operation with air as the oxidant.

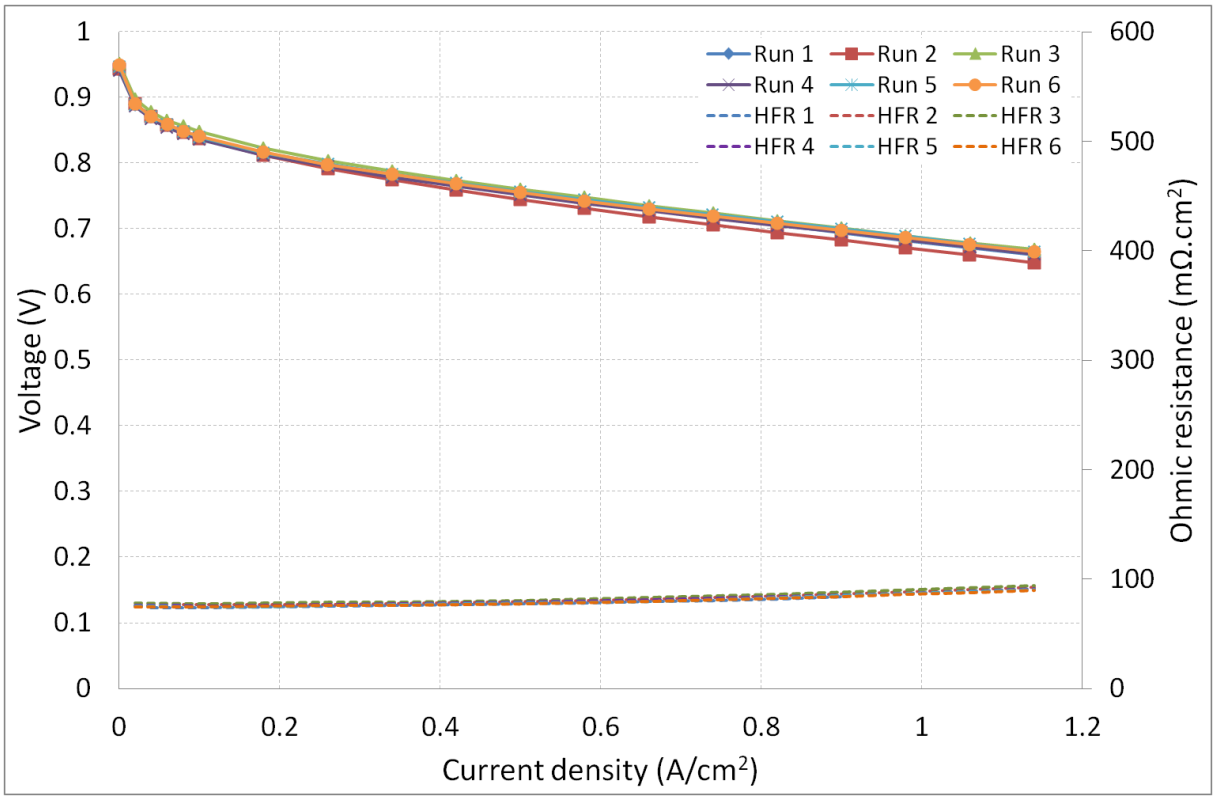

Figure 6.22: MEA performance variation at high RH with oxygen. Freudenberg H2315 I6 at cathode

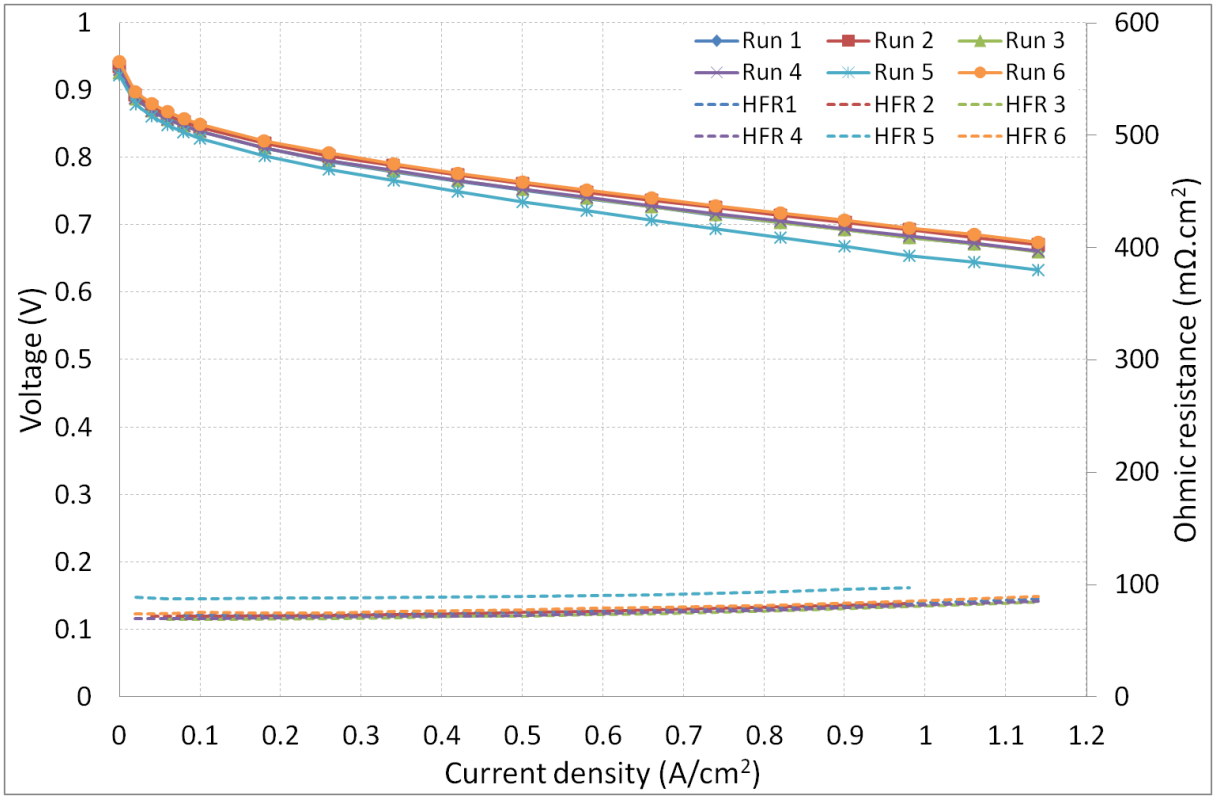

Figure 6.23: MEA performance variation at high RH with oxygen. SGL 25BA at cathode

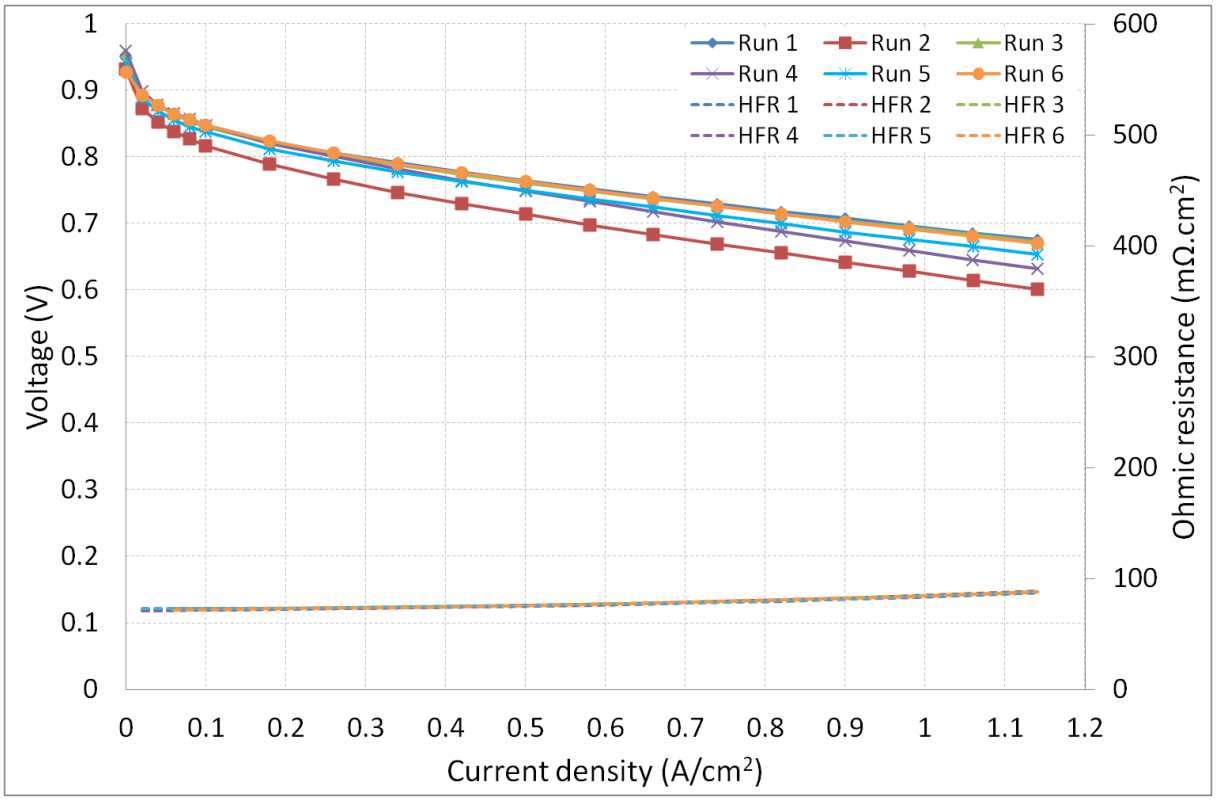

Figure 6.24: MEA performance variation at high RH with oxygen. SGL 25BC at cathode

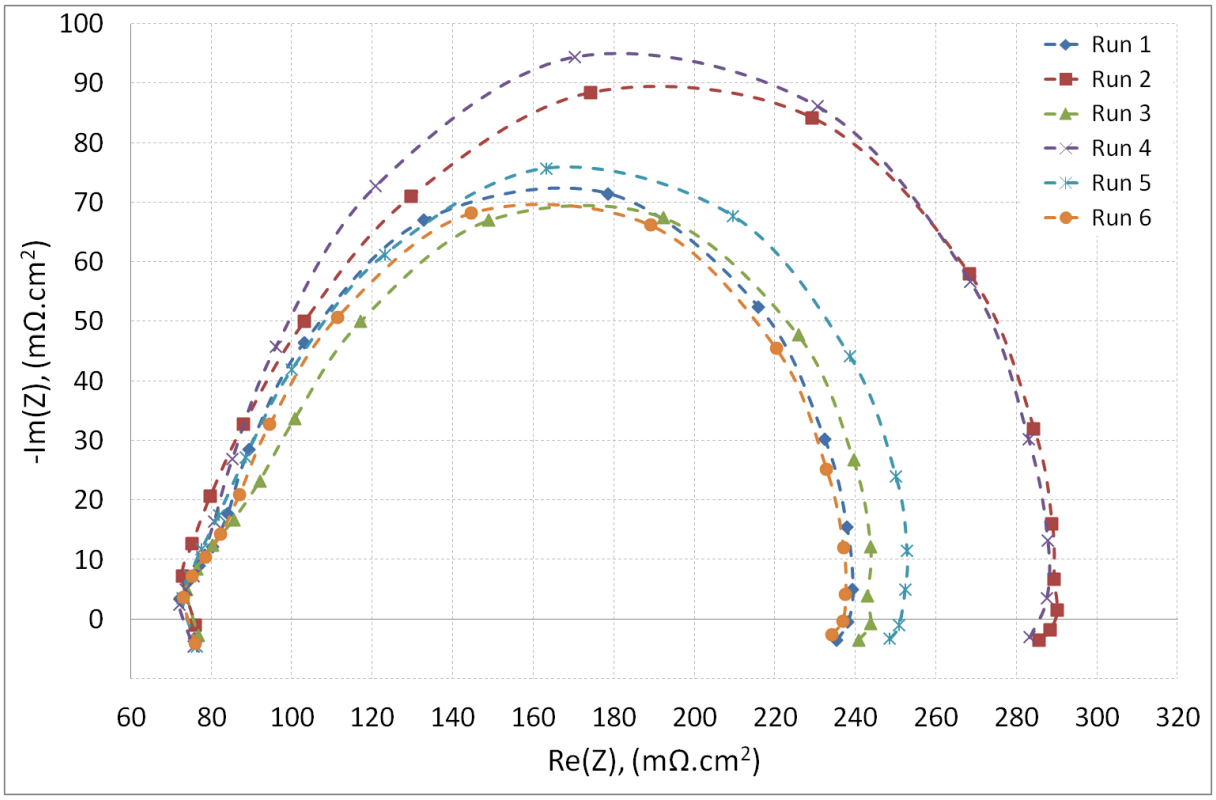

Figure 6.25: Impedance spectra at 300 mA/cm^2, high RH with oxygen. SGL 25BC at cathode

Table 6.4: Charge transfer resistances at 300 mA/cm^2 for repeat runs with different cathode PDM

Run	Freudenberg I6	SGL 25BA	SGL 25BC
	Charge transfer resistance (mΩ.cm^2)		
1	163	172	163
2	175	163	215
3	153	174	169
4	160	174	213
5	155	181	176
6	159	153	162

6.2.2 High relative humidity testing with air

Figure 6.26 to Figure 6.28 show polarization curves for repeat testing of the different GDLs at high relative humidity with air (Condition E in Table A.3). The variation is larger than that found with oxygen due to significant effect of the GDL on mass transfer resistances. Removing the outlier from the SGL 25BA data set shows that both the Freudenberg and SGL 25BA (GDLs without MPL) show relatively small variance compared with the SGL 25BC GDL (Figure 6.30). Section 6.1.2 quantified the variation in pore structure and areal weight of the different GDL materials and shows that SGL 25BC has the largest variability (see Table 6.2). Therefore there seems to be a correlation between electrochemical performance variation and variability in the physical structure of the cathode PDM.

As before, omitting the outlier from Run 5 SGL 25BA the ohmic resistances did not vary significantly for each MEA tested and therefore membrane hydration and GDL conductivity (including contact resistances) are not the cause of the performance variance.

It is obvious from Figure 6.30 that the MPL does not have a beneficial effect on performance at these conditions and could possibly have a negative effect. However, due to the similar mean values of overpotential and the relatively large variance, any conclusive result cannot be shown with statistical significance (which requires significantly different mean values and/or low variance as will be illustrated in Section 6.2.4).

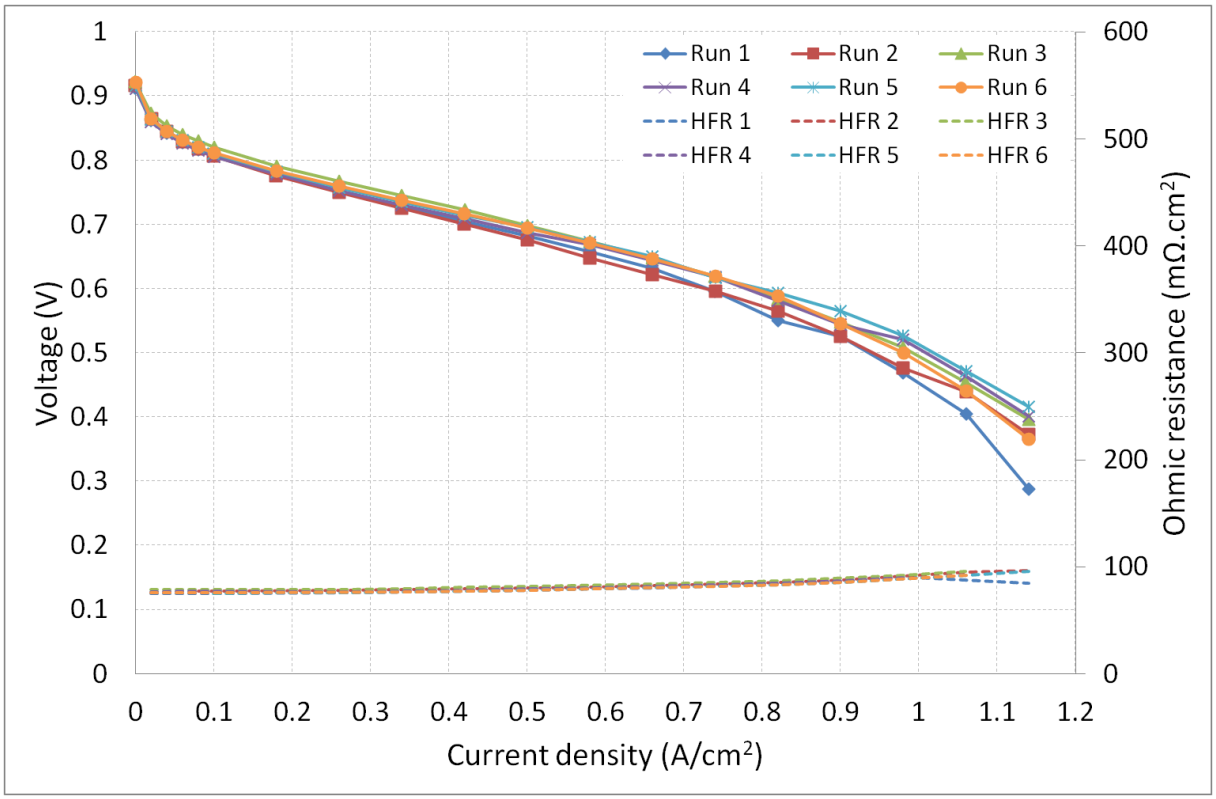

Figure 6.26: MEA performance variation at high RH with air. Freudenberg H2315 I6 at cathode

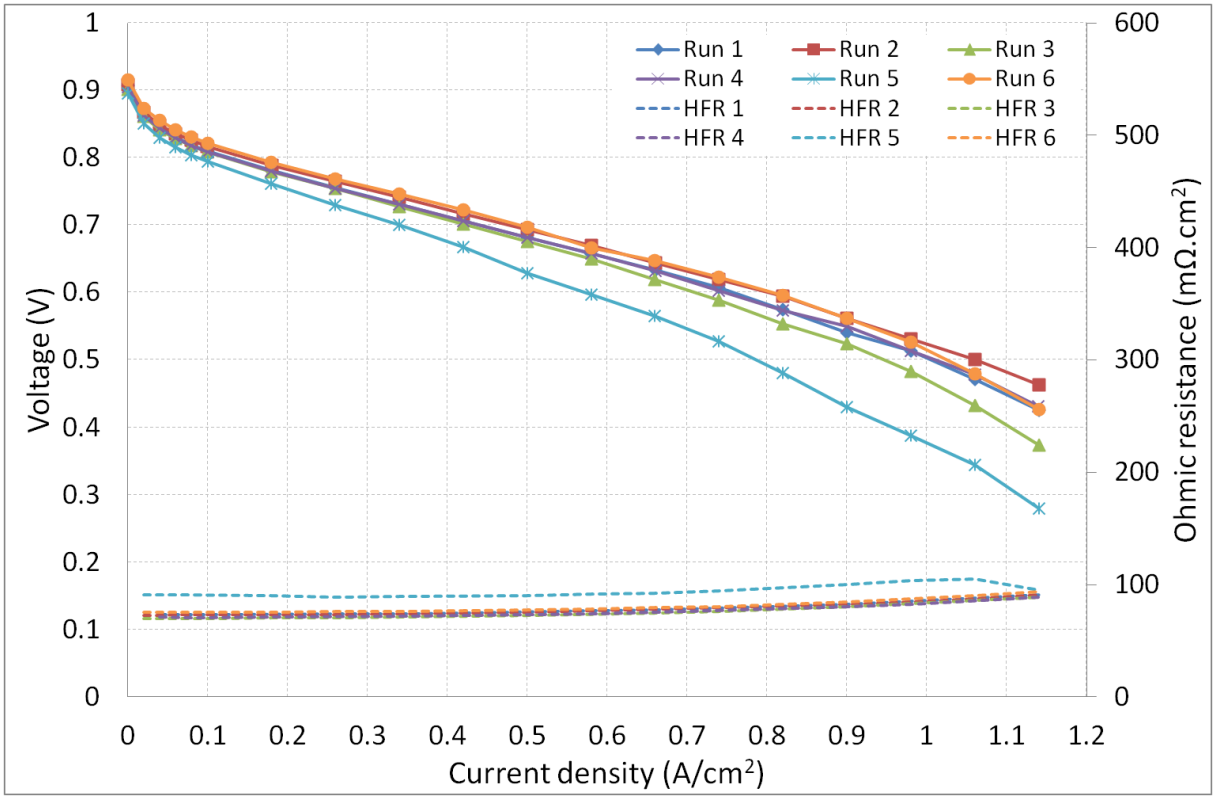

Figure 6.27: MEA performance variation at high RH with air. SGL 25BA at cathode

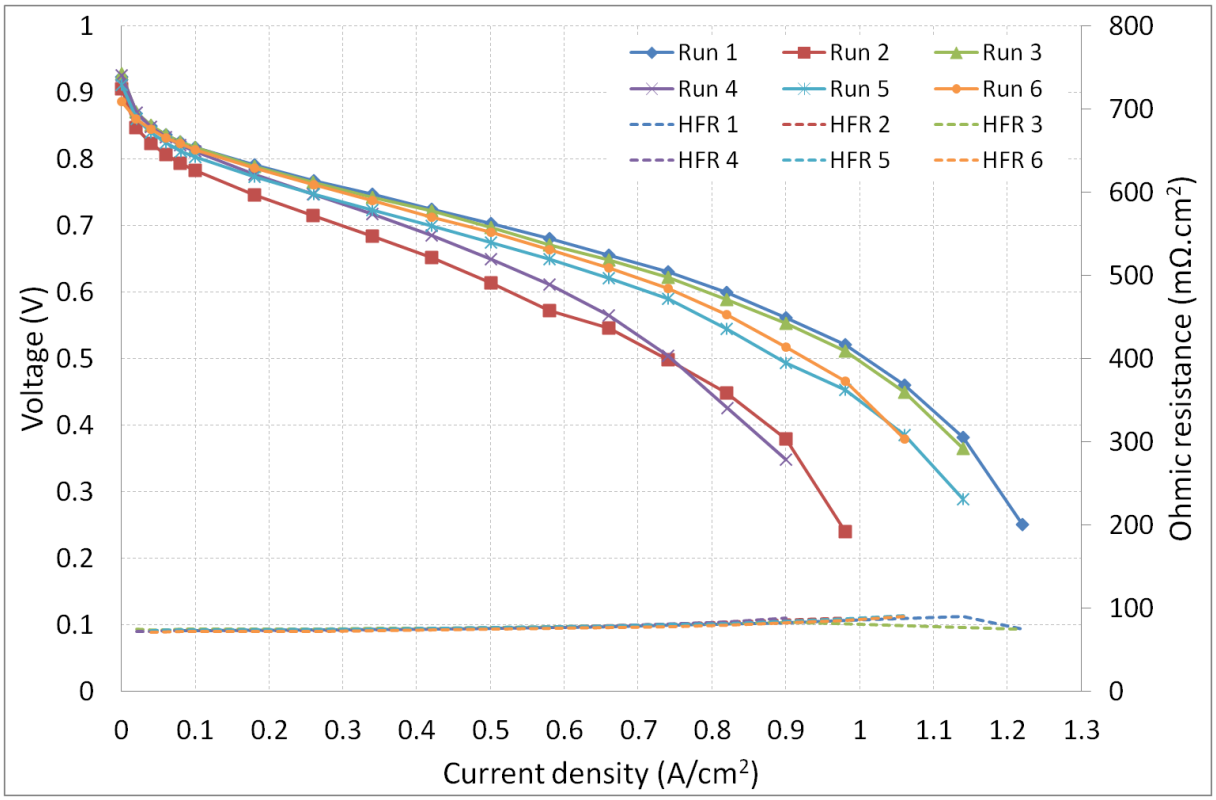

Figure 6.28: MEA performance variation at high RH with air. SGL 25BC at cathode

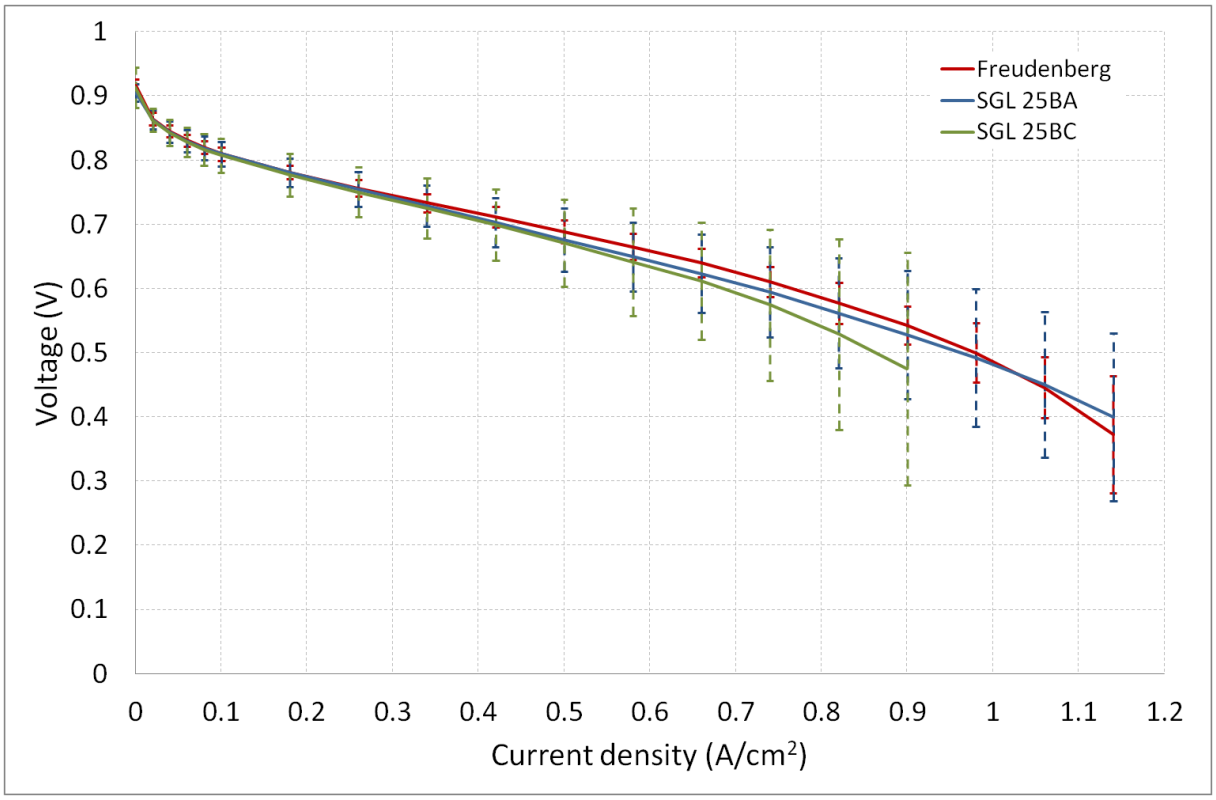

Figure 6.29: Comparison of MEA performance variation at high RH with air

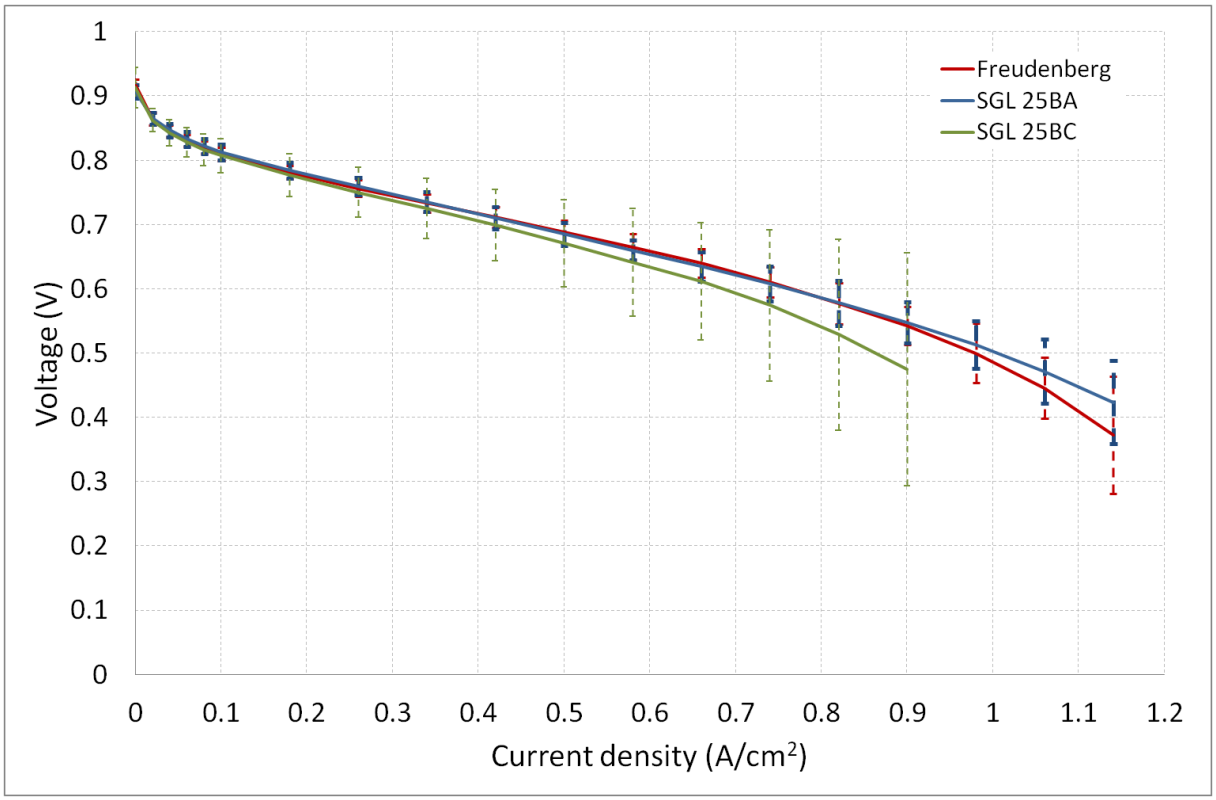

Figure 6.30: Comparison of MEA performance variation at high RH with air. SGL 25BA outlier omitted

6.2.3 Low relative humidity testing with oxygen

Figure 6.31 to Figure 6.36 show polarization curves and EIS measurements for repeat testing at low relative humidity with oxygen for the different GDLs. Previously at high relative humidity Run 2 with Freudenberg showed a slightly lower performance but the cause for this lower performance is greatly exaggerated at low RH operation. Also as previously, Run 5 for SGL 25BA shows the lowest performance but the difference between the other results is less noticeable than at high RH. The EIS plots in Figure 6.32, Figure 6.34 and Figure 6.36 clearly show that mass transfer resistances are present at these conditions even though testing with pure oxygen. However the shapes of the polarization curves are approximately linear up to 1.14 A/cm^2 and so the mass transfer resistance does not seem to have a direct effect on overpotential with increasing load.

Omitting the Freudenberg outlier (Run 2), Freudenberg and SGL 25BA show similar variance. As with the testing at high RH with air and oxygen, SGL 25 BC show the highest variance. The variance of SGL 25BC at low RH is larger than that at high RH for low and moderate current densities but similar for current densities greater than about 1 A/cm^2.

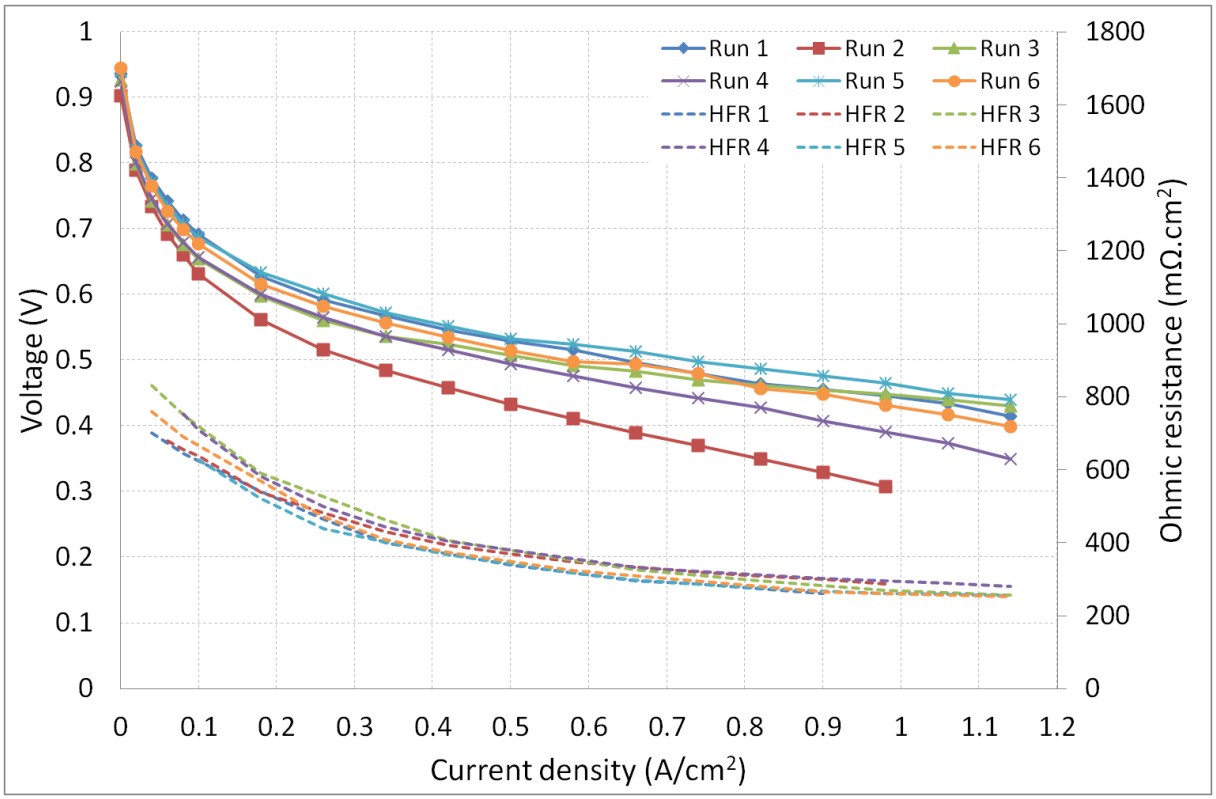

Figure 6.31: MEA performance variation at low RH with oxygen. Freudenberg H2315 I6 at cathode

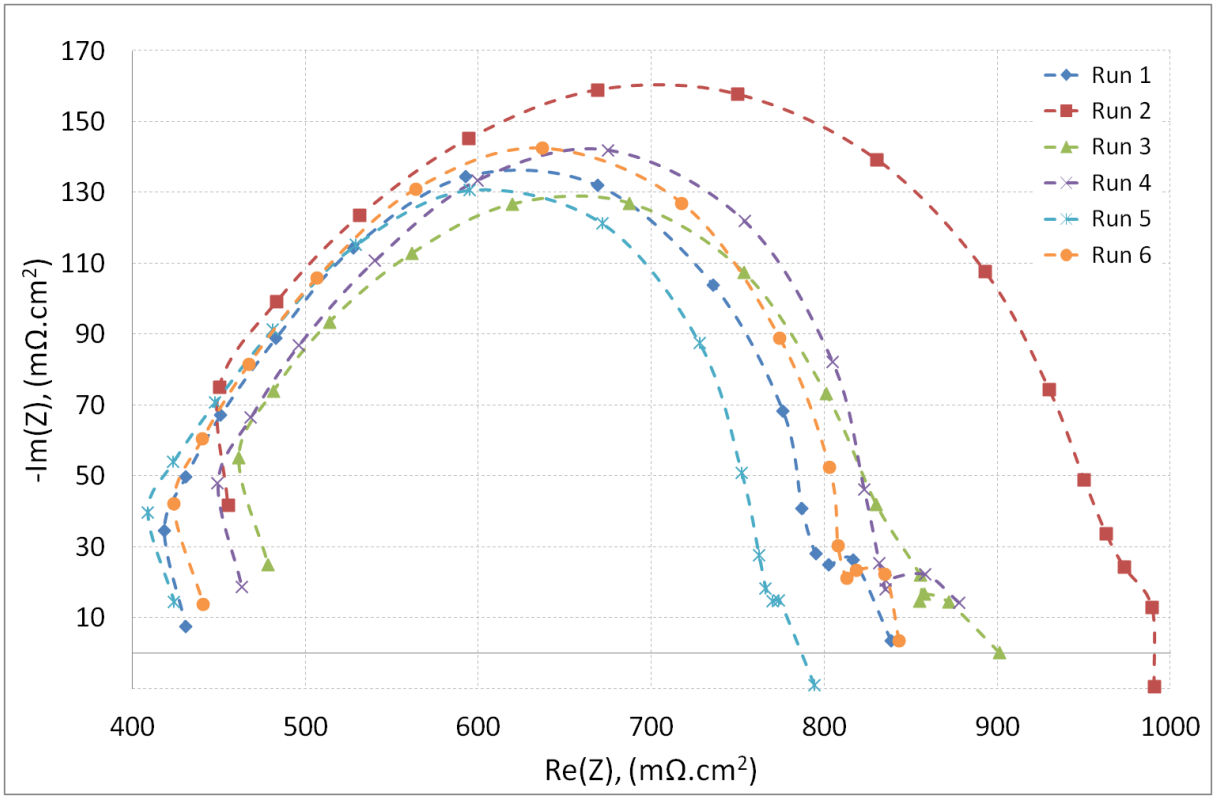

Figure 6.32: Impedance spectra at 300 mA/cm^2, low RH with oxygen. Freudenberg H2315 I6 at cathode

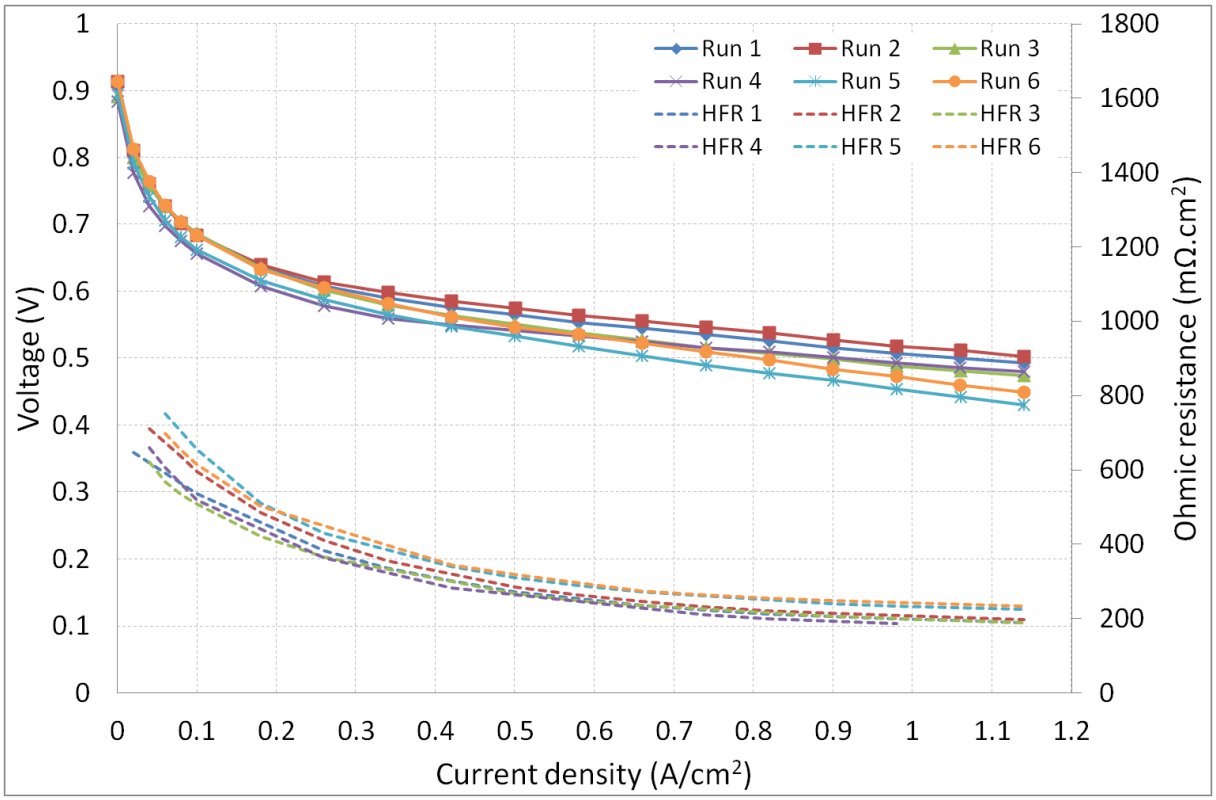

Figure 6.33: MEA performance variation at low RH with oxygen. SGL 25BA at cathode

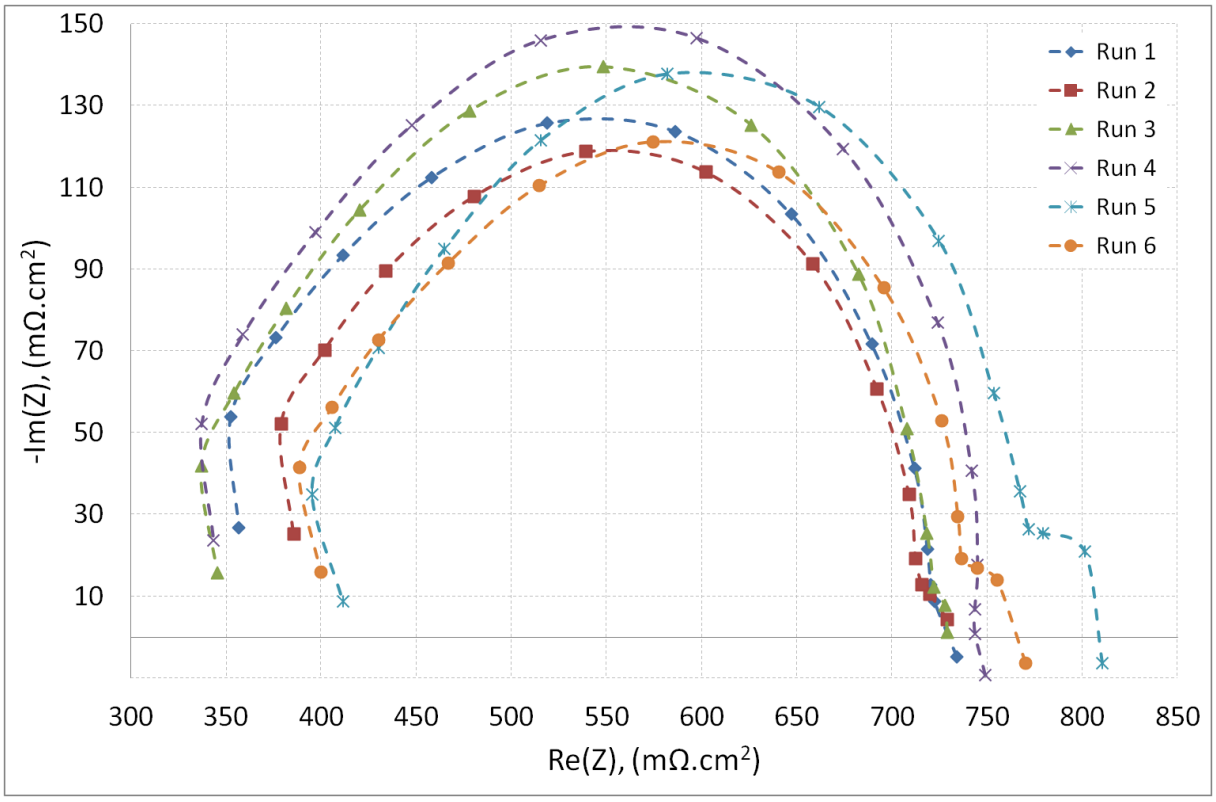

Figure 6.34: Impedance spectra at 300 mA/cm^2, low RH with oxygen. SGL 25BA at cathode

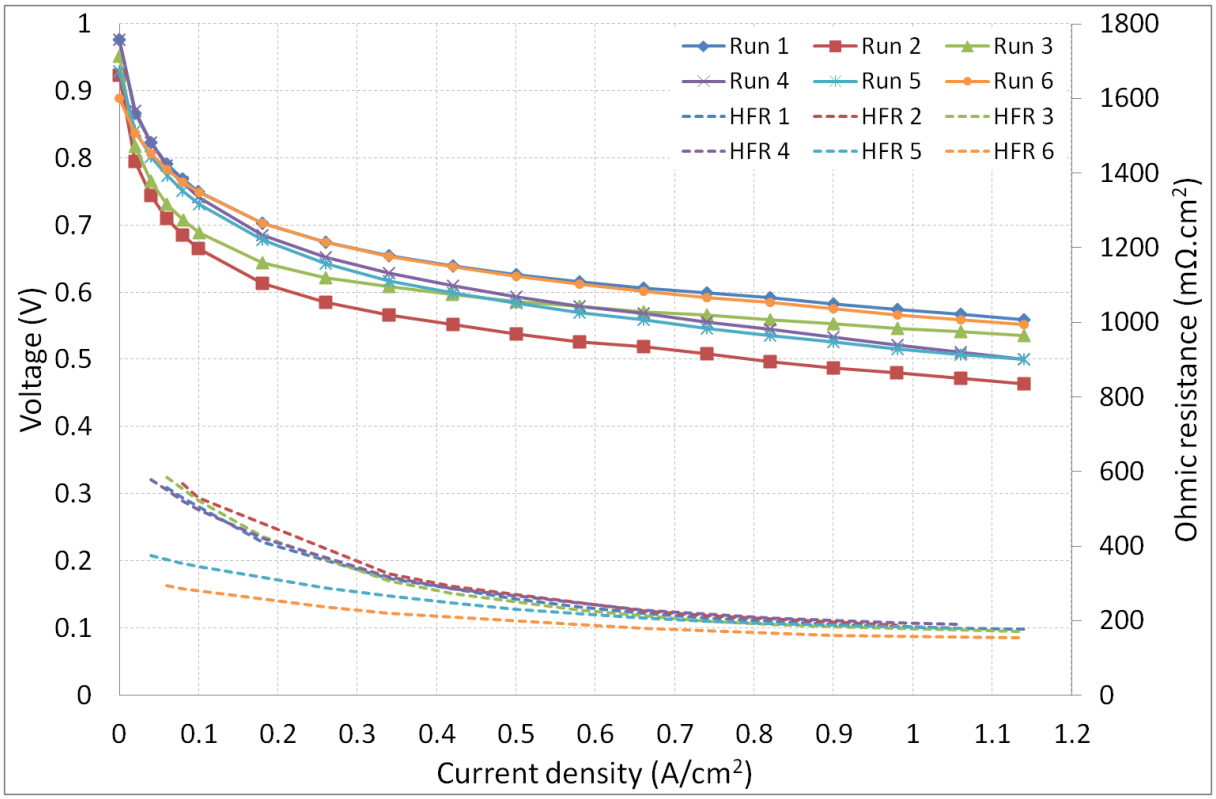

Figure 6.35: MEA performance variation at low RH with oxygen. SGL 25BC at cathode

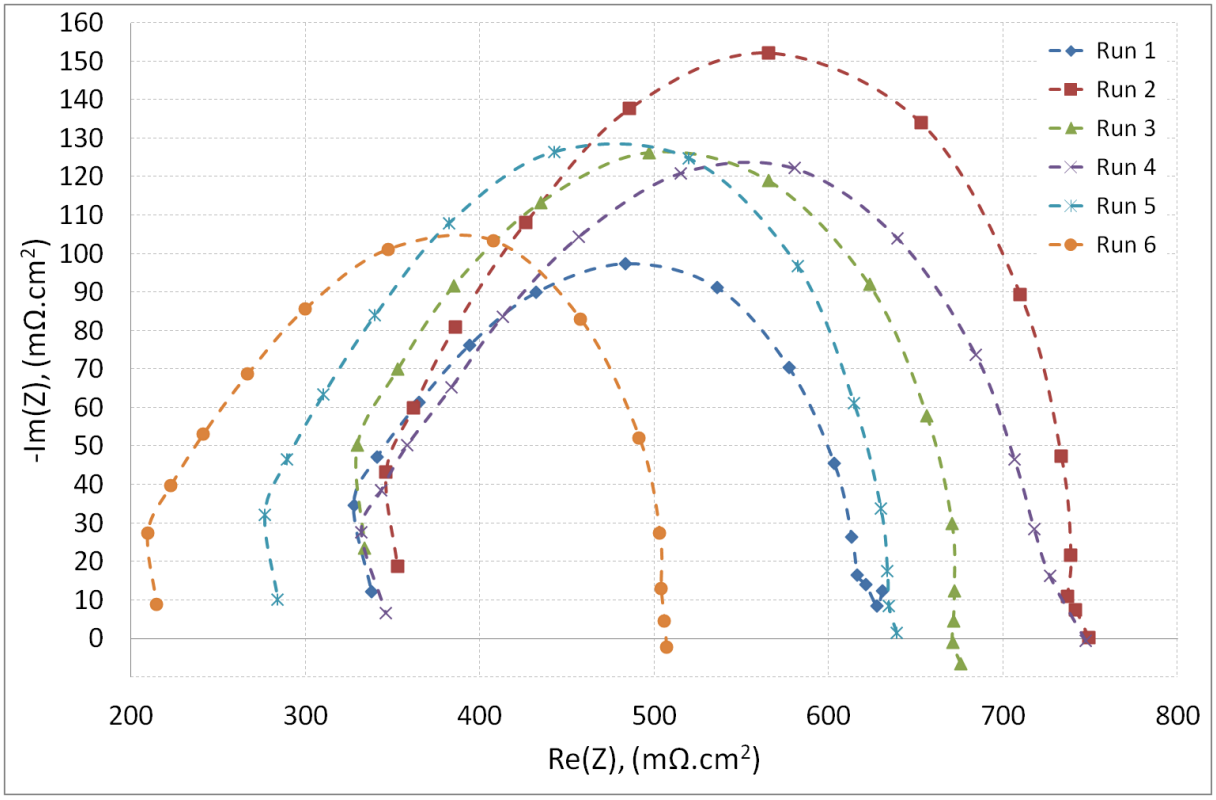

Figure 6.36: Impedance spectra at 300 mA/cm^2, low RH with oxygen. SGL 25BC at cathode

6.2.4 Low relative humidity testing with air

Figure 6.37 to Figure 6.39 show the variance in electrochemical performance for six repeats for MEAs with identical components. All MEA combinations show variation in performance, with SGL 25BA and SGL 25BC giving a spread of performances and Freudenberg affected by an outlier. The cause of this outlier is not due to ohmic resistance. As was shown and discussed earlier in the high relative humidity testing with oxygen, the outlying value is most likely due to variation in the CCM and not due to the GDL.

A comparison of the performance variance for each of the GDLs is plotted in Figure 6.40. It is evident that SGL 25BC shows highest average performance but also the largest variance in performance. With the outlier removed (Figure 6.41) Freudenberg shows the lowest variance in polarization behaviour at low RH with air. To test the effect of an MPL on PEMFC performance at low RH and mass transfer limitations (air as the oxidant) it is desirable to test against an MEA without MPL which has very small variance. In this way if the performance results of the MEA with MPL are different from the average result of the MEA without MPL, the result is likely to be statistically significant. Therefore based on these results, Freudenberg H2315 I6 would be a preferable substrate to SGL 25BA for investigating the effect of an MPL on electrochemical performance at these conditions.

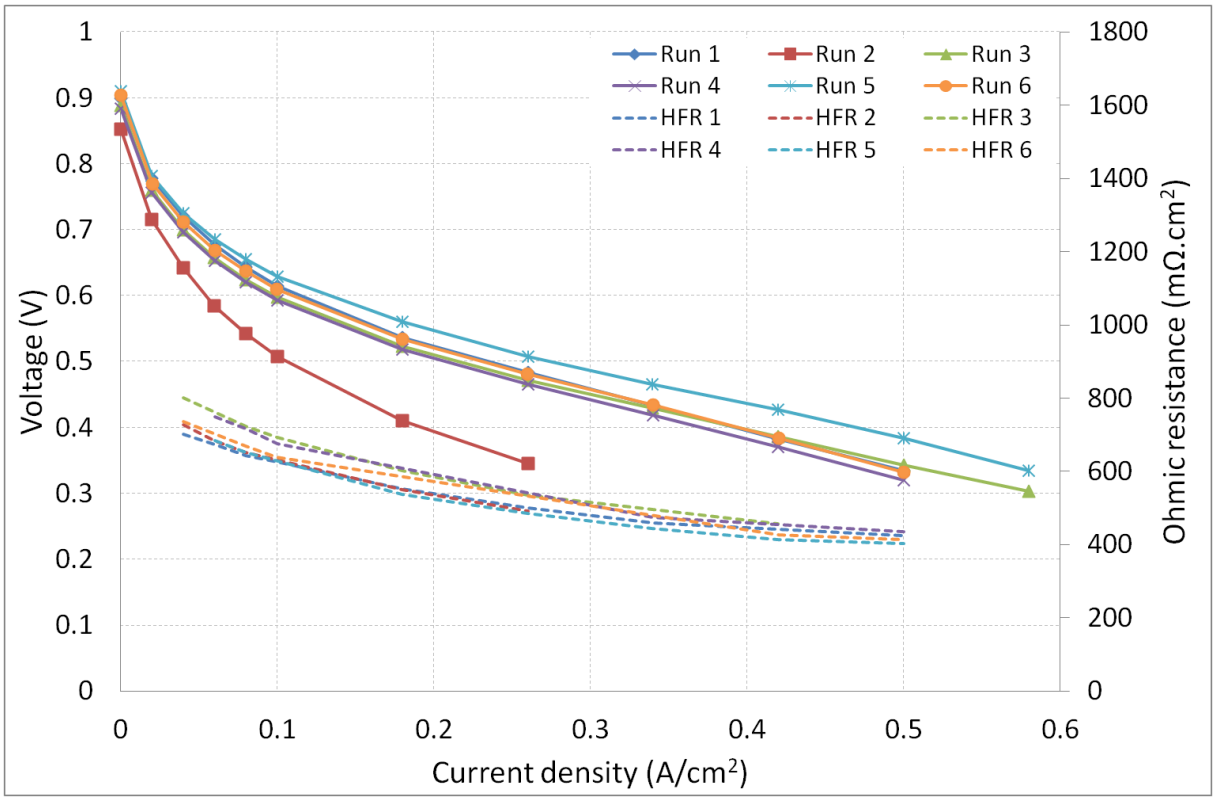

Figure 6.37: MEA performance variation at low RH with air. Freudenberg H2315 I6 at cathode

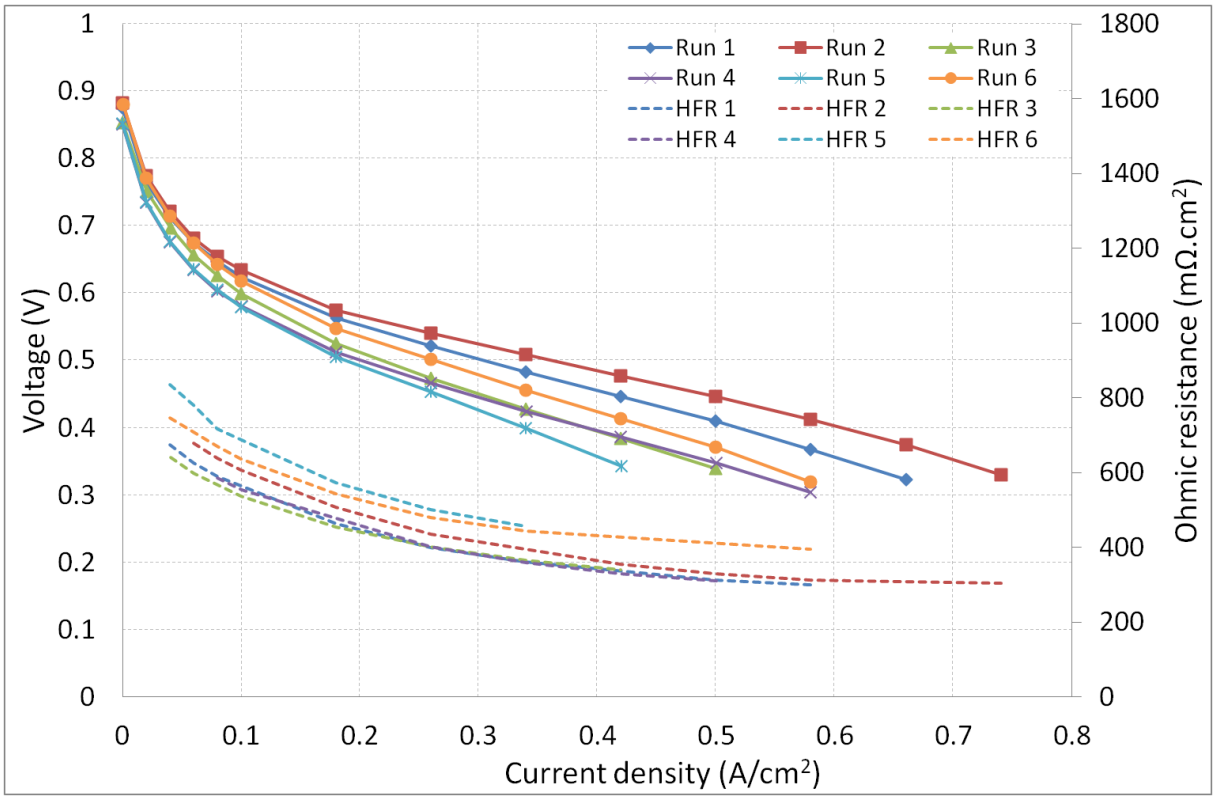

Figure 6.38: MEA performance variation at low RH with air. SGL 25BA at cathode

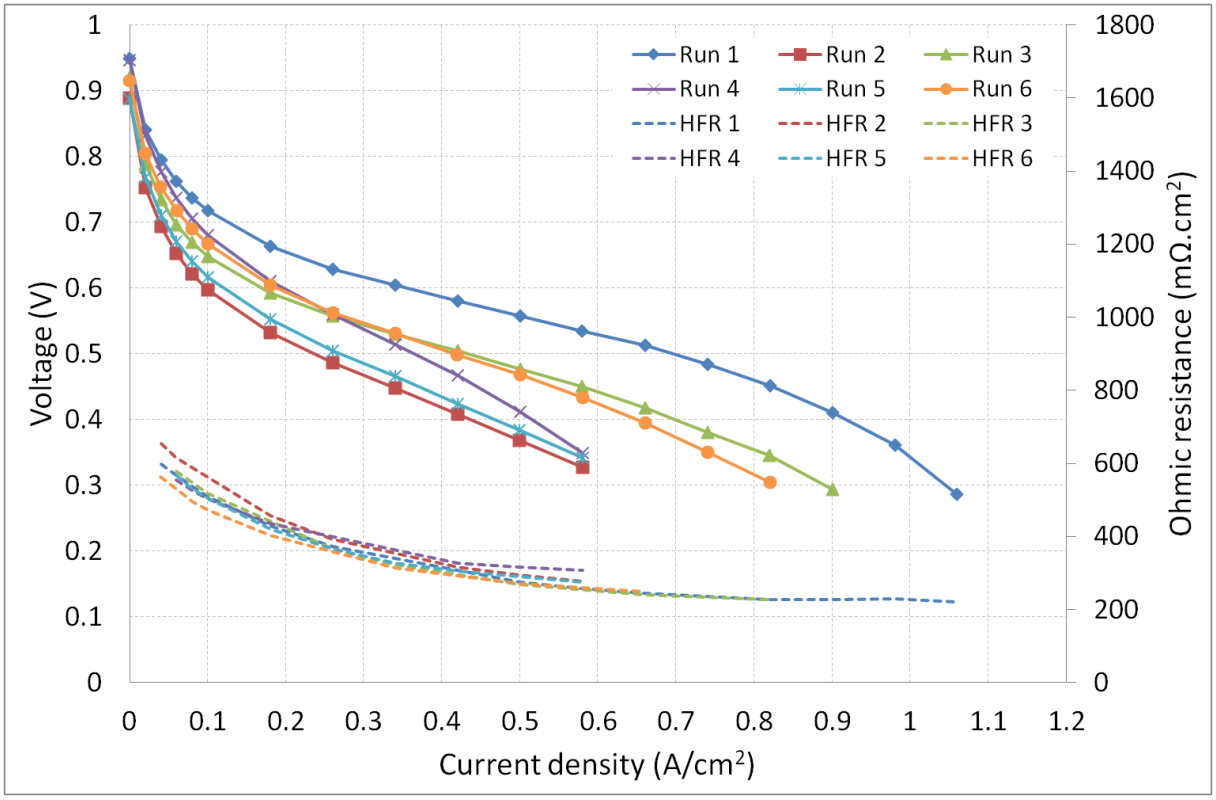

Figure 6.39: MEA performance variation at low RH with air. SGL 25BC at cathode

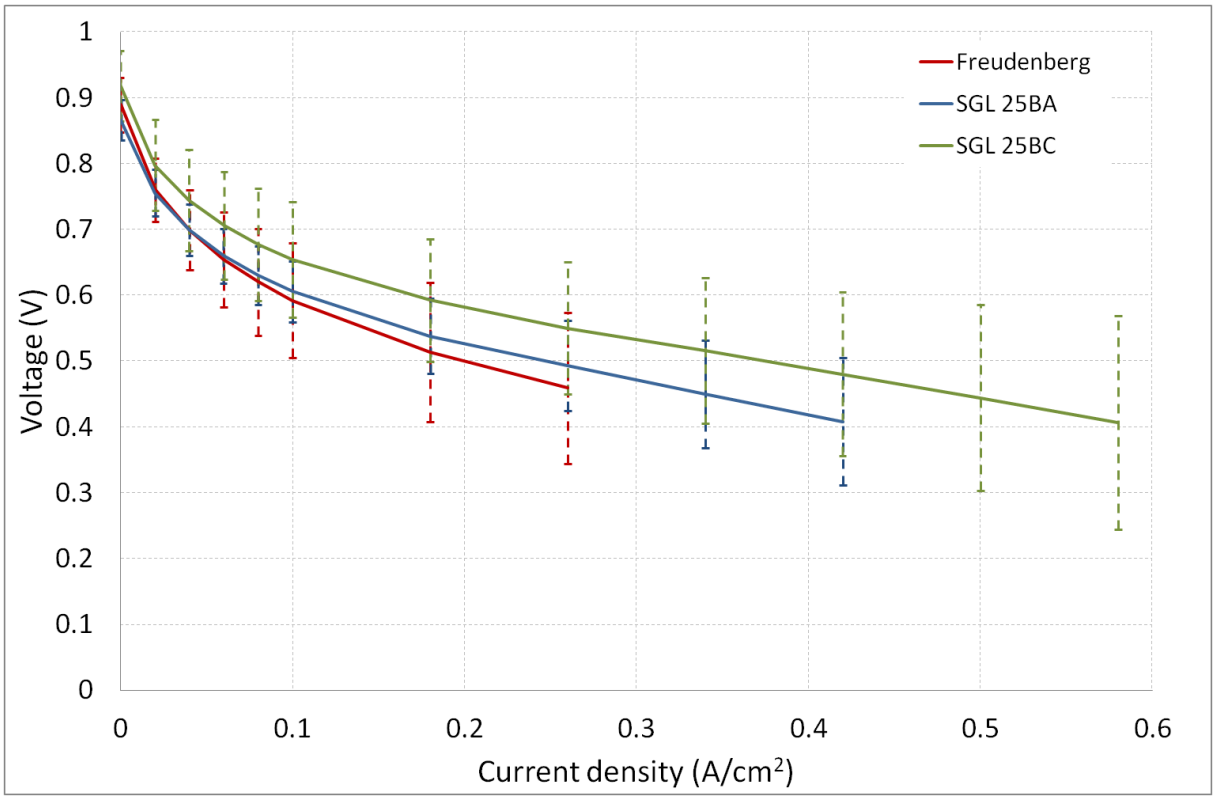

Figure 6.40: Comparison of MEA performance variation at low RH with air

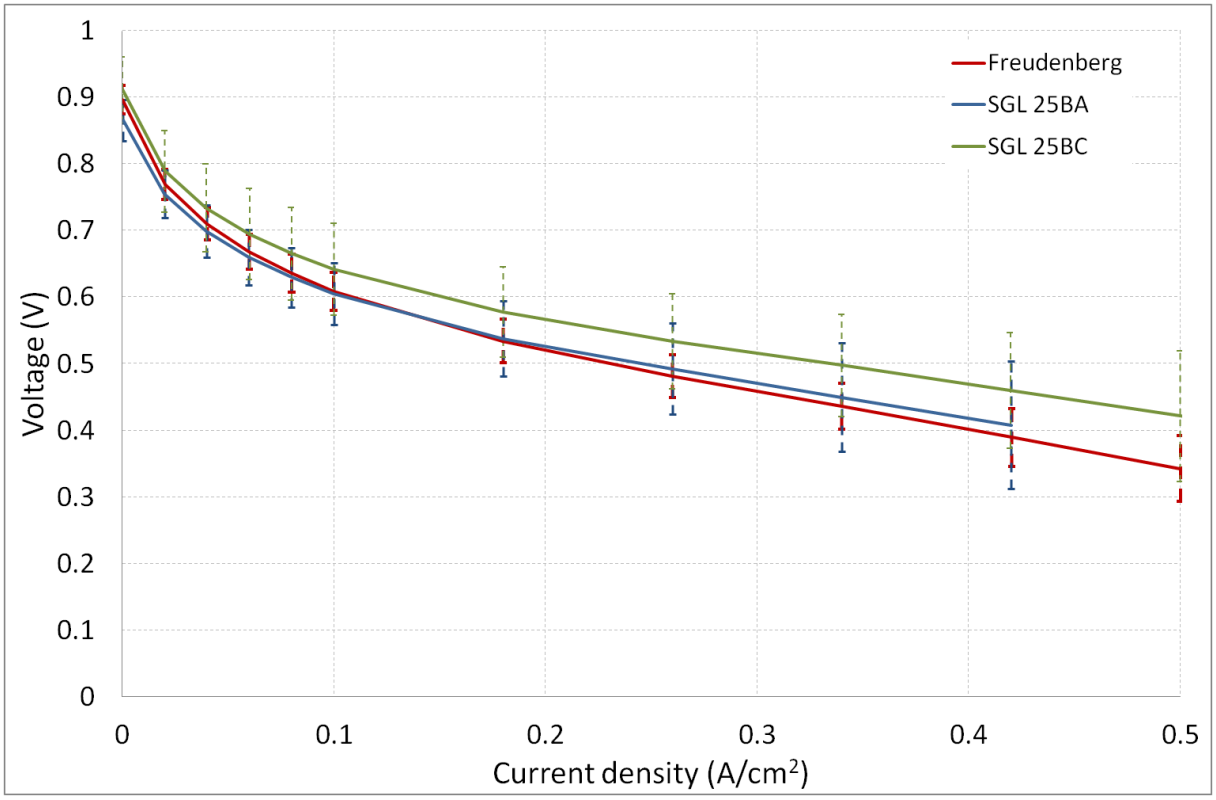

Figure 6.41: Comparison of MEA performance variation at low RH with air. Freudenberg and SGL 25BC outliers omitted

SGL 25BC is effectively an SGL 25BA substrate coated with an MPL. Therefore statistically significant differences between MEAs with the two different GDLs at the cathode can be attributed to the effect of the MPL. It is obvious that Run 1 for SGL 25BC shows uncharacteristically high performance, but even with this value removed, Figure 6.41 shows that there still seems to be a beneficial as a result of the MPL. Due to the relatively large variance in both the SGL 25BA and SGL 25BC polarization behaviour, a statistical analysis is required to determine whether the observed increase in average performance with the addition of the MPL is significant or not.

Parametric statistical tests are based on the assumption that the data comes from a certain probability distribution, usually a normal distribution. In this study, too few samples were obtained for any normality tests to be meaningful. However, once the (single) outliers are removed from the data sets, the mean and descriptive statistics of variance (error bars) describe the spread of data well (at least qualitatively). Therefore parametric tests should still give meaningful results.

The repeat runs for SGL 25BA and SGL 25BC are separate sets of (unpaired) data with similar variance. Therefore an independent two-sample t-test was used to compare the means of the two data sets to determine whether the effect of the MPL is statistically significant. Specifically the test will be used to determine whether the MPL has a positive effect on performance and therefore a one-tailed test is valid. Because the variance and difference in the means between data points is similar between 0.1 and 0.4 A/cm^2 (Figure 6.41) the test was performed at a single current density (0.26 A/cm^2) and the result treated as being general. The application and results of the t-test on the two GDL samples is shown in Table 6.5.

The null hypothesis (assumed true) is that the two means are equal. The p-value is 3.98% and therefore the probability that the null hypothesis is true is very low and is rejected. Therefore there is a very high likelihood that the MPL has a positive effect on MEA performance under the conditions of low relative humidity operation (with air) tested here.

Table 6.5: Independent two-sample one-tailed t-test on the effect of the MPL on performance

Run	SGL 25BC	SGL 25BA
1	0.487	0.522
2	0.558	0.540
3	0.560	0.473
4	0.505	0.466
5	0.562	0.453
6	-	0.502
Mean ($\bar{X}$)	0.534	0.493
Standard deviation	0.036	0.034
Unbiased variance	0.00127	0.00117
$\bar{X}_1 - \bar{X}_2$	0.0417	
$S_{X_1X_2}$	0.035	
t_{stat}	1.976	
Degrees of freedom (n-1)	9	
One-tailed test p-value	0.0398	

7 Conclusions

The MPL is an important layer in the MEA which has been found to significantly improve PEMFC performance at both high and low relative humidity operation. Research to date has used varied approaches to elucidating the function of the MPL, but its precise role is still not well understood. The lack of a well established and rigorous methodology for precise fabrication and accurate characterization and correlation of MPL physical properties with MEA electrochemical performance may be a contributing factor to the uncertainty. Particularly, the effect of MEA variance on electrochemical performance is not often considered during MPL electrochemical testing.

In this study, X-ray computed tomography was used to develop a novel method for measuring the thickness distribution of the MPL (after MEA electrochemical testing) while still contained within an assembled MEA. It was found that there is a bimodal thickness distribution for in-house doctor-blade fabricated MPLs, with the minor mode in agreement with SEM measurements and the major mode centred at a lower thickness. The large thickness distribution suggests that conventional (highly localized) MPL analysis using SEM was inadequate for holistic quantification of thickness for the in-house fabricated MPLs.

When investigating the effect of changing any layer of the MEA, all other components must be carefully controlled as any variation in fixed components in the MEA will result in uncertainty in the measured effect of the layer under study. Therefore reliability of such investigations depends on minimizing MEA variation under the testing conditions of interest to improve the likelihood of statistically significant results. The variance of MEAs assembled with Ion Power® NAFION® NR-211 CCMs, Sigracet® SGL 25BC at the anode and three different GDL combinations at the cathode; SGL 25BC, SGL 25BA and Freudenberg H2315 I6 were measured from six repeat runs. Additionally the variation in pore structure for the cathode GDLs was quantified by repeat mercury intrusion porosimetry analysis. SGL 25BC showed the largest variation in pore structure across samples and also gave the largest variance in electrochemical performance compared with SGL 25BA and Freudenberg H2315 I6. It is therefore likely that the SGL 25BC MPL has a significant effect on measured pore structure and MEA variance.

The largest MEA performance variation for all three cathode GDL combinations was measured at low relative humidity operation with air as the oxidant. Applying an independent two-sample one-tailed t-test to the results for SGL 25BA and SGL 25BC at the cathode showed that there is a high probability (> 96 %) that the MPL has a positive effect

on performance at this condition. However the MPL did not have a statistically significant beneficial effect on performance at high relative humidity operation.

The methodology developed in this study highlights the importance of reliable fabrication and characterization of MPLs and careful consideration of the effect of MEA performance variation on the statistical significance of electrochemical performance results. An established MPL research methodology using statistical inference methods may allow for a better understanding on the role of the MPL in PEMFC performance improvement.

References

- Ahn, M., Cho, Y. Cho, Y., Kim. J., Jung. N. and Sung. Y. 2011. Influence of hydrophilicity in micro-porous layer for polymer electrolyte membrane fuel cells. *Electrochimica Acta*. 56: 2450-2457.
- AMRESCO. 2011. *Triton X-100* [Safety Data Sheet]. Available: https://www.amresco-inc.com/media.acux?path=/media/products/msds/MSDS-M143.pdf [Accessed: 12 August 2014].
- Arvay, A., Yli-Rantala, E., Liu, C.H., Peng, X.H., Koski, P., Cindrella, L., Kauranen, P., Wilde, P.M. and Kannan, A.M. 2012. Characterization techniques for gas diffusion layers for proton exchange membrane fuel cells – A review. *Journal of Power Sources*. 213: 317-337.
- Atiyeh, K.H., Karan, K., Peppley, B., Phoenix, A., Halliop, E. and Pharoah, J. 2007. Experimental investigation of the role of a microporous layer on the water transport and performance of a PEM fuel cell. *Journal of Power Sources*. 170: 111-121.
- Babir, F. 2005. PEM Fuel Cells: Theory and Practice. London: Elsevier Academic Press. p75-144.
- Bender, G., Zawodzinski, T.A. and Saab, A.P. 2003. Fabrication of high precision PEFC membrane electrode assemblies. *Journal of Power Sources*. 124: 114-117.
- Benziger, J., Nehlsen, J., Blackwell, D., Brennan, T. and Itescu, J. 2005. Water flow in the gas diffusion layer of PEM fuel cells. *Journal of Membrane Science*. 261: 98-106.
- Chan, C., Zamel, N., Li, X. and Shen, J. 2012. Experimental measurement of effective diffusion coefficient of gas diffusion layer/microporous layer in PEM fuel cells. *Electrochimica Acta*. 65: 13-21.
- Chang, H., Lin, C., Chang, M., Shiu, H., Chang, W. and Tsau, F. 2011. Optimization of polytetrafluoroethylene content in cathode gas diffusion layer by the evaluation of compression effect on the performance of a proton exchange membrane fuel cell. *Journal of Power Sources*. 196: 3773-3780.
- Chen, H.-H. and Chang, M.-H. 2013. Effect of cathode microporous layer composition on proton exchange membrane fuel cell performance under different air inlet relative humidity. *Journal of Power Sources*. 232: 306-309.
- Chen, J., Xu, H., Zhang, H. and Yi, B. 2008. Facilitating mass transport in gas diffusion layer of PEMFC by fabricating microporous layer with dry layer preparation. *Journal of Power Sources*. 182: 531-539.
- Cheng. X., Yi, B., Han, M., Zhang, J., Qiao, Y. and Yu, J. 1999. Investigation of platinum utilization and morphology in catalyst layer of polymer electrolyte fuel cells. *Journal of Power Sources*. 79: 75-81.
- Chun, J.H., Park, K.T., Jo, D.H., Lee, J.Y., Kim, S.G., Park, S.H., Lee, E.S., Jyoung, J. and Kim, S.H. 2011. Development of a novel hydrophobic/hydrophilic double micro porous layer for use in a cathode as diffusion layer in PEMFC. *International Journal of Hydrogen Energy*. 36: 8422-8428.

- Cindrella, L., Kannan, A.M., Lin, J.F., Saminathan, K., Ho, Y., Lin, C.W. and Wertz, J. 2009. Gas diffusion layer for proton exchange membrane fuel cells - A review. *Journal of Power Sources*. 194: 146-160.
- Colinart, T., Chenu, A., Didierjean, S., Lottin, O. and Besse, S. 2009. Experimental study on water transport coefficient in Proton Exchange Membrane Fuel Cell. *Journal of Power Sources*. 190: 230-240.
- Cooper, K.R., Ramani, V., Fenton, J.M. and Kunz, H.R. 2005. *Experimental Methods and Data Analyses for Polymer Electrolyte Fuel Cells*. North Carolina: Scribner Associates, Inc.
- Cooper, K.R. and Smith, M. 2006. Electrical test methods for on-line fuel cell ohmic resistance measurement. *Journal of Power Sources*. 160: 1088-1095.
- Cuccaro, R., Lucariello, M., Battaglia, A. and Graizzaro, A. 2008. Research of a HySyLab internal standard procedure for single PEMFC. *International Journal of Hydrogen Energy*. 33: 3159-3166.
- Darling, R.M. and Meyers, J.P. 2003. Kinetic Model of Platinum Dissolution in PEMFCs. *Journal of The Electrochemical Society*. 150(11): A1523-A1527.
- Davard, F. and Dupuis, D. 2000. *Journal of Non-Newtonian Fluid Mechanics*. 93: 17-28.
- Deevanhxay, P., Sasabe, T., Tsushima, S. and Hirai, S. 2013. Effect of liquid water distribution in gas diffusion media with and without microporous layer on PEM fuel cell performance. *Electrochemistry Communications*. 34: 239-241.
- Dhillon, R.S. and Wuehlisch, G. 2013. Mitigation of global warming through renewable biomass. *Biomass and Bioenergy*. 48: 75-89.
- El-kharouf, A., Mason, T.J., Brett, D.J.L. and Pollet, B.G. 2012. *Ex-situ* characterisation of gas diffusion layers for proton exchange membrane fuel cells. *Journal of Power Sources*. 218: 393-404.
- Eom, K., Cho, E., Jang, J., Kim, H., Lim, T., Hong, B.K. and Lee, J. Optimization of GDLs for high-performance PEMFC employing stainless steel bipolar plates. *International Journal of Hydrogen Energy*. 38: 6249-6260.
- Escribano, S., Blachot, J.-F., Ethève, J., Morin, A. and Mosdale, R. 2006. Characterization of PEMFCs gas diffusion layers properties. *Journal of Power Sources*. 156: 8-13.
- Frey, T. and Linardi, M. 2004. Effects of membrane electrode assembly preparation on the polymer electrolyte membrane fuel cell performance. *Electrochimica Acta*. 50: 99-105.
- Gao, Y., Zhang, X., Rama, P., Chen, R., Ostadi, H. and Jiang, K. 2013. Lattice Boltzmann simulation of water and gas flow in porous gas diffusion layers in fuel cells reconstructed from micro-tomography. *Computers and Mathematics with Applications*. 65: 891-900.
- Gostick, J., Ioannidis, M.A., Fowler, M.W. and Pritzker, M. 2009. On the role of the microporous layer in PEMFC operation. *Electrochemistry Communications*. 11: 576-579.
- Herman G.T. 2009. Fundamentals of Computerized Tomography: Image Reconstruction from Projections. Second Edition. London, England: Springer.

- Hiramitsu, Y., Sato, H. and Hori. M. 2010. Prevention of the water flooding by micronizing the pore structure of gas diffusion layer for polymer electrolyte fuel cell. *Journal of Power Sources*. 195: 5543-5549.
- Hyun, D. and Kim, J. 2004. Study of external humidification method in proton exchange membrane fuel cell. *Journal of Power Sources*. 126: 98-103.
- International Union of Pure and Applied Chemistry (IUPAC). 2014. *Compendium of Chemical Terminology*. Version 2.2.3. (the "Gold Book"). Oxford: Blackwell Scientific Publications. p 916. Available: http://goldbook.iupac.org/PDF/goldbook.pdf [Accessed: 10 June 2014].
- James, J.P., Choi, H.-W. and Pharoah, J.G. 2012. X-ray computed tomography reconstruction and analysis of polymer electrolyte membrane fuel cell porous transport layers. *International Journal of Hydrogen Energy*. 37: 18216-18230.
- Janssen, G.J.M. and Overvelde, M.L.J. 2001. Water transport in the proton-exchange-membrane fuel cell: measurements of the effective drag coefficient. *Journal of Power Sources*. 101: 117-125.
- Kang, J., Jung, D.W., Park, S., Lee, J., Ko, J. and Kim, J. 2010. Accelerated test analysis of reversal potential caused by fuel starvation during PEMFCs operation. *International Journal of Hydrogen Energy*. 35: 3727-3735.
- Karimi, G., Li. X. and Teertstra, P. 2010. Measurement of through-plane effective thermal conductivity and contact resistance in PEM fuel cell diffusion media. *Electrochimica Acta*. 55: 1619-1625.
- Kitahara, T., Konomi, T. and Nakajima, H. 2010. Microporous layer coated gas diffusion layers for enhanced performance of polymer electrolyte fuel cells. *Journal of Power Sources*. 195: 2202-2211.
- Kitahara, T., Nakajima, H. and Mori, K. 2012. Hydrophilic and hydrophobic double microporous layer coated gas diffusion layer for enhancing performance of polymer electrolyte fuel cells under no-humidification at the cathode. *Journal of Power Sources*. 199: 29-36.
- Kocha, S.S. 2003. *Principles of MEA preparation*. In: Vielstich, W., Gasteiger, H.A and Lamm, A. *Handbook of Fuel Cells – Fundamentals, Technology and Applications*. Volume 3 chapter 43. Chichester, UK: Wiley. p 540-563.
- Kong, C.S., Kim, D., Lee, H., Shul, Y. and Lee, T. 2002. Influence of pore-size distribution of diffusion layer on mass-transport problems of proton exchange membrane fuel cells. *Journal of Power Sources*. 108: 185-191.
- Krantz, W.B., Greenberg, A.R., Kujundzic, A.Y. and Hosseini, S.S. 2013. Evapoporometry: A Novel Technique for Determining the Pore-Size Distribution of Membranes. *Journal of Membrane Science*. Author's accepted manuscript.
- Larminie, J. and Dicks, A. 2003. *Fuel Cell Systems Explained*. 2nd Edition. Chichester, England: John Wiley & Sons Ltd.

- Latorrata, S., Stampino, P.G., Amici, E., Pelosato, R., Cristiani, C. and Dotelli, G. 2012. Effect of rheology controller agent addition to Micro-Porous Layers on PEMFC performances. *Solid State Ionics*. 216: 73-77.
- Latorrata, S., Stampino, P.G., Cristiani, C. and Dotelli, G. 2014. Novel superhydrophobic microporous layers for enhanced performance and efficient water management in PEM fuel cells. *International Journal of Hydrogen Energy*. 39: 5350-5357.
- Lee, D. and Bae, J. 2009. Evaluation of the net water transport through electrolytes in Proton Exchange Membrane Fuel Cell. *Journal of Power Sources*. 191: 390-399.
- Lee, J., Hinebaugh, J and Bazylak, A. 2013. Synchrotron X-ray radiographic investigations of liquid water transport behaviour in a PEMFC with MPL-coated GDLs. *Journal of Power Sources*. 227: 123-130.
- Li. H., Tang. Y., Wang. Z., Shi. Z., Wu. S., Song. D., Zhang. J., Fatih. K., Zhang. J., Wang. H., Liu. Z., Abouatallah. R. And Mazza. A. 2008. A review of water flooding issues in the proton exchange membrane fuel cell. *Journal of Power Sources*. 178: 103-117.
- Lin, G. and Nguyen, T.V. 2006. A Two-Dimensional Two-Phase Model of a PEM Fuel Cell. *Journal of The Electrochemical Society*. 153(2): A372-A382.
- Maire, E. and Withers, P.J. 2014. Quantitative X-ray tomography. *International Materials Reviews*. 59(1): 1-43.
- Miller, M. and Bazylak, A. 2011. A review of polymer electrolyte fuel cell stack testing. *Journal of Power Sources*. 196: 601-613.
- Murahashi, T. Naiki, M. and Nishiyama, E. 2006. Water transport in the proton exchange membrane fuel cell: Comparison of model computation and measurements of effective drag. *Journal of Power Sources*. 162: 1130-1136.
- Nam, J., Lee, K., Hwang, G., Kim, C. and Kaviany, M. 2009. Microporous layer for water morphology control in PEMFC. *International Journal of Heat and Mass Transfer*. 52: 2779-2791.
- Nishiyama, E. and Murahashi, T. 2011. Water transport characteristics in the gas diffusion media of proton exchange membrane fuel cell – Role of the microporous layer. *Journal of Power Sources*. 196: 1847-1854.
- Niya, S.M.R. and Hoorfar, M. 2013. Study of proton exchange membrane fuel cells using electrochemical impedance spectroscopy technique – A review. *Journal of Power Sources*. 240: 281-293.
- Ostadi, H., Rama, P., Chen, R., Zhang, X. and Jiang, K. 2011. Nanotomography based study of gas diffusion layers. *Microelectronic Engineering*. 87: 1640-1642.
- Oyarce, A., Zakrisson, E., Ivity, M., Lagergren, C., Ofstad, A.B., Boden, A. and Lindbergh, G. 2014. Comparing shut-down strategies for proton exchange membrane fuel cells. *Journal of Power Sources*. 254: 232-240.
- Owejan, J.P., Owejan, J.E. and Gu, W. 2013 Impact of Platinum Loading and Catalyst Layer Structure on PEMFC Performance. *Journal of The Electrochemical Society*. 160(8): F824-F833.

- Paganin, V.A., Ticianelli, A. and Gonzalez, R. 1996. Development and electrochemical studies of gas diffusion electrodes for polymer electrolyte fuel cells. *Journal of Applied Electrochemistry*. 26: 297-304.
- Pant, L.M., Mitra, S.K. and Secanell, M. 2012. Absolute permeability and Knudsen diffusivity measurements in PEMFC gas diffusion layers and micro porous layers. *Journal of Power Sources*. 206: 153-160.
- Park, S. Lee, J. and Popov, B.N. 2008. Effect of PTFE content in microporous layer on water management in PEM fuel cells. *Journal of Power Sources*. 177: 457-463.
- Park, S. and Popov, B.N. 2009. Effect of cathode GDL characteristics on mass transport in PEM fuel cells. *Fuel*. 88(11): 2068:2073.
- Park, I-S., Li, W. and Manthiram, A. 2010. Fabrication of catalyst-coated membrane-electrode assemblies by doctor blade method and their performance in fuel cells. *Journal of Power Sources*. 195: 7078-7082.
- Park, S., Lee, J. and Popov, B. 2012. A review of gas diffusion layer in PEM fuel cells: Materials and designs. *International Journal of Hydrogen Energy*. 37: 5850-5865.
- Pasaogullari, U. and Wang, C. 2008. Two-phase transport and the role of micro-porous layer in polymer electrolyte fuel cells. *Electrochimica Acta*, 49: 4359-4369.
- Pfrang, A., Didas, S. and Tsotridis, G. 2013. X-ray computed tomography of gas diffusion layers of PEM fuel cells: Segmentation of the microporous layer. *Journal of Power Sources*. 235: 81-86.
- Prasanna, M., Cho, E.A., Lim, T.-H., and Oh, I.-H. 2008. Effects of MEA fabrication method on durability of polymer electrolyte membrane fuel cells. *Electrochimica Acta*. 53: 5434-5441.
- Qi, K. and Kaufman, A. 2002. Improvement of the water management by a microporous sublayer for PEM fuel cells. *Journal of Power Sources*. 109: 38-46.
- Ramanathan, V. and Feng, Y. 2009. Air pollution, greenhouse gases and climate change: Global and regional perspectives. *Atmospheric Environment*. 43: 37-50.
- Ramasamy, R.P., Kumbur, E.C., Mench, M.M, Liu, W. Moore, D. and Murthy, M. 2008. Investigation of macro- and micro-porous layer interaction in polymer electrolyte fuel cells. *International Journal of Hydrogen Energy*. 33: 3351-3367.
- Reshetenko, T., Bender, G., Bethune, K. and Rocheleau, R. 2012. Effects of local variations of the gas diffusion layer properties on PEMFC performance using a segmented cell system. *Electrochimica Acta*. 80: 368-376.
- Rieke, P.C. and Vanderborgh, N.E. 1987. Temperature dependence of water content and proton conductivity in polyperfluorosulfonic acid membranes. *Journal of Membrane Science*. 32: 313-328.
- Shao, Y., Yin, G. and Gao, Y. 2007. Understanding and approaches for the durability issues of Pt-based catalysts for PEM fuel cells. *Journal of Power Sources*. 171: 558-566.
- Stampino, P.G., Cristiani, C., Dotelli, G., Omati, L., Zampori, L., Pelosato, R. and Guilizzoni, M. 2009. Effect of different substartes, inks composition and rheology on coating deposition of microporous layer (MPL) for PEM-FCs. *Catalysis Today*. 147S: S30-S35.

- Starz, K.A., Auer, E., Lehmann, T. and Zuber, R. 1999. Characteristics of platinum-based electrocatalysts for mobile PEMFC applications. *Journal of Power Sources*. 84: 167-172.
- Tang, H., Wang, S., Pan, M. and Yuan, R. 2007a. Porosity-graded micro-porous layers for polymer electrolyte membrane fuel cells. *Journal of Power Sources*. 166: 41-46.
- Tang, H., Wang, S., Jiang, S.P. and Pan, M. 2007b. A comparative study of CCM and hot-pressed MEAs for PEM fuel cells. *Journal of Power Sources*. 170: 140-144.
- Tanuma, T. and Kinoshita, S. 2012. Impact of gas diffusion layers (GDLs) on MEA performance in PEFCs. *Energy Procedia.* 28: 12-29.
- Thomas, A., Maranzana, G., Didierjean, S., Dillet, J. and Lottin, O. 2014. Thermal and water transfer in PEMFCs: Investigating the role of the microporous layer. *International Journal of Hydrogen Energy*. 39: 2649-2658.
- Tseng, C. and Lo, S. 2010. Effects of microstructure characteristics of gas diffusion layer and microporous layer on the performance of PEMFC. *Energy Conversion and Management*. 51: 677-684.
- US Fuel Cell Council's (USFCC) single cell testing task force. 2006. *Single Cell Test Protocol*. Available: http://www.fchea.org/core/import/PDFs/Technical%20Resources/MatComp%20Single%20Cell%20Test%20Protocol%2005-014RevB.2%20071306.pdf [Accessed: 15 March 2013]
- Viswanathan, B and Aulice Scibioh, M. (2006). *Fuel Cells Principles and Applications*. India: Universities Press. p 272-307.
- Wargo, E.A., Schulz, V.P., Çeçen, A., Kalidindi, S.R. and Kumbur, E.C. 2013a. Resolving macro- and micro-porous layer interaction in polymer electrolye fuel cells using focused ion beam and X-ray computed tomography. *Electrochimica Acta*. 87: 201-212.
- Wargo, E.A., Kotaka, T., Tabuchi, Y. and Kumbur, E.C. 2013b. Comparison of focused ion beam versus nano-scale X-ray computed tomography for resolving 3-D microstructures of porous fuel cell materials. *Journal of Power Sources*. 241: 608-618.
- Weber, A.Z. and Newman, J. 2005. Effects of Microporous Layers in Polymer Electrolyte Fuel Cells. *Journal of The Electrochemical Society*. 152(4): A677-A688.
- Wu, J., Yuan, X.Z., Martin, J.J., Wang, H., Zhang, J., Shen, J., Wu, S. and Merida, W. 2008a. A review of PEM fuel cell durability: Degradation mechanisms and mitigation strategies. *Journal of Power Sources*. 184: 104-119.
- Wu, J., Yuan, X.Z., Wang, H., Blanco, M., Martin, J.J. and Zhang, J. 2008b. Diagnostic tools in PEM fuel cell research: Part I Electrochemical techniques. *International Journal of Hydrogen Energy*. 33: 1735-1746.
- Yang, X., Ye, Q. And Cheng, P. 2012. In-plane transport effects on hydrogen depletion and carbon corrosion induced by anode flooding in proton exchange membrane fuel cells. *International Journal of Heat and Mass Transfer*. 5: 4754-4765.
- Yousfi-Steiner, N., Mocotéguy, Ph., Candusso, D. and Hissel, D. 2009. A review on polymer electrolyte membrane fuel cell catalyst degradation and starvation issues: Causes, consequences and diagnostic for mitigation. *Journal of Power Sources*. 194: 130-145.

- Yu, X. and Ye, S. 2007. Recent advances in activity and durability enhancement of Pt/C catalytic cathode in PEMFC Part II: Degradation mechanism and durability enhancement of carbon supported platinum catalyst. *Journal of Power Sources*. 172: 145-154.
- Yuan, X., Wang, H., Sun, J.C. and Zhang, J. 2007. AC impedance technique in PEM fuel cell diagnosis - A review. *International Journal of Hydrogen Energy*. 32: 4365-4380.
- Zawodzinski, T.A., Derouin, C., Radzinski, S., Sherman, R.J., Smith, V.T. Springer, T.E. and Gottesfeld, S. 1993. Water Uptake and Transport Through Nafion 117 Membranes. *Journal of The Electrochemical Society*. 140: 1041-1047.
- Zhan, Z., Xiao, J., Zhang, Y., Pan, M. and Yuan, R. 2007. Gas diffusion through differently structured gas diffusion layers of PEM fuel cells. *International Journal of Hydrogen Energy*. 32: 4443-4451.
- Zhiani, M. and Majidi, S. 2013. Effect of MEA conditioning on PEMFC performance and EIS response under steady state condition. *International Journal of Hydrogen Energy*. 38: 9819-9825.
- Zientek, M.L., Causey, J.D., Parks, H.L., and Miller, R.J. 2014. *Platinum-Group Elements in Southern Africa – Mineral Inventory and an Assessment of Undiscovered Mineral Resources*: U.S. Geological Survey Scientific Investigations Report 2010-5090-Q. Available: http://pubs.usgs.gov/sir/2010/5090/q/pdf/sir2010-5090Q.pdf [Accessed 10 June 2014].

Appendix A

A.1 Operating Conditions

Table A.1: Polarization curve parameters for MEA variance testing

Test condition	Value
Hydrogen	
Flow type	constant
Stoichiometry @ 1A/cm^2	1.5
Air	
Flow type	constant
Stoichiometry @ 1A/cm^2	2
Repeat polarization curves	3
Oxygen	
Flow type	constant
Stoichiometry @ 1A/cm^2	10
Repeat polarization curves	3
Activation region current step (A)	0.5
Ohmic region current step (A)	2
Assumed transition region (A/cm^2)	0.1
Stabilization period after load change (minutes)	4
Repeat voltage measurements over 1 minute	4
Cell temperature equilibration tolerance (^{o}C)	0.2
HFR at each data point	10 kHz

Table A.2: Electrochemical impedance spectroscopy parameters for MEA variance testing

Parameter	Value
Fuel	Hydrogen
Oxidant(s)	Air and oxygen
Hydrogen flow rate (nl/min)	0.26
Oxidant flow rate (nl/min)	0.87
Frequency range (Hz)	0.1 – 13 000
Number of measurements	18

Table A.3: Fuel cell operating conditions

Condition	A	B	C	D	E
Cell temperature (^{o}C)	80	≈25	80	70	70
Anode					
RH (%)	100	≈100		40	100
Pressure (bara)	1	1	1	1	1
Constant flow (l/min)	0.26	≈0.4	0.4	0.26	0.26
Cathode					
RH (%)	100	≈100		bypassed	100
Pressure (bara)	1	1	1	1	1
Constant flow (l/min)	0.87	≈0.8	0.8	0.87	0.87

Appendix B

B.1 Sample polarization curve and EIS raw data

Table B.1: Raw polarization curve data. Freudenberg I6 Run 3 Condition E with air oxidant.

PC 1						
Cell temp (^{o}C)	Current density (A/cm^2)		Voltage (V)			Avg. voltage (V)
69.4	0	0.927	0.926	0.926	0.925	0.926
69.7	0.0200	0.876	0.876	0.876	0.876	0.876
70.0	0.0400	0.856	0.856	0.856	0.856	0.856
70.0	0.0600	0.841	0.841	0.841	0.841	0.841
70.0	0.0800	0.830	0.830	0.830	0.830	0.830
70.1	0.0997	0.820	0.820	0.820	0.820	0.820
70.2	0.1800	0.791	0.791	0.791	0.790	0.791
70.1	0.2598	0.766	0.766	0.766	0.766	0.766
70.1	0.3400	0.744	0.744	0.744	0.744	0.744
70.1	0.4200	0.722	0.722	0.722	0.722	0.722
70.1	0.5000	0.699	0.697	0.698	0.698	0.698
70.2	0.5802	0.676	0.677	0.677	0.676	0.677
70.1	0.6600	0.647	0.649	0.649	0.649	0.649
70.2	0.7400	0.623	0.622	0.623	0.622	0.622
70.2	0.8201	0.585	0.588	0.587	0.587	0.587
70.2	0.9000	0.546	0.543	0.552	0.546	0.547
70.2	0.9799	0.526	0.521	0.524	0.520	0.523
70.2	1.0599	0.469	0.478	0.466	0.479	0.473
70.4	1.1400	0.403	0.389	0.406	0.412	0.402

PC 2						
Cell temp (^{o}C)	Current density (A/cm^2)		Voltage (V)			Avg. voltage (V)
70.0	0	0.923	0.923	0.923	0.922	0.923
70.0	0.0200	0.873	0.873	0.873	0.873	0.873
70.0	0.0400	0.854	0.854	0.854	0.854	0.854
70.0	0.0600	0.840	0.840	0.840	0.840	0.840
70.0	0.0800	0.829	0.829	0.829	0.829	0.829
70.0	0.1001	0.820	0.820	0.820	0.820	0.820
70.1	0.1800	0.791	0.791	0.791	0.791	0.791
70.1	0.2597	0.767	0.767	0.767	0.767	0.767
70.1	0.3396	0.743	0.743	0.743	0.743	0.743
70.2	0.4198	0.721	0.720	0.721	0.720	0.720
70.2	0.5000	0.696	0.696	0.696	0.695	0.696
70.2	0.5800	0.672	0.674	0.672	0.673	0.673
70.1	0.6600	0.646	0.647	0.647	0.647	0.647
70.2	0.7401	0.615	0.619	0.616	0.616	0.616
70.2	0.8200	0.584	0.582	0.584	0.583	0.583
70.2	0.9000	0.557	0.557	0.558	0.557	0.557
70.2	0.9800	0.516	0.514	0.516	0.508	0.514
70.2	1.0600	0.455	0.467	0.467	0.469	0.464
70.2	1.1401	0.409	0.399	0.392	0.416	0.404

PC 3						
Cell temp (^{o}C)	Current density (A/cm^{2})		Voltage (V)			Avg. voltage (V)
70.0	0	0.924	0.923	0.923	0.923	0.923
70.0	0.0200	0.874	0.874	0.874	0.873	0.874
70.0	0.0400	0.854	0.854	0.854	0.854	0.854
70.0	0.0600	0.841	0.840	0.841	0.840	0.840
70.0	0.0800	0.830	0.830	0.830	0.830	0.830
70.0	0.1000	0.820	0.820	0.820	0.820	0.820
70.0	0.1800	0.791	0.791	0.791	0.791	0.791
70.0	0.2600	0.767	0.767	0.767	0.767	0.767
70.2	0.3400	0.745	0.745	0.745	0.745	0.745
70.1	0.4200	0.722	0.723	0.723	0.723	0.723
70.2	0.5000	0.698	0.698	0.699	0.699	0.698
70.1	0.5800	0.674	0.673	0.674	0.674	0.674
70.2	0.6602	0.647	0.647	0.648	0.648	0.648
70.2	0.7398	0.619	0.618	0.619	0.619	0.619
70.2	0.8199	0.588	0.584	0.583	0.586	0.585
70.1	0.8997	0.553	0.543	0.550	0.548	0.548
70.2	0.9800	0.510	0.505	0.507	0.509	0.508
70.4	1.0597	0.457	0.449	0.452	0.458	0.454
70.4	1.1400	0.396	0.394	0.397	0.397	0.396

Table B.2: Raw polarization curve data. Fruedenberg I6 Run 3 Condition E with pure oxygen oxidant.

PC 1						
Cell temp (^{o}C)	Current density (A/cm^{2})		Voltage (V)			Avg. voltage (V)
70.0	0	0.958	0.957	0.956	0.955	0.956
70.0	0.0201	0.905	0.905	0.905	0.905	0.905
69.9	0.0397	0.887	0.887	0.887	0.887	0.887
70.0	0.0599	0.874	0.874	0.874	0.874	0.874
70.0	0.0800	0.864	0.864	0.864	0.864	0.864
70.0	0.1002	0.855	0.855	0.855	0.855	0.855
70.2	0.1798	0.831	0.831	0.831	0.831	0.831
70.1	0.2600	0.812	0.812	0.812	0.812	0.812
70.2	0.3400	0.797	0.797	0.797	0.797	0.797
70.1	0.4200	0.783	0.783	0.783	0.783	0.783
70.1	0.5000	0.770	0.770	0.770	0.770	0.770
70.0	0.5800	0.758	0.758	0.758	0.758	0.758
70.1	0.6600	0.746	0.746	0.746	0.746	0.746
70.1	0.7399	0.734	0.734	0.734	0.734	0.734
70.1	0.8200	0.723	0.723	0.723	0.723	0.723
70.1	0.9000	0.712	0.712	0.712	0.712	0.712
70.1	0.9797	0.701	0.701	0.701	0.701	0.701
70.2	1.0600	0.690	0.690	0.689	0.689	0.690
70.2	1.1400	0.677	0.677	0.677	0.677	0.677

PC 2						
Cell temp (^{o}C)	Current density (A/cm^{2})	Voltage (V)				Avg. voltage (V)
69.9	0	0.953	0.953	0.953	0.952	0.953
70.0	0.0200	0.900	0.900	0.900	0.900	0.900
70.0	0.0399	0.881	0.882	0.882	0.882	0.882
70.0	0.0598	0.869	0.869	0.869	0.869	0.869
70.0	0.0797	0.859	0.859	0.859	0.859	0.859
70.0	0.1000	0.851	0.850	0.851	0.851	0.851
70.1	0.1800	0.826	0.826	0.826	0.826	0.826
70.1	0.2597	0.807	0.807	0.807	0.807	0.807
70.1	0.3400	0.791	0.791	0.791	0.791	0.791
70.2	0.4199	0.777	0.777	0.777	0.777	0.777
70.1	0.4998	0.764	0.764	0.764	0.764	0.764
70.1	0.5800	0.751	0.751	0.751	0.751	0.751
70.2	0.6600	0.739	0.739	0.739	0.739	0.739
70.1	0.7399	0.727	0.727	0.727	0.727	0.727
70.1	0.8199	0.716	0.716	0.716	0.716	0.716
70.2	0.8998	0.705	0.705	0.705	0.705	0.705
70.1	0.9802	0.694	0.694	0.694	0.694	0.694
70.2	1.0601	0.683	0.683	0.683	0.683	0.683
70.2	1.1400	0.672	0.672	0.672	0.672	0.672

PC 3						
Cell temp (^{o}C)	Current density (A/cm^{2})	Voltage (V)				Avg. voltage (V)
70.0	0	0.952	0.952	0.951	0.951	0.952
70.0	0.0200	0.898	0.898	0.898	0.898	0.898
70.0	0.0401	0.879	0.879	0.879	0.879	0.879
70.0	0.0599	0.866	0.866	0.866	0.866	0.866
70.0	0.0799	0.857	0.857	0.857	0.857	0.857
70.0	0.0999	0.848	0.848	0.848	0.848	0.848
70.0	0.1798	0.823	0.823	0.823	0.823	0.823
70.1	0.2600	0.804	0.804	0.804	0.804	0.804
70.2	0.3399	0.788	0.788	0.788	0.788	0.788
70.1	0.4200	0.774	0.774	0.774	0.774	0.774
70.1	0.4998	0.760	0.760	0.760	0.761	0.760
70.2	0.5800	0.748	0.748	0.748	0.748	0.748
70.1	0.6600	0.735	0.735	0.735	0.736	0.735
70.1	0.7400	0.724	0.724	0.724	0.724	0.724
70.1	0.8199	0.712	0.712	0.713	0.713	0.712
70.1	0.9000	0.701	0.701	0.701	0.701	0.701
70.2	0.9798	0.690	0.690	0.690	0.690	0.690
70.2	1.0600	0.679	0.679	0.679	0.679	0.679
70.1	1.1400	0.669	0.668	0.668	0.669	0.669

Table B.3: Raw EIS data 300 mA/cm^2. Fruedenberg I6 Run 3 Condition E with pure oxygen oxidant.

Frequency, Hz	Re (Z), Ω	-Im (Z), Ω
0.1	9.01	-0.17
0.3	9.14	-0.08
0.7	9.22	0.02
1.5	9.26	0.22
3.1	9.2	0.44
6.3	9.06	0.89
12.7	8.63	1.59
25.5	7.57	2.33
51.1	6.02	2.47
102.3	4.77	1.93
204.7	4.09	1.3
409.5	3.77	0.87
819.1	3.54	0.62
1638.3	3.36	0.46
3276.7	3.21	0.33
6553.5	3.11	0.19
13107.1	3.25	-0.11

B.2 Single cell testing script

```
'////////////////////////////////////////////////////////////////////////////
/////
'// Copyright(c)  Hydrogen South Africa Catalysis (University of Cape Town)
'// Title:         Single cell testing
'// Author:        Greg Crymble
'// Date:          10 March 2014
'// Description:   Calls desired subroutines for cell testing
'// Comments:      Instruction from Nabeel Hussain
'//
'////////////////////////////////////////////////////////////////////////////
/////

Include "ExcelAutomation.fwsl"
Include "TrueData.fwsl"
Include "HySA-Test Information Library.fwsl"
Include "HySA-Startup Checklist Library.fwsl"
Include "HySA-User Input Library.fwsl"
Include "HySA-Cell Compression Library.fwsl"
Include "HySA-Leak Test Library.fwsl"
Include "HySA-Bubbler Drain and Fill Library.fwsl"
Include "HySA-Heating Library.fwsl"
Include "HySA-Constant Current Conditioning Library.fwsl"
Include "HySA-Cyclic Conditioning Library.fwsl"
Include "HySA-Polcurve Library.fwsl"
Include "HySA-EIS Library.fwsl"
Include "HySA-EIS to Excel Library.fwsl"
Include "HySA-Shutdown Library.fwsl"

'all user defined variables must be global to allow subroutines access to
the values
Dim Dotestinfo, Docellcomp, Doleaktest, Dobubblerdrain,
Doheating_conditioning, Dopolcurve, DoEIS, Doshutdown
'Test selection
Dim logdata, user, path, pathname, experiment,logbookref, descrip,
samplecode, decal, dectemp, decforce, decpressure, dectime, decsupport,
fuelcellinfo
Dim fixture_pressure
'Compression
Dim anodelktest
'Leak test
Dim active_area,cell_temp,anode_back_pressure, cathode_back_pressure,
anode_bubbler_temp,cathode_bubbler_temp,anode_feed_temp,cathode_feed_temp
'Heating
Dim condition_cycles, stoich_a,stoich_c,cyclic
'Cyclic Conditioning
Dim cond_currden, cond_time
'Constant current conditioning
Dim stoich_air, stoich_ox,
anodestoich,maxcurrent_air,maxcurrent_ox,minvoltage_air,minvoltage_ox,numcu
rve_air,numcurve_ox,rest,numrep,ohminc,acinc,stabtime,minflow_cathode,minfl
ow_anode,helox,hfrup, hfrdown, tempeq, temptol, tempeqtime
'Polarization curves
Dim stfreq,Endfreq,EISoxidant,EIS_anodeflow,EIS_cathodeflow
'EIS
Dim shtdwn

ManualControl = True                          ' activation of manual
operation on the p&i-view
```

```
Trace = False                                    ' activation program trace
TagEventHandling = True

TagWriteMode = 0

Main

Sub Main

shtdwn=0
fixture_pressure=4.8
anodelktest=7
active_area=25
cell_temp=70
anode_feed_temp = cell_temp+40
'necessary to prevent condensation
cathode_feed_temp = cell_temp+40
anode_back_pressure=1
cathode_back_pressure=1
anode_bubbler_temp=50.4        '40% RH
cathode_bubbler_temp=0
stoich_a=2
stoich_c=2
cyclic=1
condition_cycles = 12
stoich_air=0
stoich_ox=0
anodestoich=0
maxcurrent_air=30
maxcurrent_ox=30
minvoltage_air=0.3
minvoltage_ox=0.3
numcurve_air=3
numcurve_ox=3
rest=15
numrep=4
ohminc=2
acinc=0.5
stabtime=4
minflow_cathode=0.87
minflow_anode=0.26
helox=0
hfrdown=1
hfrup=0
tempeq=6
temptol=0.5
tempeqtime=10
stfreq=20000
Endfreq=0.1

EIS_anodeflow=0.26
EIS_cathodeflow=0.87

pathname="D:\Fuel Cell Testing\Greg\Data\"

CELLCOMPRESSION
LEAKTEST

Dotestinfo=1
Docellcomp=0
Doleaktest=0
```

```
Dobubblerdrain=0
Doheating_conditioning=0
Dopolcurve=0
DoEIS=0
Doshutdown=0

USERINPUT

Docellcomp=1
Doleaktest=1
Dobubblerdrain=1
Doheating_conditioning=1
Dopolcurve=1
DoEIS=1

BUBBLERDRAINANDFILL

HEATING

'if two polarization curves are run on the same day then unique identifier
is required
Dim ID
ID=1

Dim d,dy,dm,dd,datestr
    d=date
    dy=DatePart("yyyy",d)
    dm=DatePart("m",d)
    dd=DatePart("d",d)
    datestr=dd & "_" & dm & "_" & dy

TESTINFO ID, datestr

CYCLIC_CONDITIONING ID,datestr

'Tune control parameters

Tag("T901000_RD")=30
Tag("T901000_RI")=300
Tag("T901000_RP")=10

Sleep 1*1000*10

PrintLine vbCrLf & "cell PID gains"
PrintLine "P= " & Tag("T901000_RP")
PrintLine "I= " & Tag("T901000_RI")
PrintLine "D= " & Tag("T901000_RD")
PrintLine vbCrLf

POLCURVE ID,datestr

'EIS with air
EISoxidant=0
EIS2EXCEL 1,datestr,300
EIS2EXCEL 2,datestr,300

'EIS with oxygen
EISoxidant=1
EIS2EXCEL 1,datestr,300
EIS2EXCEL 2,datestr,300
EIS2EXCEL 1,datestr,1000
```

```
EIS2EXCEL 2,datestr,1000

'Change conditions to high RH

anode_bubbler_temp=70
cathode_bubbler_temp=70

Tag("T161000_W1")=anode_bubbler_temp
Tag("T261000_W1")=cathode_bubbler_temp

While Tag("T161000_X1")-anode_bubbler_temp+2<0
    Sleep 1*1000
Wend

While Tag("T261000_X1")-cathode_bubbler_temp+2<0
    Sleep 1*1000
Wend

    d=date
    dy=DatePart("yyyy",d)
    dm=DatePart("m",d)
    dd=DatePart("d",d)
    datestr=dd & "_" & dm & "_" & dy

ID=2

TESTINFO ID,datestr

CYCLIC_CONDITIONING ID,datestr

'Tune control parameters

Tag("T901000_RD")=30
Tag("T901000_RI")=300
Tag("T901000_RP")=10

Sleep 1*1000*10

PrintLine vbCrLf & "cell PID gains"
PrintLine "P= " & Tag("T901000_RP")
PrintLine "I= " & Tag("T901000_RI")
PrintLine "D= " & Tag("T901000_RD")
PrintLine vbCrLf

POLCURVE ID,datestr

'EIS with air
EISoxidant=0
EIS2EXCEL 3,datestr,300
EIS2EXCEL 4,datestr,300
EIS2EXCEL 3,datestr,1200
EIS2EXCEL 4,datestr,1200

'EIS with oxygen
EISoxidant=1
EIS2EXCEL 3,datestr,300
EIS2EXCEL 4,datestr,300
EIS2EXCEL 3,datestr,1200
EIS2EXCEL 4,datestr,1200

shtdwn=1
```

```
SHUTDOWN

PrintLine "'-------------------------------------------------------------
"
PrintLine "          Single cell testing finished at " & Now
PrintLine "      The system is now in unlimited manual operation mode"
PrintLine "-------------------------------------------------------------
"

TestPointName = "manual operation"
    ManualControl = True
    Trace              = False

    While ( True )
      Sleep 1000
    Wend

End Sub
```

B.3 Polarization curve library

```
'////////////////////////////////////////////////////////////////////////
/////
'// Copyright(c)  Hydrogen South Africa Catalysis (University of Cape Town)
'// Title:          Polarization Curve Library
'// Authors:        Greg Crymble, Nabeel Hussain
'// Date:           10 March 2014
'// Description:    Polarization curve with variable step-size and HFR
'//                 Transition from Activation to Ohmic region at 0.1 A/cm2
'////////////////////////////////////////////////////////////////////////
/////

Sub POLCURVE(arg,arg2)

     Dim tol2,ImpRe,Impi,l

    'create excel file
    Dim str            'file name
    str=pathname & arg2 & " Polarisation Curve(s) " & " ID" & arg & ".xlsx"

    CreateOrOpenExcelFile str,""

    Dim ox,fin,colshift2

    If numcurve_air<>0 Then
        ox=0                                          'test with air first
    Else
        ox=1
    End If

    fin=0      'allows pol curve script to loop to test with air and oxygen
    colshift2=0

    Dim P(12)                  'array to store voltage readings (up to 12)
```

```
    PrintLine " "
    PrintLine "Polarization curve measurements, refer to the Script window
to follow automated procedure"
    PrintLine "Do not open or modify any excel documents while the script
is running"
    PrintLine "After the test has finished remember to save all documents
before closing "
    PrintLine " "

    Dim c,hfrc,cc
    c=4
'column number
    hfrc=1
'column number for impedance
    cc=1

While fin=0

    Dim
i,v,v0,minvoltage,maxcurrent,k,kk,x,lin,ichange,numcurve,y,z,cathodestoich,
temptime,oxpressure

    y=0
'number of curves achieved
    z=1
'dummy variable for testing point of transition from activation to ohmic
region

    Tag("E602000_W1")=0
'OCV
    Tag("E600000_Y3")=0
'Disconnect load

    'Set minimum flows with air to start
    Dim actualanodeflow, actualcathodeflow
    actualanodeflow=Tag("F104000_X1")
    actualcathodeflow=Tag("F204000_X1")

    Tag("Q111000_Y3")=0
'deactivate stoich control
    Tag("Q211000_Y3")=0
'deactivate stoich control

    'check if nitrogen is flowing and flow rate set points are high
(potential shut down situation when valves opened due to temp rise)
    If Tag("U303100_Y3")=-1 Then
        Tag("F104000_W1")=0.5
'approx 25 Nl/min (same as N2 flow)
    End If

    If Tag("U304100_Y3")=-1 Then
        Tag("F204000_W1")=0.5
'approx 25 Nl/min (same as N2 flow)
```

```
    End If

    If Tag("U202000_Y3")=0  And Tag("U232000_Y3")=0 Then
        Tag("U202000_Y3")=-1
'open air flow to cathode
    End If
    Tag("U102000_Y3")=-1
'open hydrogen flow to cathode

    'start with hydrogen flow setting
    While actualanodeflow-minflow_anode+0.1<0
        Tag("F104000_W1")=Tag("F104000_W1")+0.1
        Sleep 30*1000
        actualanodeflow=Tag("F104000_X1")
    Wend
    Tag("F104000_W1")=minflow_anode

    'set oxidant flow
    While actualcathodeflow-minflow_cathode+0.1<0
        Tag("F204000_W1")=Tag("F204000_W1")+0.1
        Sleep 20*1000
        actualcathodeflow=Tag("F204000_X1")
    Wend
    Tag("F204000_W1")=minflow_cathode
    Sleep 30*1000

    Tag("E600000_Y3")=-1
    Tag("E602000_W1")=2.5

    If ox=0 Then
'start test with air
        If Tag("U202000_Y3")=0 Then
            Tag("U202000_Y3")=-1                                    'open air
flow to cathode
            Sleep 10*1000*60
        End If
        cathodestoich=stoich_air
        maxcurrent=maxcurrent_air
        minvoltage=minvoltage_air
        numcurve=numcurve_air
    Else
'parameters for test with oxygen or helox
        'if testing with helox the minimum flow at the cathode must be
scaled due to the calibration of the mass flow controller (for oxygen)
        If helox=1 Then
            minflow_cathode=minflow_cathode*1.363
            Tag("F204000_W1")=minflow_cathode
        End If
        If Tag("U232000_Y3")<>-1 Then
            oxpressure=0
            While oxpressure=0
                If Tag("P231000_X1")-8>0 Then
                    Tag("U232000_Y3")=-1
```

```
                    PrintLine vbCrLf & "Please wait 10 minutes from " & Now
& " for the Polarisation curve to begin"
                    Sleep 10*1000*60
                    oxpressure=1
                Else
                    msgbox("Oxygen pressure below 8 bar, please increase
pressure and click OK to continue with test")
                End If
            Wend
        End If
        cathodestoich=stoich_ox
        maxcurrent=maxcurrent_ox
        minvoltage=minvoltage_ox
        numcurve=numcurve_ox
    End If

    PrintLine "Lower voltage limit = " & minvoltage & "V"
    PrintLine "Maximum current limit = " & maxcurrent & "A"
    PrintLine "Number of repeat readings = " & numrep
    PrintLine "Number of repeat polarisation curves = " & numcurve
    If tempeq=6 Then
        PrintLine "Cell temperature control activated"
    End If

    Dim hfrstart,hfrtime                                        'to
determine if HFR measurement fails

    PrintLine " "
    PrintLine "Returning to OCV and switching off load"
    PrintLine " "

    'bring currrent to zero in steps of 2
    i=Tag("E602000_X1")

    While i-2>0
        i=i-2
        Tag("E602000_W1")=i
        Sleep 20*1000
    Wend

    While y-numcurve<>0
'repeat procedure until number of desired curves are completed

        TestPointName="Measure PolCurve"                        ' write
into [test point name] of p&i-d
        Tag("H840000_X1") = Tag("H840000_X1") + 1                ' test
point number + 1
    Sleep 2000
        curvename = "Polcurve " & arg2    & " " & ox & y &" ID" & arg    '
unique identifier
        Sleep 5*1000                                                '
wait 5 sec
```

```
        'column headings
        ExcelAutomationWriteCell str,"table1",2,c,"Cell temp (degC)"
        ExcelAutomationWriteCell str,"table1",2,c+1,"Current density
(A/cm2)"
        ExcelAutomationWriteCell str,"table1",2,c+2,"Voltage (V)"
        ExcelAutomationWriteCell str,"table1",2,c+numrep+2,"Avg. voltage
(V)"
        If ox=0 Then
            ExcelAutomationWriteCell str,"table1",1,c,"Forward sweep (air)"
            ExcelAutomationWriteCell str,"table1",1,c+numrep+4,"Reverse
sweep (air)"
        ElseIf helox=0 Then
            ExcelAutomationWriteCell str,"table1",1,c,"Forward sweep
(oxygen)"
            ExcelAutomationWriteCell str,"table1",1,c+numrep+4,"Reverse
sweep (oxygen)"
        Else
            ExcelAutomationWriteCell str,"table1",1,c,"Forward sweep
(helox)"
            ExcelAutomationWriteCell str,"table1",1,c+numrep+4,"Reverse
sweep (helox)"
        End If
        ExcelAutomationWriteCell str,"table1",2,c+numrep+4,"Cell temp
(degC)"
        ExcelAutomationWriteCell str,"table1",2,c+numrep+5,"Current density
(A/cm2)"
        ExcelAutomationWriteCell str,"table1",2,c+numrep+6,"Voltage (V)"
        ExcelAutomationWriteCell str,"table1",2,c+(2*numrep)+6,"Avg.
voltage (V)"

        'Impedence meaurement column headings
        If hfrdown=1 Then
            ExcelAutomationWriteCell str,"table2",2,cc,"Current density
(A/cm2)"
            ExcelAutomationWriteCell str,"table2",2,cc+1,"Real
impedence(mOhm.cm2)"
            ExcelAutomationWriteCell str,"table2",2,cc+2,"Im.
impedence(mOhm)"
            If ox=0 Then
                ExcelAutomationWriteCell str,"table2",1,cc,"Forward sweep
(air)"
                cc=cc+4
            ElseIf helox=0 Then
                ExcelAutomationWriteCell str,"table2",1,cc,"Forward sweep
(oxygen)"
                cc=cc+4
            Else
                ExcelAutomationWriteCell str,"table2",1,cc,"Forward sweep
(helox)"
                cc=cc+4
            End If
        End If
```

```
        If hfrup=1 Then
            ExcelAutomationWriteCell str,"table2",2,cc,"Current density
(A/cm2)"
            ExcelAutomationWriteCell str,"table2",2,cc+1,"Real
impedence(mOhm.cm2)"
            ExcelAutomationWriteCell str,"table2",2,cc+2,"Im.
impedence(mOhm)"
            If ox=0 Then
                ExcelAutomationWriteCell str,"table2",1,cc,"Reverse sweep
(air)"
                cc=cc+4
            ElseIf helox=0 Then
                ExcelAutomationWriteCell str,"table2",1,cc,"Reverse sweep
(oxygen)"
                cc=cc+4
            Else
                ExcelAutomationWriteCell str,"table2",1,cc,"Reverse sweep
(helox)"
                cc=cc+4
            End If
        End If

        'Write testing parameters to file
        ExcelAutomationWriteCell str,"table1",1,1,"Set point values"
        ExcelAutomationWriteCell str,"table1",2,1,"Cell temperature set
point"
        ExcelAutomationWriteCell str,"table1",2,2,Tag("T901000_W1")
        ExcelAutomationWriteCell str,"table1",3,1,"Anode humidifier"
        ExcelAutomationWriteCell
str,"table1",3,2,Round(Tag("T161000_X1"),2)
        If Tag("Q110000_Y3")=0 Then
            ExcelAutomationWriteCell str,"table1",3,3,"Bypassed"
        End If
        ExcelAutomationWriteCell str,"table1",4,1,"Cathode humidifier"
        ExcelAutomationWriteCell
str,"table1",4,2,Round(Tag("T261000_X1"),2)
        If Tag("Q210000_Y3")=0 Then
            ExcelAutomationWriteCell str,"table1",4,3,"Bypassed"
        End If
        ExcelAutomationWriteCell str,"table1",5,1,"Backpressure"
        ExcelAutomationWriteCell
str,"table1",5,2,Round(Tag("P209000_X1"),2)
        ExcelAutomationWriteCell str,"table1",6,1,"Anode min flow"
        ExcelAutomationWriteCell str,"table1",6,2,minflow_anode
        ExcelAutomationWriteCell str,"table1",7,1,"Cathode min flow"
        ExcelAutomationWriteCell str,"table1",7,2,minflow_cathode
        ExcelAutomationWriteCell str,"table1",8,1,"Anode stoich"
        ExcelAutomationWriteCell str,"table1",8,2,anodestoich
        ExcelAutomationWriteCell str,"table1",9,1,"Air stoich"

        If stoich_air=-1 Then
            ExcelAutomationWriteCell str,"table1",9,2,"NA"
        Else
```

```
            ExcelAutomationWriteCell str,"table1",9,2,stoich_air
        End If

        If helox=0 Then
            ExcelAutomationWriteCell str,"table1",10,1,"Oxygen stoich"
        Else
            ExcelAutomationWriteCell str,"table1",10,1,"Helox stoich"
        End If

        If stoich_ox=-1 Then
            ExcelAutomationWriteCell str,"table1",10,2,"NA"
        Else
            ExcelAutomationWriteCell str,"table1",10,2,stoich_ox
        End If

        Tag("E602000_W1") = 0
' set current to 0
        Sleep 10*1000        '10s

        k=3
'updates the row number when writing to file
        kk=3
        inc=acinc
'before ohmic region curve will be non-linear (use small step size)
        lin=0
'is data linear?
        z=1

        PrintLine "Started at " & Now & vbCrLf

        i=0

        Tag("E600000_Y3")= -1
' connect load
        Sleep 30*1000

        v=Tag("E601000_X1")
        PrintLine "OCV= " & v & "V"
'display OCV
        PrintLine "OCV current= " & Tag("E602000_X1") & "A"
'display actual cell current

        Dim actual_celltemp,Setpoint_celltemp

        actual_celltemp=Tag("T901000_X1")

        Dim g
'indexing variable
        For g=0 To numrep-1
            P(g)=Tag("E601000_X1")
'first voltage measurement (OCV)
            PrintLine P(g) & "V"
            Sleep rest*1000
```

```
        Next

        SaveChartPoint curvename
'save the last read voltage value at OCV

        'find average voltage
        v0=0

        For g=0 To numrep-1
            v0=v0+P(g)
        Next
        v0=v0/numrep
'average OCV

        PrintLine Round(v0,3) & "V (average OCV)"

        'Write cell potentials (and associated current density) to file
        ExcelAutomationWriteCell str,"table1",k,c,Round(actual_celltemp,3)
        ExcelAutomationWriteCell
str,"table1",k,c+1,Tag("E602000_X1")/active_area

        For g=0 To numrep-1
        ExcelAutomationWriteCell str,"table1",k,c+g+2,P(g)
        Next
        'Write average voltage
    ExcelAutomationWriteCell str,"table1",k,c+numrep+2,Round(v0,3)

        i=i+inc
        k=k+1

    '-------------------------------------------------------------------------
-----------------------------------
        Tag("E602000_W1")=i

        'obtain second data point to extrapolate voltage

        Sleep (stabtime*60*1000)   'wait before voltage reading
        PrintLine Tag("E602000_X1") & "A"

        actual_celltemp=Tag("T901000_X1")
        For g=0 To numrep-1
            P(g)=Tag("E601000_X1")
            PrintLine P(g) & "V"
            Sleep rest*1000
        Next

        SaveChartPoint curvename
'save the value

        'find average voltage
        v=0

        For g=0 To numrep-1
```

```
            v=v+P(g)
        Next
        v=v/numrep
'average voltage reading

        PrintLine Round(v,3) & "V (average)"
        Dim actcurrden
        actcurrden=Tag("E602000_X1")/active_area

        'Write cell potentials (and associated current) to file
        ExcelAutomationWriteCell str,"table1",k,c,Round(actual_celltemp,3)
        ExcelAutomationWriteCell str,"table1",k,c+1,actcurrden

        For g=0 To numrep-1
        ExcelAutomationWriteCell str,"table1",k,c+g+2,P(g)
        Next
        'Write average voltage
    ExcelAutomationWriteCell str,"table1",k,c+numrep+2,Round(v,3)

        If hfrdown=1 Then
                    'take HFR meaurement here
                    ''''''''''''''''''''''''''''''''''''''''''''''
                    hfrstart=Now
                    Tag("E620000_Y3")=-1
                    TrueDataImpedance 10000, "HFR impedance 10 kHz"
' Impedance at 10kHz (HFR)
                    hfrtime=DateDiff("s",hfrstart,Now)

                    If hfrtime>120 Then'HFR took more than 2 mins
indicating an error in measurement
                        PrintLine "HFR failed at " & Tag("E602000_X1")& "A"
                    Else
                        ImpRe=Tag("E624001_X1")
                        Impi=Tag("E624002_X1")

                        'Write Impedence measurements to file
                        ExcelAutomationWriteCell
str,"table2",kk,hfrc,actcurrden    'current density
                        ExcelAutomationWriteCell
str,"table2",kk,hfrc+1,ImpRe*active_area                'impedence real
                        ExcelAutomationWriteCell
str,"table2",kk,hfrc+2,Impi            'impedence imaginary
                        kk=kk+1
                    End If

                    Tag("E620000_Y3")=0
                    Sleep 5000    'sleep 5s
                End If

        k=k+1
        i=i+inc
        Dim speqav
        speqav=1
```

```
        l=1

'-------------------------------------------------------------------------
-----------------------------------------

        While (Tag("E602000_W1")+inc-maxcurrent)<=0 And l=1

            PrintLine "While Loop execute"

            Dim extrapv
            extrapv=(2*v)-v0

            PrintLine "extrapolated v= " & Round(extrapv,3)
            PrintLine "minv= " & minvoltage

            'ensure that set point current is reached. If not then
terminate loop
            Dim Setcurr, actualcurr
            Setcurr=Tag("E602000_W1")
            actualcurr=Tag("E602000_X1")

            If Setcurr-actualcurr-0.5>0 Then                    'If set
point current not reached prevent further current stepping
                speqav=0
            End If

            If extrapv-minvoltage>=0 And speqav=1 Then
' extrapolate to ensure voltage does not drop below min value upon current
increment (v-(v0-v)>minV)

                'check flow rate is sufficient before drawing current
                Dim anflow,catflow

                anflow=anodestoich*(((i/(2*96500))*60)*22.4)

            If (anflow-minflow_anode>0) Then
' no backpressure so min flow not required
                    Tag("F104000_W1")=anflow
                Else
                    Tag("F104000_W1")=minflow_anode
                End If

                If ox=0 Then
'test with air
                    catflow=cathodestoich*(((i/(4*96500))*60)*22.4)/0.21
                    If (catflow-minflow_cathode>0) Then
                        Tag("F204000_W1")=catflow
                        PrintLine vbCrLf & "LOAD FOLLOWING" & vbCrLf
                    Else
                        Tag("F204000_W1")= minflow_cathode
                    End If
                ElseIf helox=0     Then
'test with oxygen
```

```
                    catflow=cathodestoich*(((i/(4*96500))*60)*22.4)
                    If (catflow-minflow_cathode>0) Then
                        Tag("F204000_W1")=catflow
                        PrintLine vbCrLf & "LOAD FOLLOWING" & vbCrLf
                    Else
                        Tag("F204000_W1")= minflow_cathode
                    End If
                Else
'test with helox

catflow=1.363*cathodestoich*(((i/(4*96500))*60)*22.4)/0.21
                    If (catflow-minflow_cathode>0) Then
                        Tag("F204000_W1")=catflow
                    Else
                        Tag("F204000_W1")= minflow_cathode
                    End If

                End If

                Sleep 5000    '5s

                Tag("E602000_W1")=i
                PrintLine "set value= " & i & "A"

                PrintLine "execute"

                Sleep (stabtime*60*1000)       'wait for stabilization
before taking readings

                actual_celltemp=Tag("T901000_X1")
                Setpoint_celltemp=Tag("T901000_W1")

                temptime=stabtime*60

                If tempeq=6 Then
                    While Setpoint_celltemp + temptol - actual_celltemp < 0
And temptime - tempeqtime*60 < 0    'max wait tempeqtime*60
                        Sleep 5*1000
                        actual_celltemp=Tag("T901000_X1")
                        temptime=temptime+5
                    Wend
                End If

            If temptime=tempeqtime*60 Then
                PrintLine "Temperature tolerance not met" & vbCrLf
            End If

                PrintLine "actual value= " & Tag("E602000_X1")& "A"

                For g=0 To numrep-1
                    P(g)=Tag("E601000_X1")
                    PrintLine P(g) & "V"
                    Sleep rest*1000
```

```
                Next

                SaveChartPoint curvename                                ' save
the value

                v0=v
'move position of v0 for extrapolation

                'find average voltage
                v=0

                For g=0 To numrep-1
                    v=v+P(g)
                Next
                v=v/numrep
'average voltage reading

                PrintLine Round(v,3) & "V (average)"
                PrintLine "Cell temp = " & Round(Tag("T901000_X1"),3) & "
degC"

                If z=1 Then
                    If lin=0 Then    'data non linear
                        If Tag("E602000_W1") + acinc - active_area*0.1 >=
0.1 Then
                            inc=ohminc
                            PrintLine "Ohmic region"
                            lin=1
                            ichange=i        'point at which the transition
from activation region to ohmic occurs, used to change increment size on up
sweep
                            PrintLine "Transition from kinetic to ohmic
region at: " & ichange & "A"
                            z=-1
                        End If
                    End If
                End If

                actcurrden=Tag("E602000_X1")/active_area

                'Write cell potentials (and associated current) to file
                ExcelAutomationWriteCell
str,"table1",k,c,Round(actual_celltemp,3)
                ExcelAutomationWriteCell str,"table1",k,c+1,actcurrden

                For g=0 To numrep-1
                    ExcelAutomationWriteCell str,"table1",k,c+g+2,P(g)
                Next
                'Write average voltage
            ExcelAutomationWriteCell str,"table1",k,c+numrep+2,Round(v,3)

                If hfrdown=1 Then
                    'take HFR meaurement here
```

```
                    '''''''''''''''''''''''''''''''''''''''''''''
                    hfrstart=Now
                    Tag("E620000_Y3")=-1
                    TrueDataImpedance 10000, "HFR impedance 10 kHz"
' Impedance at 10kHz (HFR)
                    hfrtime=DateDiff("s",hfrstart,Now)

                    If hfrtime>120 Then'HFR took more than 2 mins
indicating an error in measurement
                        PrintLine "HFR failed at " & Tag("E602000_X1")& "A"
                    Else
                        ImpRe=Tag("E624001_X1")
                        Impi=Tag("E624002_X1")

                        'Write Impedence measurements to file
                        ExcelAutomationWriteCell
str,"table2",kk,hfrc,actcurrden    'current density
                        ExcelAutomationWriteCell
str,"table2",kk,hfrc+1,ImpRe*active_area                 'impedence real
                        ExcelAutomationWriteCell
str,"table2",kk,hfrc+2,Impi            'impedence imaginary
                        kk=kk+1
                    End If

                    Tag("E620000_Y3")=0
                    Sleep 5000    'sleep 5s
                End If

                k=k+1
                i=i+inc
            Else
                l=0        'if voltage gets too low, assign value to 'l'
such that the while loop terminates
            End If

        Wend

        i=Tag("E602000_W1")

        PrintLine "Actual Current at end of down sweep= " &
Tag("E602000_X1") & "A"
        PrintLine "Set Current at end of down sweep= " & i & "A"

        If l=1 Then
            PrintLine "Current limit reached"
        ElseIf l=0 And speqav=1 Then
            PrintLine "Voltage limit reached"
        Else
            PrintLine "Current step failed"
        End If
        k=k-1
        kk=3
```

```
        If hfrdown=1 Then
            hfrc=hfrc+4
        End If
''''''''''''''''''''''''''''''''''''''''''''''''''''''''''''''''''''''''''''
'

    While k>3 And i>0
'up sweep

        'step down current before changing flow rate
        Tag("E602000_W1")=i

        Sleep 5000    '5s

        anflow=anodestoich*(((i/(2*96500))*60)*0.082*273)       'no
backpressure so min flow not required.
     If (anflow-minflow_anode>0) Then
            Tag("F104000_W1")=anflow
        Else
            Tag("F104000_W1")=minflow_anode
        End If

        If ox=0 Then
            catflow=cathodestoich*(((i/(4*96500))*60)*22.4)/0.21
            If (catflow-minflow_cathode>0) Then
                Tag("F204000_W1")=catflow
                PrintLine vbCrLf & "LOAD FOLLOWING" & vbCrLf
            Else
                Tag("F204000_W1")= minflow_cathode
            End If
        ElseIf helox=0 Then
            catflow=cathodestoich*(((i/(4*96500))*60)*22.4)
            If (catflow-minflow_cathode>0) Then
                Tag("F204000_W1")=catflow
                PrintLine vbCrLf & "LOAD FOLLOWING" & vbCrLf
            Else
                Tag("F204000_W1")= minflow_cathode
            End If
        Else
            catflow=1.363*cathodestoich*(((i/(4*96500))*60)*22.4)
            If (catflow-minflow_cathode>0) Then
                Tag("F204000_W1")=catflow
            Else
                Tag("F204000_W1")= minflow_cathode
            End If
        End If

        PrintLine "set value= " & Round(i,3) & "A"
        PrintLine "execute"

        Sleep (stabtime*60*1000)           'wait for voltage to stabilize

        PrintLine "actual value= " & Tag("E602000_X1")& "A"
```

```
        actual_celltemp=Tag("T901000_X1")
        Setpoint_celltemp=Tag("T901000_W1")

        temptime=stabtime*60

        If tempeq=6 Then
            While Setpoint_celltemp + temptol - actual_celltemp < 0     And
temptime - tempeqtime*60 < 0
                Sleep 5*1000
                actual_celltemp=Tag("T901000_X1")
                temptime=temptime+5
            Wend
            While Setpoint_celltemp - temptol - actual_celltemp > 0     And
temptime - tempeqtime*60 < 0
                Sleep 5*1000
                actual_celltemp=Tag("T901000_X1")
                temptime=temptime+5
            Wend
        End If

        If temptime=tempeqtime*60 Then
            PrintLine "Temperature tolerance not met" & vbCrLf
        End If

        For g=0 To numrep-1
            P(g)=Tag("E601000_X1")
            PrintLine P(g) & "V"
            Sleep rest*1000
        Next

        SaveChartPoint curvename                    'save the value

        'find average voltage
        v=0

        For g=0 To numrep-1
            v=v+P(g)
        Next
        v=v/numrep
'average voltage reading

        PrintLine Round(v,3) & "V (average)"
        PrintLine "Cell temp = " & Round(Tag("T901000_X1"),3) & " degC" &
vbCrLf

        If lin=1 Then
        'check region
            If Abs(Round((i-ichange),1))<0.2 Then
                inc=acinc
                PrintLine "Activation region"
                lin=0
            End If
```

```
        End If

        actcurrden=Tag("E602000_X1")/active_area

        'Write cell potentials (and associated current) to file
        ExcelAutomationWriteCell
str,"table1",k,c+numrep+4,Round(actual_celltemp,3)
        ExcelAutomationWriteCell str,"table1",k,c+numrep+5,actcurrden

        For g=0 To numrep-1
            ExcelAutomationWriteCell str,"table1",k,c+numrep+g+6,P(g)
        Next

        'Write average voltage
    ExcelAutomationWriteCell str,"table1",k,c+(2*numrep)+6,Round(v,3)

        If hfrup=1 Then
            'take HFR meaurement here
                '''''''''''''''''''''''''''''''''''''''''''''''''''''
                    hfrstart=Now
                    Tag("E620000_Y3")=-1
                    TrueDataImpedance 10000, "HFR impedance 10 kHz"
' Impedance at 10kHz (HFR)
                    hfrtime=DateDiff("s",hfrstart,Now)

                    If hfrtime>120 Then'HFR took more than 2 mins
indicating an error in measurement
                        PrintLine "HFR failed at " & Tag("E602000_X1")& "A"
                    Else
                        ImpRe=Tag("E624001_X1")
                        Impi=Tag("E624002_X1")

                        'Write Impedence measurements to file
                        ExcelAutomationWriteCell
str,"table2",kk,hfrc,actcurrden    'current density
                        ExcelAutomationWriteCell
str,"table2",kk,hfrc+1,ImpRe*active_area                'impedence real
                        ExcelAutomationWriteCell
str,"table2",kk,hfrc+2,Impi            'impedence imaginary
                        kk=kk+1
                    End If

                    Tag("E620000_Y3")=0
                    Sleep 5000    'sleep 5s
        End If
                    k=k-1
'update row number
                    i=i-inc
'step current
    Wend

    'last check at OCV
    Tag("E602000_W1")=0
```

```
    Sleep 10000    '10s
    PrintLine "OCV current= " & Tag("E602000_X1") & "A"

    actual_celltemp=Tag("T901000_X1")

    For g=0 To numrep-1
        P(g)=Tag("E601000_X1")
        PrintLine P(g) & "V"
        Sleep rest*1000
    Next

    SaveChartPoint curvename
'save the values

    'find average voltage
    v=0

    For g=0 To numrep-1
        v=v+P(g)
    Next
    v=v/numrep
'average voltage reading

    PrintLine Round(v,3) & "V (average)"

    actcurrden=Tag("E602000_X1")/active_area

    'Write cell potentials (and associated current) to file
    ExcelAutomationWriteCell
str,"table1",k,c+numrep+4,Round(actual_celltemp,3)
    ExcelAutomationWriteCell str,"table1",k,c+numrep+5,actcurrden

    For g=0 To numrep-1
        ExcelAutomationWriteCell str,"table1",k,c+numrep+g+6,P(g)
    Next

    'Write average voltage
   ExcelAutomationWriteCell str,"table1",k,c+(2*numrep)+6,Round(v,3)

    If hfrup=1 Then
'take HFR meaurement here
        '''''''''''''''''''''''''''''''''''''''''''''''''''''
        Tag("E620000_Y3")=-1
        TrueDataImpedance 10000, "impedance 10 kHz"
'Impedance at 10kHz (HFR)

        ImpRe=Tag("E624001_X1")
        Impi=Tag("E624002_X1")

        'Write Impedence measurements to file
        ExcelAutomationWriteCell str,"table2",kk,hfrc,actcurrden
'Current density
        ExcelAutomationWriteCell str,"table2",kk,hfrc+1,ImpRe*active_area
```

```
'Impedence real
        ExcelAutomationWriteCell str,"table2",kk,hfrc+2,Impi
'Impedence imaginary
        Tag("E620000_Y3")=0
        Sleep 5000     'sleep 5s
    End If

    'bring back to OCV
    PrintLine "returning to OCV"

    i=Tag("E602000_X1")
    inc=2
        While i-inc>0
            i=i-inc
            Tag("E602000_W1")=i
            Sleep 20000
        Wend

    Tag("E602000_W1")=0

    c=c+(2*numrep)+8
    y=y+1

    If hfrup=1 Then
        hfrc=hfrc+4
    End If

    If y-numcurve<>0 Then
        PrintLine vbCrLf & "Beginning next polarisation curve at " & Now
    End If

    Wend

    If ox=1 Or numcurve_ox=0 Then
        fin=fin+1
'If pol curves with oxygen completed or not desired then exit loop
    End If

    ox=1
    c=c+1

Wend
'Loop to repeat polcurves with oxygen

If helox=1 And numcurve_ox>0 Then
'Reset min flow if test performed with helox
    minflow_cathode=minflow_cathode/0.363
End If

Tag("F104000_W1") = minflow_anode
'Set minimum flows
Tag("F204000_W1") = minflow_cathode
Tag("U202000_Y3") = -1
```

```
'Open air flow to cathode
Tag("E602000_W1") = active_area*0.2
'Constant current operation
Sleep 20*1000*60


 End Sub 'polcurve
```